AN ELECTRON PARAMAGNETIC RESONANCE STUDY OF A MANGANESE (IV) ION IN A TRIGONAL ENVIRONMENT

BY

COLIN RUSSELL BYFLEET
B.A., University of Cambridge, 1964

A THESIS SUBMITTED IN PARTIAL FULFILMENT OF
THE REQUIREMENTS FOR THE DEGREE OF

DOCTOR OF PHILOSOPHY

in the Department
of
Chemistry

We accept this thesis as conforming to the required standard

THE UNIVERSITY OF BRITISH COLUMBIA

March, 1969

In presenting this thesis in partial fulfilment of the requirements for an advanced degree at the University of British Columbia, I agree that the Library shall make it freely available for reference and Study. I further agree that permission for extensive copying of this thesis for scholarly purposes may be granted by the Head of my Department or by his representatives. It is understood that copying or publication of this thesis for financial gain shall not be allowed without my written permission.

Colin Byfleet

Department of Chemistry

The University of British Columbia
Vancouver 8, Canada

Date March 13 1964

ABSTRACT

An electron spin resonance study has been carried out at room temperature, on a magnetically dilute single crystal of ammonium 9-molybdomanganate. A general method for fitting E.S.R. results to a spin Hamiltonian has been devised, and the results of the above study have been used as an example of this method. The values of the parameters thus determined were $|D| = 0.861 \pm 0.001$ cm^{-1}; $g_{//} = 1.9920 \pm 0.0004$ cm^{-1}; $g_{\perp} = 1.9880 \pm 0.0004$ cm^{-1}; $|A_{//}| = 0.00760 \pm 0.00004$ cm^{-1}; $|A_{\perp}| = 0.00684 \pm 0.00004$ cm^{-1}.

A review of previous theoretical calculations on d^3 has been given, and a ligand field approach has been taken in an attempt to interpret the observed parameters. This was successful for the zero field splitting and hyperfine coupling constants, but not for the g-values.

The experimental results from a study of an irradiated, single crystal of deuterated ammonium paramolybdate tetrahydrate have also been fitted to a suitable spin Hamiltonian.

The principal axes of the $\underline{\underline{g}}$ and $\underline{\underline{A}}$ tensors were found not to be coincident, and a method for treating the experimental results in this situation has been given.

This study showed that the doublet splitting observed earlier, in the E.S.R. spectrum of the irradiated, undeuterated compound, was most probably due to a captured proton. An interpretation of the observed g-values and hyperfine coupling constants has been given, using a molecular orbital approach.

TABLE OF CONTENTS

Table of Contents (cont'd.)

TABLES

Tables (cont'd.)

FIGURES

Figures (cont'd.)

Figures (cont'd.)

ACKNOWLEDGMENT

I would like to express my sincere thanks to Dr. W.C. Lin for suggesting this problem, for his untiring assistance and guidance, and for many hours of stimulating discussion.

I am very grateful to Dr. C.A. McDowell for making the excellent facilities of the Department available to me; to Dr. D.P. Chong for clarifying many points in perturbation theory and, together with Dr. F.G. Herring and Mr D.E. Kennedy, for supplying computer sub-routines.

My thanks are also due to Mr J. Sallos and Mr T. Markos for keeping the E.S.R. equipment in excellent condition, and to my wife for her help in the preparation of this manuscript.

Finally, I would like to acknowledge the receipt of an assistantship from the Department of Chemistry, a University of British Columbia scholarship, and two scholarships from the National Research Council of Canada.

Symbols Used but Undefined in the Text

$\hbar$ = $h/2\pi$ = Planck's constant

∇_i = $(\partial/\partial x_i, \partial/\partial y_i, \partial/\partial z_i)$

m = electron rest mass

e = electronic charge

c = velocity of light

g_e = g-value of free electron

β_e = absolute value of Bohr magneton

β_N = nuclear magneton

g_N = nuclear g-factor

H = magnetic field

$\underline{s}$, $\underline{S}$ = electron spin momentum vector

$\underline{I}$ = nuclear spin momentum vector

$\underline{l}$ = orbital angular momentum vector

$\delta(r_{ik})$ = Dirac δ-function

Q = nuclear quadrupole moment

$g_{\parallel}$ = g_{zz}, z-component of g-tensor

$g_{\perp}$ = $\frac{1}{2}(g_{xx} + g_{yy})$

$A_{\parallel}$ = A_{zz}, z-component of hyperfine coupling tensor, A

$A_{\perp}$ = $\frac{1}{2}(A_{xx} + A_{yy})$

P = quadrupole coupling tensor

M_s = eigenvalue of electron spin vector

M_I = eigenvalue of nuclear spin vector

e, a, t, etc., are one-electron group theoretical labels

E, A, T, etc., are electronic state group theoretical labels

NOTE: the symbols e and e_g etc., are used interchangeably

$E(^4A_1)$ etc., are the energies of $^4A_1$ electronic states with respect to the ground state of the system.

PART I

1. Introduction

Electron spin resonance spectra of transition metal complexes have been widely studied (1-4), and the information obtained by this method has led to a greater understanding of the detailed electronic structure of these compounds. Three theoretical approaches have been used to interpret the experimental results, these being the crystal field (5), ligand field (6) and molecular orbital (7,8) theories. The latter approach is most successful, although most applications have been to d^1 or d^9 systems, since calculations involving more than one free electron become very tedious.

Ligand field theory is formally very similar to crystal field ideas, where the ion under study is considered to be co-ordinated by oppositely charged ions or dipoles; no allowance being made for covalency effects, which have been observed as, for instance, super-hyperfine interactions with the ligand nuclei (9). Various parameters are allowed to vary from their free ion value in ligand field theory, in a physically justifiable way, to account for covalency.

Manganese occurs in several valence states, +2, +3, +4, +6 and +7. Of these the first four have the possibility of being paramagnetic and much E.S.R. work has been done on the $d^5 Mn^{2+}$ system. The major part of this work is concerned with a d^3 system in which the central transition metal ion is manganese in its +4 valence state; namely, $(NH_4)_6Mo_9O_{32}Mn.8H_2O$, ammonium 9-molybdomanganate, a typical heteropolymolybdate.

There are very few Mn^{+4} compounds and MnO_2 is the only one commonly found. This has led to a very small number of previous E.S.R. studies being done on Mn^{+4} systems (11-22). In fact, all the previous work has been on crystals of compounds like SnO_2 or $SrTiO_3$ having Mn^{+4} as an impurity ion replacing Sn^{+4} or Ti^{+4} in the lattice, and leading to a

magnetically dilute MnO_2 system.

In the present system the Mn^{+4} ion is part of a well defined polymolybdate complex, a system which may have many different ions in the central position. These have not been studied by E.S.R., but would seem to offer a large field for further study, which would enable comparisons to be made between different ions in very similar environments.

Magnetically concentrated systems give unresolved E.S.R. spectra due to dipole-dipole interactions between neighbouring ions (23). The polymolybdate ion under study is a very large unit, and it was hoped that the pure crystals would have a sufficiently large distance between neighbouring ions to give fully resolved spectra. In fact, this distance was found to be just not large enough since the fine structure lines were easily observed, but these had a line width of about 350 gauss, which obscured the underlying hyperfine structure. Accordingly all the experiments were carried out on crystals of the isomorphic Ni^{4+} compound containing a small amount of Mn^{4+}.

The most commonly studied d^3 system is Cr^{3+} although V^{2+} (2-4) has also been investigated. Unfortunately ^{53}Cr (the only isotope with nuclear spin) has a small nuclear moment and is only about 10% abundant in naturally occurring chromium, and these two factors have led to relatively few observations of its hyperfine structure. The most abundant isotopes of both Mn^{4+} and V^{2+} both have fairly large nuclear moments, and this leads to much easier observation of hyperfine structure. A description of the main features to be expected in the E.S.R. spectra of these d^3 systems will be useful.

A free d^3 ion has a ^4F ground state (10). In a complex with regular octahedral co-ordination, the angular momentum is "quenched" leading to a $^4A_{2g}$ (6) ground state, which is orbitally non-degenerate. Only one

line would be observable in the E.S.R. spectrum of such a complex, since the levels would be split by a magnetic field in a simple linear fashion as shown below in Fig. 1(a) and transitions occur between levels having M_S values differing by ± 1.

Figure 1

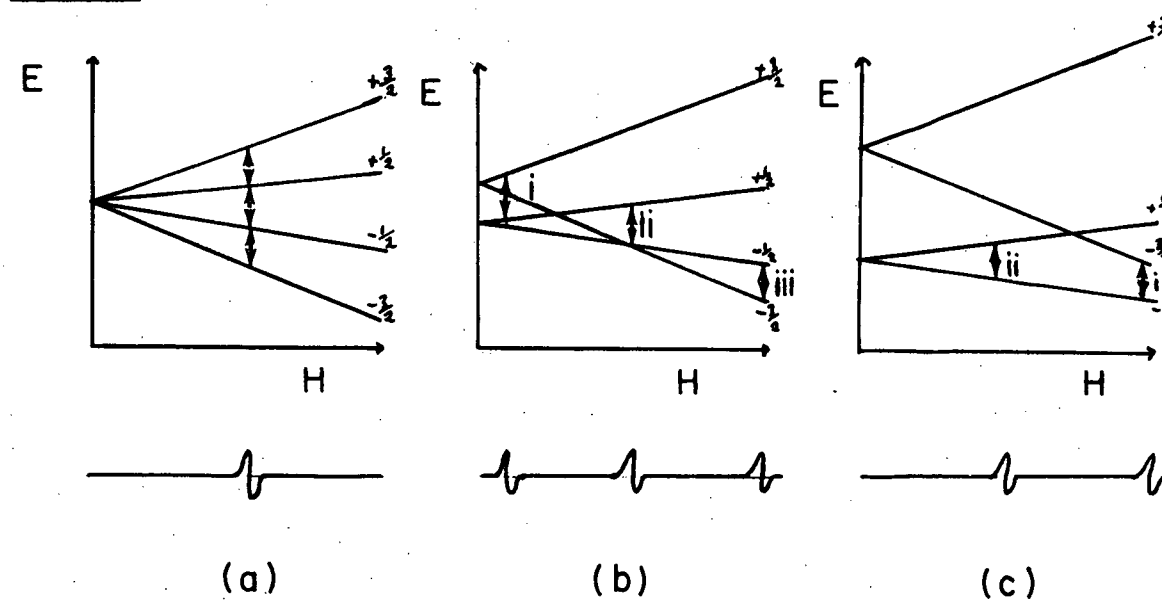

There is however, the possibility of distortion of the complex from the Jahn-Teller (24) effect, and also of spin-orbit coupling with higher levels. These two effects together lead to partial removal of the spin degeneracy, producing two doublets as predicted by Kramers (25) theorem; the energy separation being known as zero field splitting (Z.F.S.). This situation is shown in Fig. 1(b) and it can be seen that three lines are in general observable, if the Z.F.S. is small in magnitude. Large splittings lead to the situation in Fig. 1(c), where transition (i) of Fig. 1(b) is no longer possible with the available microwave quanta, and transition (iii) may be at too high a field to be observable; so only one transition (ii) is observed in general.

Figs. 1(b) and 1(c) are shown with the direction of the magnetic field parallel to the direction of distortion. For other orientations the

energy levels are curved, since the eigenstates are mixtures of the simple M_s functions. The zero field splitting of the Mn^{4+} complex described later is 1.722 cm^{-1}, and graphs of energy levels versus magnetic field for various orientations, using this value for the Z.F.S. are shown in Fig. 2. These were calculated by numerically diagonalizing the fine structure matrix given later (Equ. #18), for a series of values of the magnetic field, using chosen values of D, $g_{//}$ and $g_{\perp}$ (0.861 cm^{-1}, 1.992, 1.988 respectively).

The available microwave quantum was approximately 0.3 cm^{-1}, and so the transitions indicated were the only ones observed. The magnetic field was not strong enough to enable the possible transition at 20,000 gauss to be observed.

FIGURE 2 : Energy level diagram for a spin quartet in a magnetic field

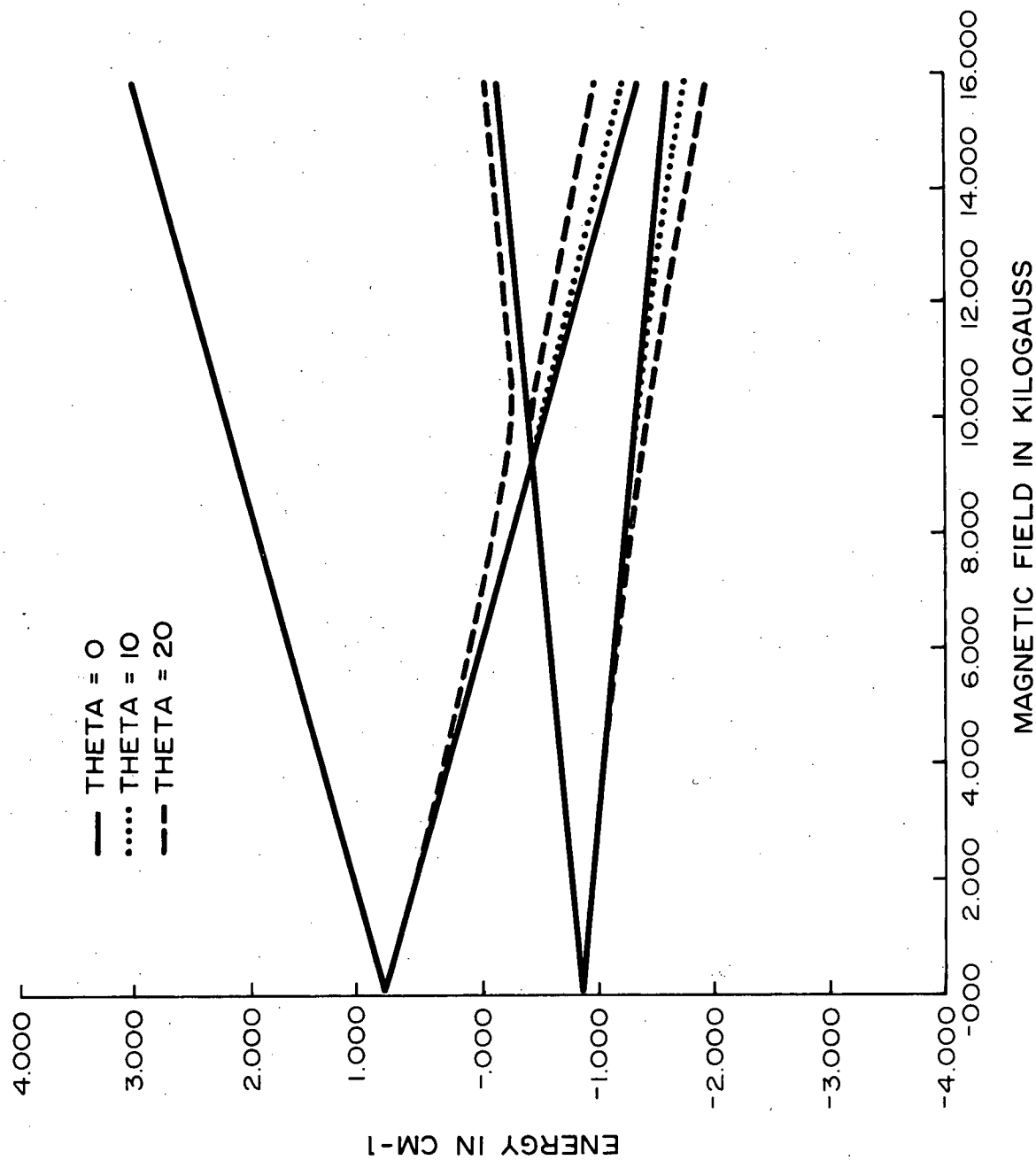

FIGURE 2A

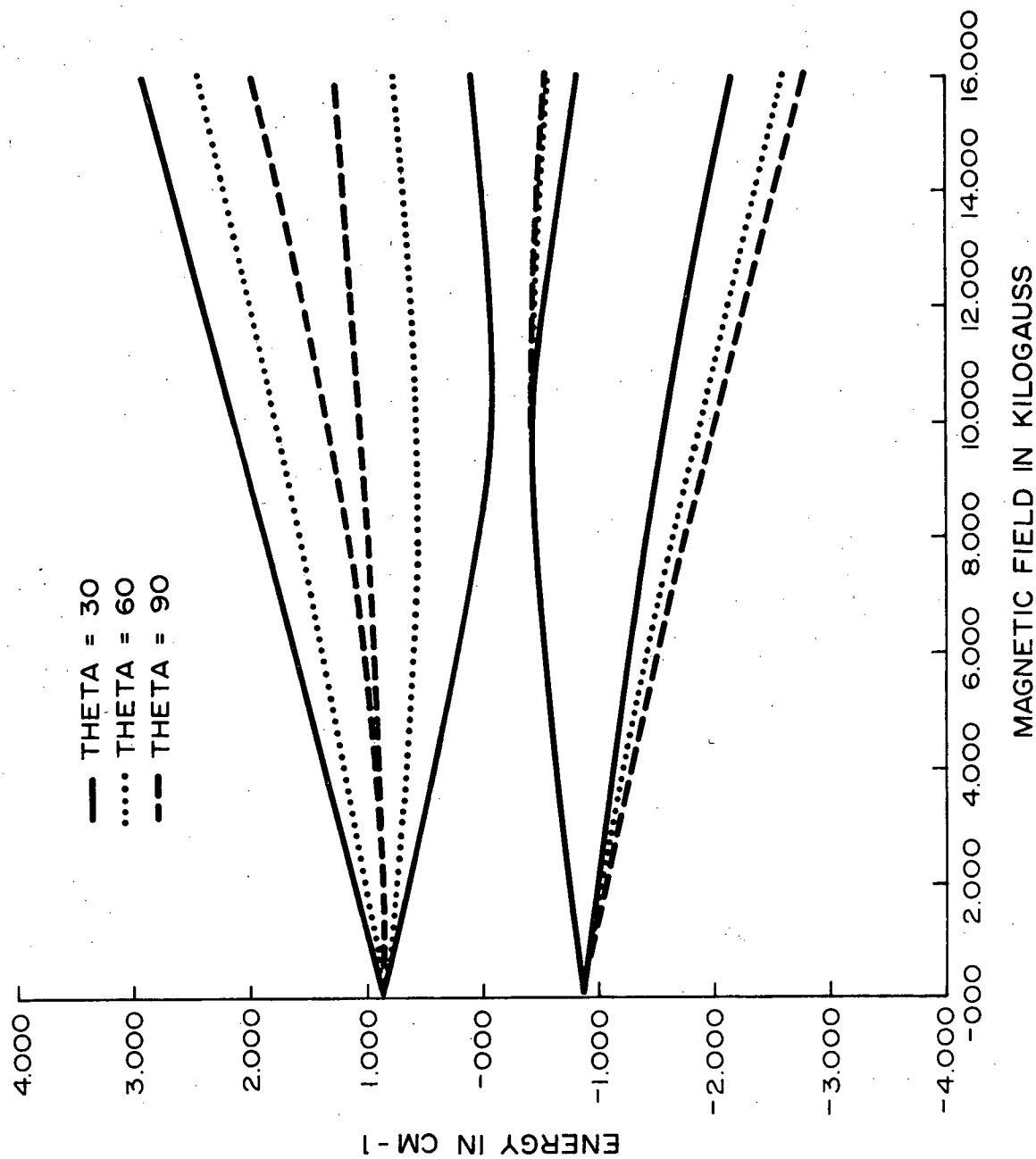
THETA = 30
THETA = 60
THETA = 90
4.000
3.000
2.000
1.000
-000
-1.000
-2.000
-3.000
-4.000
-000
2.000
4.000
6.000
8.000
10.000
12.000
14.000
16.000
ENERGY IN CM-1
MAGNETIC FIELD IN KILOGAUSS

2. Theoretical

The calculation of electronic energy levels for paramagnetic molecules in a magnetic field requires the consideration of a Hamiltonian of the form below, which includes magnetic as well as electric interactions.

$$\mathcal{H} = \mathcal{H}_o + \mathcal{H}_1 + \mathcal{H}_2$$

where $\mathcal{H}_o = -(\hbar^2/2m)\sum_i^n \nabla_i^2 + \phi$

ϕ being the total electrostatic potential.

$$\mathcal{H}_1 = \mathcal{H}_{zs} + \mathcal{H}_{zo} + \mathcal{H}_{zI} + \mathcal{H}_{ss} + \mathcal{H}_{ls} + \mathcal{H}_{l's} + \mathcal{H}_{sI} + \mathcal{H}_{lI} + \mathcal{H}_Q$$

and $\mathcal{H}_2 = \mathcal{H}_{ll} + \mathcal{H}_{cs} + \mathcal{H}_{II}$ ...(1)

The nine terms in $\mathcal{H}_1$ are given in approximate decreasing order of magnitude, and their explicit forms are given below.

A. Zeeman Interactions

The interactions with a magnetic field of electron and nuclear spin magnetic moments can be written as

$$\mathcal{H}_{zs} + \mathcal{H}_{zI} = g_e \beta_e \underline{H} \cdot \sum_i^n \underline{s}_i - \beta_N \underline{H} \cdot \sum_k^N g_{Nk}\, \underline{I}_k \qquad \ldots(2)$$

where the sums run over the number of electrons (n) and nuclei (N). There is a similar interaction between a magnetic field and the electrons' orbital magnetic moment which is of the form (6)

$$\mathcal{H}_{zo} = \frac{e}{mc} \sum_i^n (\underline{p}_i \cdot \underline{A}_i) + \frac{e^2}{2mc^2} \sum_i^n \underline{A}_i^2 \qquad \ldots(3)$$

where $\underline{p}_i$ is the linear momentum operator and $\underline{A}_i$ is the vector potential of the magnetic field. For a constant magnetic field $\underline{A}_i = \frac{1}{2}\underline{H} \times \underline{r}_i$ where $\underline{r}_i$ is the position vector of the i-th electron, and thus

$$\mathcal{H}_{zo} = \beta_e \underline{H} \cdot \sum_i^n (\underline{r}_i \times \underline{p}_i) + \underline{H} \cdot \sum_i^n \frac{e^2}{8mc^2} (r_i^2 \underline{\underline{U}} - \underline{r}_i \underline{r}_i) \cdot \underline{H}$$

where $\underline{\underline{U}}$ is the unit dyadic

$$\sim \beta_e \underline{H} \cdot \sum_i^n \underline{1}_i \qquad \ldots(4)$$

The last term is very small and is neglected since it is the same for all energy levels and thus contributes nothing to E.S.R. However,

it is important when calculating diamagnetic susceptibilities. The form given for $\mathcal{H}_{zo}$ is correct only for systems having a well-defined axis, or centre, about which angular momenta can be calculated.

B. Spin-Orbit Coupling

According to the special theory of relativity an electron moving in an electric field "feels" part of this field as magnetic, and the interaction of the magnetic moment of the electron with this magnetic field gives rise to the phenomenon of spin-orbit coupling. It may be shown (6) using Dirac's theory that the contribution to the Hamiltonian is

$$\mathcal{H}_{ls} = \frac{-e}{2m^2c^2r}\frac{dA_o}{dr}\,\underline{l}.\underline{s} = \xi(r)\,\underline{l}.\underline{s} \qquad \ldots(5)$$

for one electron in a central field, A_o being the electrostatic potential of that field. For a nucleus of charge Ze then A_o is Ze/r and thus $\mathcal{H}_{ls}$ is positive since $\frac{dA_o}{dr}$ will be negative. To generalise this for a system of n electrons, including electron repulsion, two approximations are used. Each electron is considered to obey the same formula, and then a summation is carried out over the total number of electrons. Also since $\xi(r)$ varies as $\frac{1}{r^3}$ it is assumed that most of the contribution to $\mathcal{H}_{ls}$ comes from regions close to the nucleus, where the electric field should be nearly spherical. Thus

$$\mathcal{H}_{ls} = \sum_{i}^{n}\sum_{k}^{N} \xi_k(r_{ki})\,\underline{l}_{ki}\cdot\underline{s}_i \qquad \ldots(6)$$

where the potential in which the electron moves is given by

$$A_o = \sum_{k}^{N}\frac{Z_k e}{r_{ki}} - \sum_{i\neq j}\frac{e}{r_{ij}}$$

It is conventional to set the radial integral

$$\int R_{nl}^2\,\xi(r).r^2dr$$

equal to $\hbar^{-2}\zeta_{nl}$ where ζ_{nl} is called the spin orbit constant for a

nl orbital.

A very small contribution to $\mathcal{H}_{ls}$ comes from the electron - other orbit interaction, where the electron's magnetic moment interacts with the magnetic field set up by the orbital motions of other electrons besides itself. This may be written as (26)

$$\mathcal{H}_{l's} = \frac{-e^2h}{2mc^2} \sum_{i>j} \frac{1}{r_{ij}^3} \underline{s}_i \cdot (\underline{r}_{ij} \times \underline{p}_j) \qquad \ldots(7)$$

C. Electron-Electron Dipolar Interaction

This is the straightforward interaction of two magnetic dipoles a distance r_{ij} apart, and is given by

$$\mathcal{H}_{ss} = g_e^2 \beta_e^2 \sum_{i\ j} \underline{s}_i \cdot (r_{ij}^2 \underline{\underline{U}} - 3\underline{r}_i \underline{r}_j) r_{ij}^{-5} \cdot \underline{s}_j \qquad \ldots(8)$$

D. Electron Spin-Nuclear Spin Interaction

Since there exists a finite probability of finding the electron at the nucleus, at least for s-electrons, then this produces a singularity which must be considered when writing the form for this interaction. The explicit formula is

$$\mathcal{H}_{sI} = g_e g_N \beta_e \beta_N \sum_{i,k} \underline{s}_i \cdot \{ [r_{ik}^2 \underline{\underline{U}} - 3\underline{r}_{ik} \underline{r}_{ik}] r_{ik}^{-5} - \frac{8\pi}{3} \delta(\underline{r}_{ik}) \} \cdot \underline{I}_k \qquad \ldots(9)$$

The first term is correct for p, d and f electrons, which all have zero probability of being at the nucleus and has the same form as $\mathcal{H}_{ss}$ since electrons also do not coexist at the same point. The second term is due to Fermi (27) and is a first-order approximation which gives the same matrix elements as the terms arising from Dirac's equation. It is called the contact term by convention.

E. Nuclear Spin-Electron Orbit Interaction

$$\mathcal{H}_{lI} = g_e g_N \beta_e \beta_N \sum_{i,k} (\underline{l}_{ik} \cdot \underline{I}_k) r_{ik}^{-3} \qquad \ldots(10)$$

This term has to be considered sometimes (28) since it can give, in

conjunction with spin-orbit coupling, a second order contribution to the hyperfine interaction conventionally called "pseudo-dipolar" hyperfine interaction.

F. Nuclear Quadrupole Interaction

This is often a very small term whose main effect is to increase the transition probability of "spin-forbidden" lines in E.S.R. spectra. The explicit form is

$$\mathcal{H}_Q = \sum_{i,k}^{n,N} \left\{ \frac{e^2 Q_k}{2I_k(I_k-1)} \left[\underline{I}_k \cdot (r_{ik}^2 \underline{\underline{U}} - 3\underline{r}_{ik}\underline{r}_{ik}) r_{ik}^{-5} \cdot \underline{I}_k \right] \right\} \qquad \ldots(11)$$

G. Smaller Interactions

The three terms in $\mathcal{H}_2$ namely, orbit-orbit interaction, nuclear chemical shift and nuclear spin-nuclear spin dipole interactions are all very small. It has never been necessary to include them to account for observed E.S.R. spectra since experimental accuracy would need to be improved by several orders of magnitude for them to be detectable.

When written in the form given above the general Hamiltonian is not readily applicable to the interpretation of experimental results. In general, it is found convenient first to describe these results with a Hamiltonian involving only electron-spin and nuclear-spin operators, known as a "spin-Hamiltonian", which is not necessarily uniquely defined for any given system.

The idea of a spin Hamiltonian was suggested and developed by Abragam and Pryce (29,30) and has recently been treated in a more general fashion by Koster and Statz (31).

The simple Zeeman effect is represented by operators $\mathcal{H}_{zo}$ and $\mathcal{H}_{zs}$ above and is

$$\beta_e \underline{H} \cdot \left(\sum_i \underline{l}_i + g_e \sum_i \underline{s}_i \right) \qquad \ldots(12)$$

whereas in the spin Hamiltonian this is written as

$$\beta_e \underline{H} \cdot \underline{\underline{g}} \cdot \underline{s} \qquad \ldots(13)$$

where $\underline{\underline{g}}$ is a second rank tensor and implicitly includes the orbital contributions to the Zeeman term. The derivation is shown clearly by Pryce (30) and involves calculating spin orbit coupling effects with second order perturbation theory and comparing matrix elements of (Equ. #12 and #13).

Kramers' theorem (25) states that odd electron systems will have spin multiplicity in the ground state of at least 2, which can only be removed by a magnetic field. This result, together with the Jahn-Teller theorem (24), ensures that ground states of non-linear molecules will be orbitally non-degenerate with a maximum spin degeneracy of 2 in the case of odd electron systems.

These lowest doublets are not pure spin states owing to the effects of spin-orbit coupling. It is just this orbital contribution which causes $\underline{\underline{g}}$ to vary with direction in a crystal and to deviate from the free-electron value. These deviations are most noticeable for metal complexes, spin-orbit coupling in organic radicals being very small for atoms of the first period. Since the excited states above the orbitally non degenerate ground state may be only a few hundred cm^{-1} away in metal complexes, then $\underline{\underline{g}}$ can deviate very considerably from 2.00232.

A general spin Hamiltonian for one nuclear spin may be written as

$$\beta_e \, \underline{H} \cdot \underline{\underline{g}} \cdot \underline{s} + \underline{s} \cdot \underline{\underline{D}} \cdot \underline{s} + \underline{s} \cdot \underline{\underline{A}} \cdot \underline{I} - g_N \beta_N \underline{H} \cdot \underline{I} + \underline{I} \cdot \underline{\underline{P}} \cdot \underline{I} \qquad \ldots(14)$$

The tensor $\underline{\underline{D}}$ arises from one of two terms in Equ. #1. The straightforward dipolar term $\mathcal{H}_{ss}$ or a second order spin orbit coupling term from $\mathcal{H}_{ls}$ can contribute to $\underline{\underline{D}}$. For organic triplets the dipolar term is of primary importance whereas for transition metal complexes this is usually less than 5% of the total (32). The axis systems in which $\underline{\underline{g}}$ and $\underline{\underline{D}}$ are

diagonal may be different. In organic triplets, because of the two different interactions leading to $\underline{\underline{g}}$ and $\underline{\underline{D}}$; and in some metal complexes where a triplet interaction is observed along a metal-metal bond (33).

The hyperfine tensor A arises in a similar manner from at least two different terms. It may or may not (34) be parallel to the $\underline{\underline{g}}$ or $\underline{\underline{D}}$ tensors. $\underline{\underline{A}}$ comes from term $\mathcal{H}_{sI}$ in Equ. #1 and also as a "pseudo-dipolar hyperfine interaction" (35) from perturbation interactions of $\mathcal{H}_{1's}$ and $\mathcal{H}_{1I}$.

The quadrupolar interaction P may be parallel to the hyperfine tensor A if term $\mathcal{H}_{sI}$ is the primary contribution to the latter or in some general direction determined by the local electric fields in the molecule.

For systems with $\underline{S}$ greater than 1/2 it may be necessary to carry this perturbation derivation of the spin Hamiltonian to higher orders. Bleaney (36) has shown that Equ. #2 is always sufficient for S = 1, but for S = 3/2 and higher, a term in $(\underline{S})^3\underline{H}$ is allowed and for S = 2 and greater, terms in $\underline{S}^4$ are allowed. The coefficient of these higher order terms may well be negligibly small in many cases, but $\underline{S}^4$ terms have been necessary for most S-state ions (37).

In general, the tensors $\underline{\underline{g}}$, $\underline{\underline{A}}$, $\underline{\underline{D}}$ and $\underline{\underline{P}}$ have six components (g_{xx}, $g_{xy} = g_{yx}$, ... g_{zz}), but for an axially symmetric system with $\underline{\underline{g}}$, $\underline{\underline{D}}$ and $\underline{\underline{A}}$ all coaxial we can write in the principal axis co-ordinate system,

$$\mathcal{H} = \beta_e(g_{\parallel}S_zH_z + g_{\perp}(S_xH_x + S_yH_y)) + D(S_z^2 - 1/3\ S(S+1)) + A_{\parallel}S_zI_z + A_{\perp}(S_xI_x + S_yI_y) + P(I_z^2 - 1/3\ I(I+1)) \quad \ldots(15)$$

This Hamiltonian represents the Mn^{4+} complex in this work with P = 0 within the limits of the experiments.

3. Sample, Preparation and Structure

Ammonium 9-Molybdomanganate $(NH_4)_6MnMo_9O_{32}.8H_2O$

This salt was readily prepared by the method of Friedheim and Samuelson (76) and a good yield of bright orange-red rhombohedral crystals were obtained. The isomorphous, diamagnetic nickel^{4+} salt was prepared by the same method and mixed crystals of the two salts prepared by slow aqueous evaporation. The ratio Ni:Mn was 16:1 and in view of the very large size of the heteropoly anion was sufficient to remove dipolar effects from neighbouring paramagnetic centres.

The structure was determined by Waugh et al. (77) and the crystal belongs to the D_3^7 - R32 space group. Only one formula unit exists per unit cell and the structure is shown in Fig. 3. The point group of the complex ion is D_3 (differing from D_{3d} in having no reflexion planes).

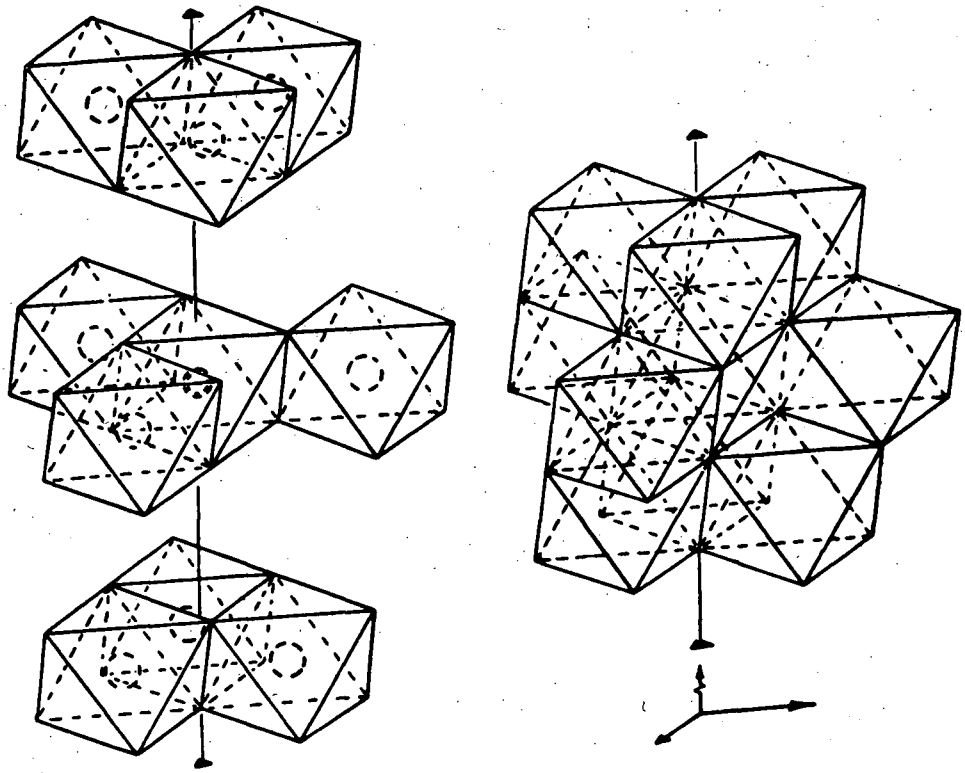

Figure 3 : Diagram of molecular structure of ammonium 9-molybdomanganate. Oxygen atoms occupy positions at the vertices of the octahedra, and molybdenum atoms the centres of these octahedra marked with a single broken circle. The sole manganese atom is at the mid-point of the central octahedron, and is marked with a double broken circle. The left view is exploded along the trigonal axis for clarity.

4. Experimental Methods and Results

A standard 9.5MHz E.S.R. spectrometer was used for all measurements. A schematic diagram is given in Fig. 4. The magnet was a Varian model V-3927-3 with 12" pole tips and a gap of 2 3/4" controlled by a VFR 2501 Fieldial Mk. II. A V-3921-3 rotating base was used in conjunction with a V.4533 cylindrical cavity. A maximum field of 12,200 gauss was obtainable with the above equipment, and for the very high field measurements at about 15,000 gauss the sample was transferred to a similar spectrometer with a V.3600 magnet. The microwave frequency was measured with a Hewlett-Packard 5246L Frequency Counter, using a 5256A Plug-In attachment and the Fieldial was calibrated with an N.M.R. probe and magnetometer constructed by the Electronics Group, Department of Chemistry, U.B.C.

The crystal was mounted in a sample holder supplied by Magna Devices which enabled the crystal to be rotated in the vertical plane, whilst situated in the cavity. Very precise alignment of the crystal was then possible in the magnetic field.

A typical crystal is shown in Fig. 5 and the axis system used throughout is shown. In the case of the Mn^{4+} molybdate the crystal axes are coincident with the molecular axes.

The graphs of energy levels versus magnetic field shown in Fig. 2 indicate the possible field for transitions to occur given the selection rule $\Delta M_s = \pm 1$. A typical spectrum is shown in Fig. 6. This is the $'|+\tfrac{1}{2}\rangle' - '|-\tfrac{1}{2}\rangle'$ transition for $\theta = 30^{\circ}$ (where the states are labelled in the zero field notation), and the six hyperfine lines due to the 5/2 spin of the ^{55}Mn nucleus are very easily distinguished. The small lines in the wings and between the hyperfine components are probably due to super-hyperfine effects from the surrounding Mo nuclei and

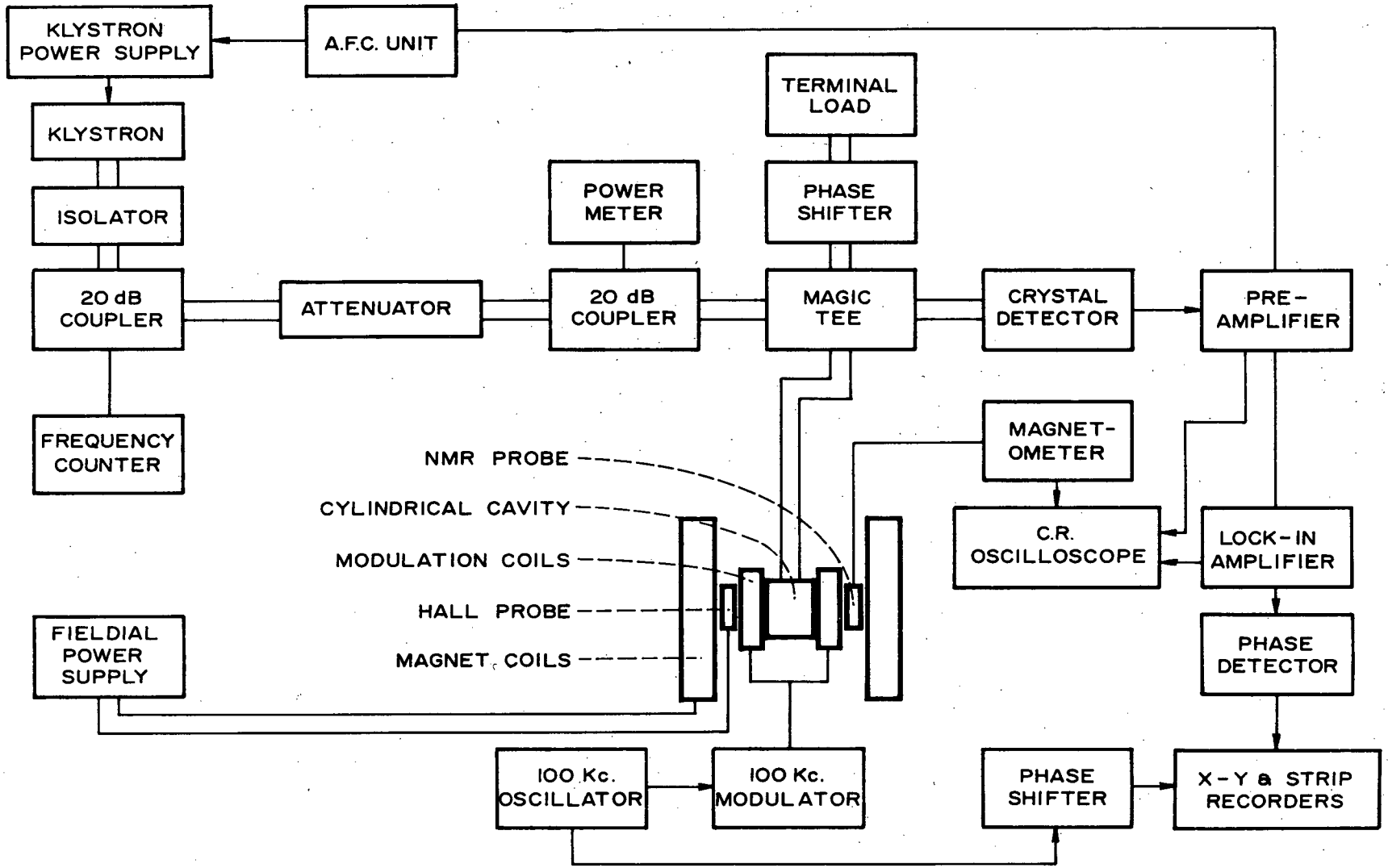

Figure 4

Block diagram of 100 kc. E.S.R. Spectrometer

FIGURE 5 : A typical crystal of ammonium 9-molybdomanganate

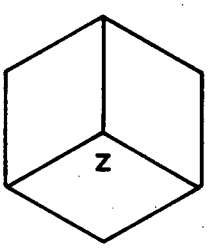

Plan

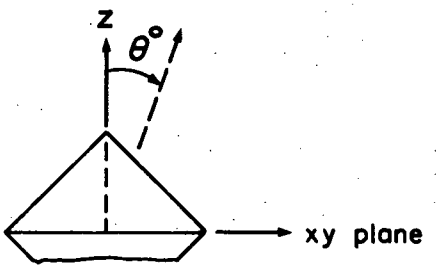

Side Elevation

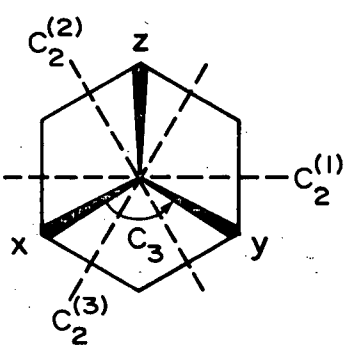

Coordinate axis for orbital manifold ($z \equiv$ 4 fold axis of octahedron)

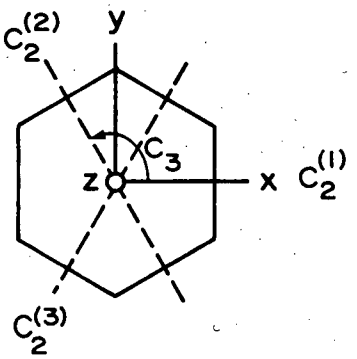

Coordinate axis for spin manifold ($z \equiv$ 3 fold axis of octahedron)

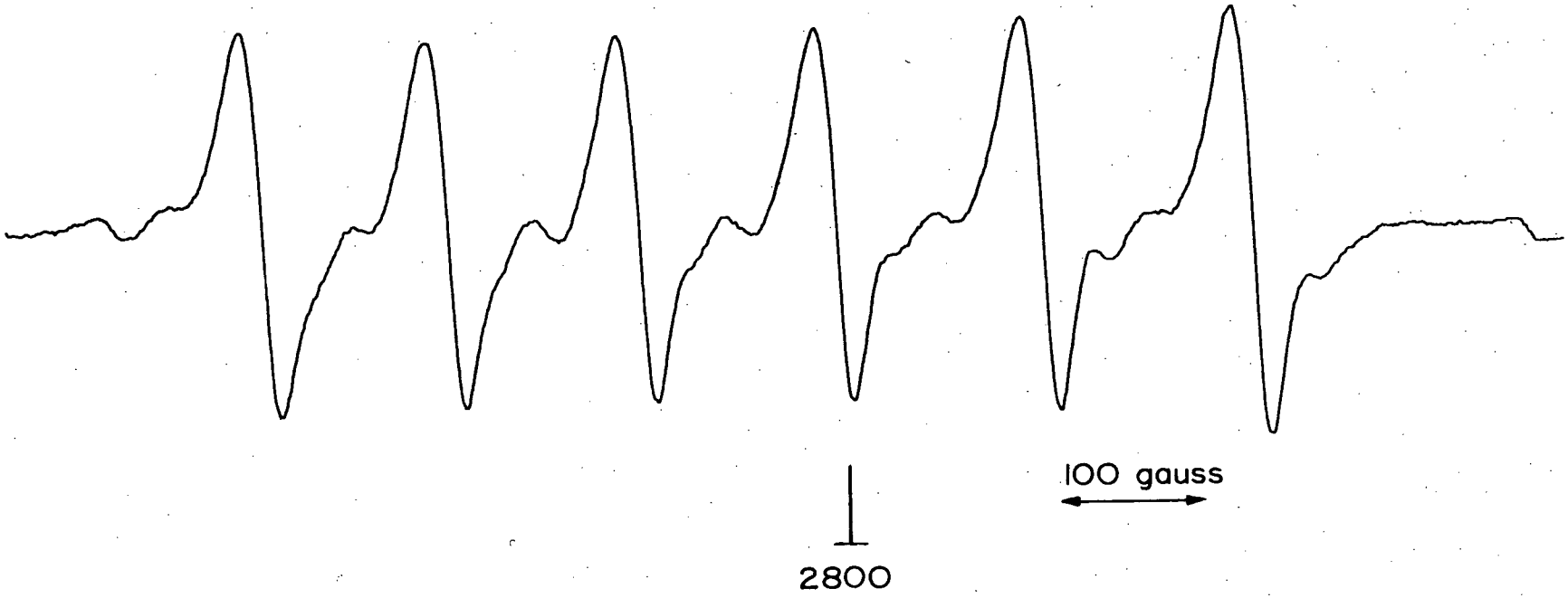

FIGURE 6 : A typical spectrum of the $\langle -\frac{1}{2} | - | +\frac{1}{2} \rangle$ transition ($\theta = 30^{o}$), for a magnetically dilute single crystal of ammonium 9-molybdomanganate

this possibility is discussed later.

Similar spectra were taken every 10^{o} around all three axes and these showed the crystal to be axially symmetric within experimental error. Use of the vertical rotation property of the Magna Devices crystal holder, in conjunction with the rotating magnet now made it possible to align the crystal very precisely in the magnetic field. As can be seen from Fig. 2 the $|+\frac{1}{2}\rangle$ - $|-\frac{1}{2}\rangle$ transition occurs at its highest field when the molecular axis is parallel to the magnetic field, and this was the criterion used in aligning the crystal.

The accuracy of this alignment was estimated to be 0.25^{o} from the mean of several attempts. With the crystal accurately aligned with the magnetic field, then because of the strictly axial symmetry, accurate spectra were obtainable at every 5^{o} from the z-axis to the x-y plane, simply by rotating the magnet through the required angle.

The '$|+\frac{1}{2}\rangle$ ' - '$|-\frac{1}{2}\rangle$' transition is the only one observable at all orientations with the available x-band microwave quantum. The variation of the position of this line with orientation provided the data from which most of the spin-Hamiltonian parameters could be established. The value of D is however, not found from this data, since the positions of the transitions are very insensitive to the actual size of the zero field splitting, when this is larger than the microwave quantum.

Since the rotating magnet was restricted to about 12 kilogauss, and no other transitions except the $|+\frac{1}{2}\rangle$ - $|-\frac{1}{2}\rangle$ were observed for $\theta=0^{o}$, it was decided to mount the crystal in a non-rotating magnet which could reach somewhat more than 15 kilogauss. After realigning the crystal by the method described above, a transition was luckily observed at around 15,000 gauss and was ascribed to the $|-\frac{1}{2}\rangle$ -$|-3/2\rangle$

transition (see Fig. 2). This enabled D to be calculated with certainty

For $\theta = 0^o$ $\quad E(|+\tfrac{1}{2}\rangle) = -D + \tfrac{1}{2}g_{\parallel}\beta_e H$

$\quad E(|-\tfrac{1}{2}\rangle) = -D - \tfrac{1}{2}g_{\parallel}\beta_e H$

$\quad E(|-3/2\rangle) = +D - 3/2\ g_{\parallel}\beta_e H$

Then $\quad E(|-3/2\rangle) - E(|-\tfrac{1}{2}\rangle) = 2D - g_{\parallel}\beta_e H_1$

$= h\nu$

And $\quad E(|+\tfrac{1}{2}\rangle) - E(|-\tfrac{1}{2}\rangle) = g_{\parallel}\beta_e H_2$

$= h\nu$

Whence D, knowing $g_{\parallel}$, H_1, H_2 and $h\nu$

Since the horizontal rotation in this experiment was measured by a small 6" diameter protractor the accuracy of alignment was not as great as with the rotating magnet and thus D has a rather larger experimental error than the other measured parameters. As the magnetic field is moved away from the molecular axis, the $|-\tfrac{1}{2}\rangle$ - $|-3/2\rangle$ transition occurs at an increased magnetic field, and since the magnet only just covered the $\theta = 0^o$ transition, it was not possible to observe it for any other angle.

At angles near to $\theta = 0^o$ the $|+\tfrac{1}{2}\rangle$ & $|-3/2\rangle$ states have energy curves which make transitions between them possible at two values of the magnetic field. These transitions have zero transition moment at 0^o, and are weakly allowed (23) for $\theta \neq 0^o$ due to mixing of the basis M_s states by the magnetic field, as is indicated by the curvature of the energy levels in Fig. 2, for angles other than $\theta = 0^o$. At about $\theta = 30^o$ the energy separation is greater than the available microwave quantum and so transitions are not obtainable. Weak transitions were observed in the 7000 g and 11,000 g regions for values of θ up to 25^o; these

lines were very weak and the hyperfine structure was not easily interpreted due to the low signal to noise ratio. A typical spectrum for this transition ($\theta = 15^{o}$) is shown in Fig. 7.

Weak transitions are also possible (38) at angles near 90^{o} between the upper two energy levels in Fig. 2. The transition moment decreases from a maximum at 90^{o} to zero at $\theta = 0^{o}$ and in fact this line could only be observed for $\theta = 90^{o}$ and this spectrum is shown in Fig. 8.

This discussion has assumed the $\pm\frac{1}{2}$ states to lie lower than the $\pm 3/2$ states, and the graphs in Fig. 2 were drawn on this assumption (i.e. D is positive). For a negative D value the labels of the states would be changed, although the E.S.R. spectra would be unchanged.

All the observed fine structure transitions are plotted in Fig. 9 as open circles, and the continuous line indicates the theoretical positions in the regions where transitions were observed and the dotted line, the regions where the transition probability is not zero but too small to observe signals.

The spin Hamiltonian

$$\mathcal{H} = \beta_e (g_{\parallel} S_z H \cos\theta + g_{\perp} S H \sin\theta) + D(S_z^2 - 1/3\ S^2) + A_{\parallel} S_z I_z + A_{\perp}(S_x I_x + S_y I_y) \quad \ldots(16)$$

was found to reproduce the experimental results well when used in a basis of $|M_s\ M_I\rangle$ product functions with S = 3/2 and I = 5/2.

Because of the complex inter-relationship between the five parameters, it is not trivial to extract them from a given set of experimental data. Bleaney (39) has given a set of equations describing the field positions, using D and A as perturbations, and accurate to second order in both.

These equations are not applicable to systems with $D > g\beta_e H$, and so a different approach was taken. We may write Equ. #16 as

$$\mathcal{H} = \mathcal{H}_o + \mathcal{H}_1 + \mathcal{H}_2 \quad \ldots(17)$$

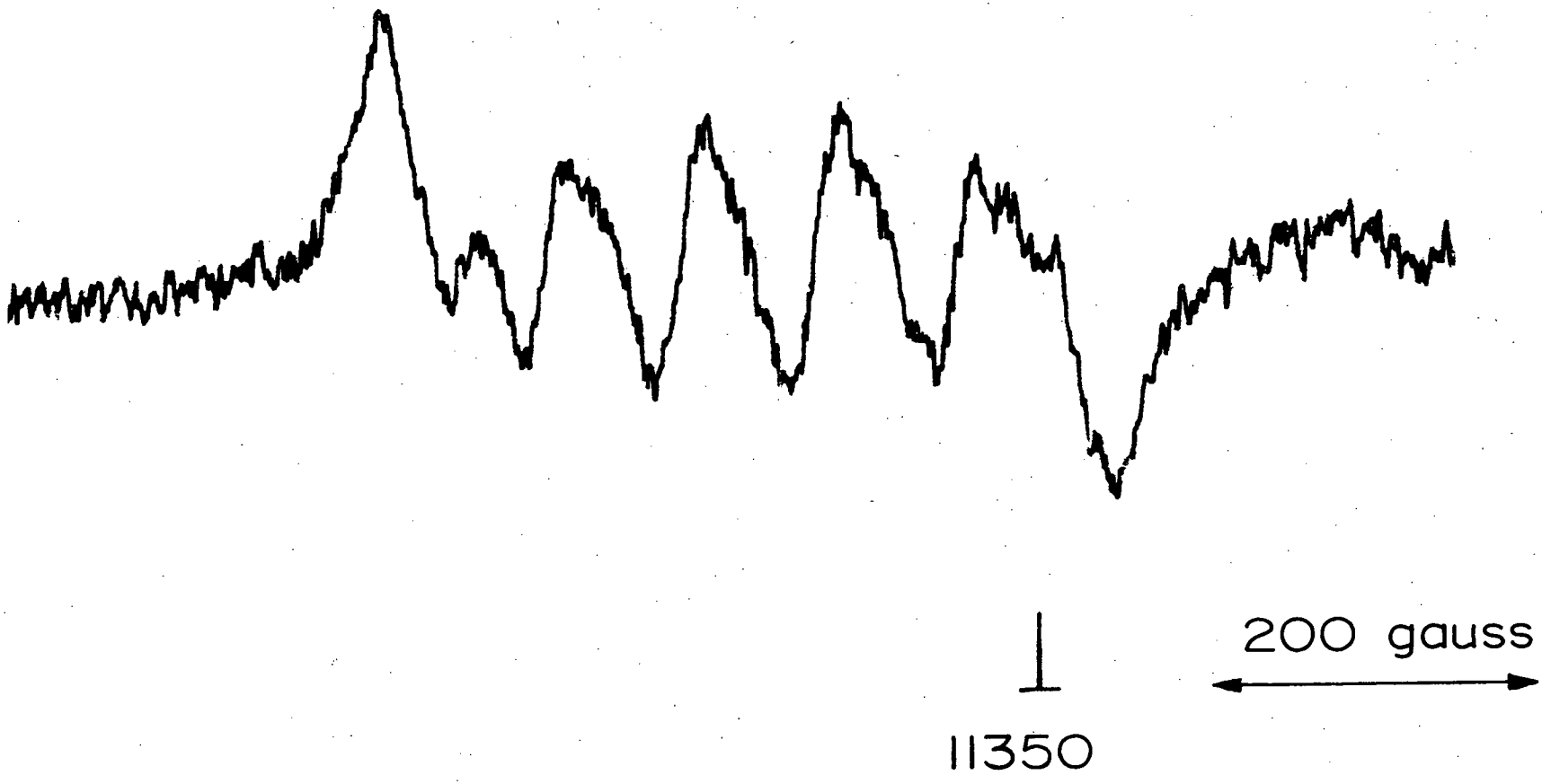

FIGURE 7 : A typical spin-forbidden transition (θ = 15°), for a magnetically dilute single crystal of ammonium 9-molybdomanganate

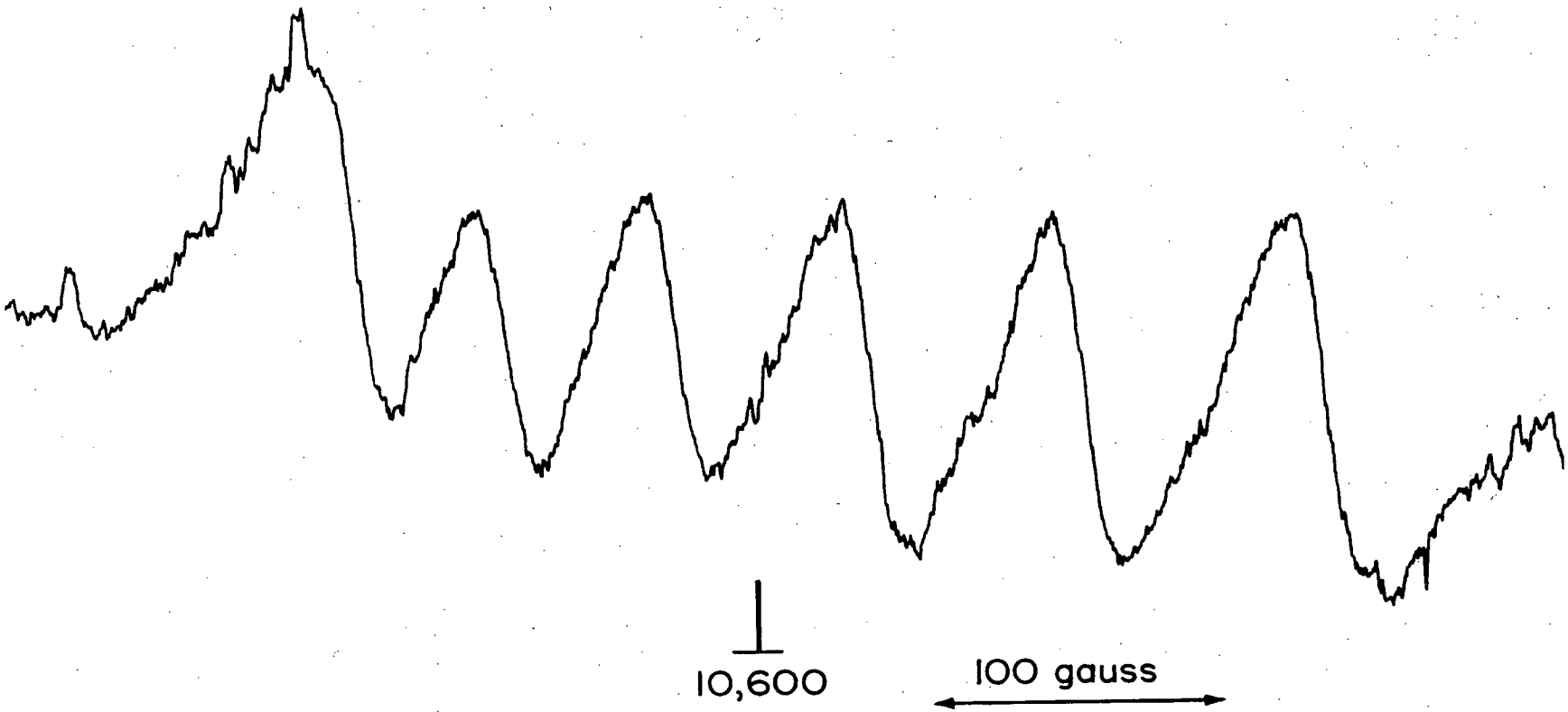

FIGURE 8 : The spin-forbidden transition observed at $\theta = 90^{o}$, for a magnetically dilute single crystal of ammonium 9-molybdomanganate

FIGURE 9 : The observed fine structure transitions

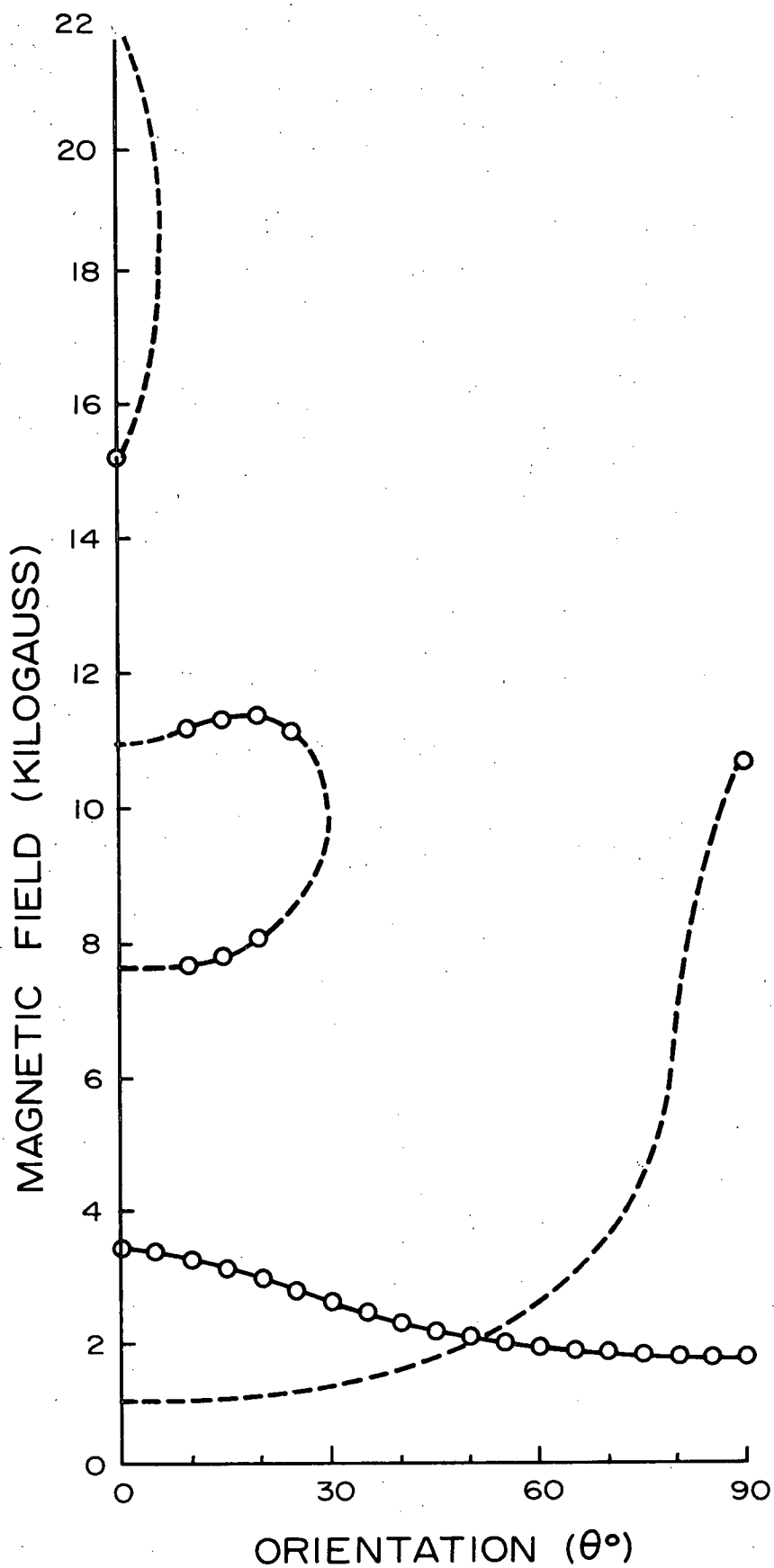

where $\mathcal{H}_o = D(S_z^2 - 1/3\ \underline{S}^2)$

$\mathcal{H}_1 = H\beta_e(g_{\parallel}S_z\cos\theta + g_{\perp}S_{\perp}\sin\theta)$

$\mathcal{H}_2 = A_{\parallel}S_zI_z + A_{\perp}(S_xI_x + S_yI_y)$ ...(18)

$\mathcal{H}_1$ can now be considered as the perturbing Hamiltonian with the magnetic field as a perturbation parameter. Expressed in matrix form in the $|M_s\rangle$ basis we have

$$\mathcal{H}_o = \begin{array}{c} \begin{matrix} -\frac{1}{2} & +\frac{1}{2} & -3/2 & +3/2 \end{matrix} \\ \begin{pmatrix} -D & & & \\ & -D & & \\ & & +D & \\ & & & +D \end{pmatrix} \end{array}$$

and

$$\mathcal{H}_1 = \beta_e H \begin{array}{c} \begin{matrix} -\frac{1}{2} & +\frac{1}{2} & -3/2 & +3/2 \end{matrix} \\ \begin{pmatrix} -A & 2B & \sqrt{3}B & 0 \\ 2B & A & 0 & \sqrt{3}B \\ \sqrt{3}B & 0 & -3A & 0 \\ 0 & \sqrt{3}B & 0 & 3A \end{pmatrix} \end{array}$$

where

$A = \frac{1}{2}g_{\parallel}\cos\theta$

$B = \frac{1}{2}g_{\perp}\sin\theta$

A general introduction to perturbation theory is given in Appendix I, and from this we see that since $\mathcal{H}_o$ contains two pairs of degenerate levels, $\mathcal{H}_1$ must be partially diagonalised in the 2 x 2 diagonal blocks before carrying out the perturbation, in order to find the correct zeroth order wave functions.

A perturbation treatment was then carried out on each of the basis states in turn and the resulting energies and wave functions expressed as polynomials in the perturbation parameter H. This was done to third order in the wave functions and seventh order in energy. A difference polynomial in H was then constructed for any two chosen energies, and, with the correct field independent term, a root of this polynomial was

found by an extended Newton-Raphson (40) procedure. In order to do this numerically, initial rough values of D, $g_{//}$ and $g_{\perp}$ were chosen from the experimental data. For example:

$|-\tfrac{1}{2}\rangle - |+\tfrac{1}{2}\rangle$ transition

$$\langle -\tfrac{1}{2}'|\,\mathcal{H}_1\,|-\tfrac{1}{2}'\rangle = F_1(H) = a_1H + a_2H^2 + \ldots + a_7H^7$$

$$\langle +\tfrac{1}{2}'|\,\mathcal{H}_1\,|+\tfrac{1}{2}'\rangle = F_2(H) = b_1H + b_2H^2 + \ldots + b_7H^7 \qquad \ldots(19)$$

where the primes indicate perturbed wave functions. The field independent (zeroth order) term of the difference polynomial is then

$$\Delta E_o = \langle +\tfrac{1}{2}|\,\mathcal{H}_o\,|+\tfrac{1}{2}\rangle - \langle -\tfrac{1}{2}|\,\mathcal{H}_o\,|-\tfrac{1}{2}\rangle - h\nu \qquad \ldots(20)$$

where $h\nu$ is the microwave energy.

Thus, we have for the difference polynomial

$$\Delta E(H) = \Delta E_o + F_2(H) - F_1(H) = 0$$

$$= \Delta E_o + H(b_1 - a_1) + H^2(b_2 - a_2) + \ldots + H^7(b_7 - a_7) \qquad \ldots(21)$$

and this can be solved for $H_{transition}$ by the Newton-Raphson method, provided a first guess at $H_{transition}$ is supplied. Correct wave functions at this transition field are found by using the previous wave function polynomials and this new value for $H_{transition}$.

The Hamiltonian $\mathcal{H}_o + \mathcal{H}_1$ was then treated as solved, with eigenvalues and eigenstates obtained in the above manner. We have next to consider the perturbation of these solutions by $\mathcal{H}_2$. Up to now all calculations have been done in the $|M_s\rangle$ basis, i.e. assuming no hyperfine effects. In order to include these effects calculations must be done from now on in the complete $|M_sM_I\rangle$ basis.

When expressed in this basis we have for $\underline{S}.\underline{\underline{A}}.\underline{I}$ the matrix shown in Table 1. However, to express this in the basis $|M_s'M_I\rangle$ where the $|M_s'\rangle$ are the solutions of $\mathcal{H}_o + \mathcal{H}_1$ we need to transform the matrix by the correct unitary transformation, which was obtained from the first

TABLE 1 : Matrix of the operator $\underline{S}.\underline{\underline{A}}.\underline{I}$ in the basis $M_S M_I$ with $S = 3/2$ and $I = 5/2$

M_S	M_I	5/2	3/2	1/2	-1/2	-3/2	-5/2
3/2	5/2	$\frac{15A}{4}$	$\sqrt{15}B/2$				
	3/2	$\frac{9A}{4}$	$\sqrt{6}B$				
	1/2	$\frac{3A}{4}$	$3\sqrt{3}B/2$				
	-1/2	$-\frac{3A}{4}$	$\sqrt{6}B$				
	-3/2	$-\frac{9A}{4}$	$\sqrt{15}B/2$				
	-5/2	$-\frac{15A}{4}$					
1/2	5/2	$\sqrt{15}B/2$	$\frac{5A}{4}$	$\sqrt{5}B$			
	3/2	$\sqrt{6}B$	$\frac{3A}{4}$	$2\sqrt{2}B$			
	1/2	$3\sqrt{3}B/2$	$\frac{A}{4}$	3B			
	-1/2	$\sqrt{6}B$	$-\frac{A}{4}$	$2\sqrt{2}B$			
	-3/2	$\sqrt{15}B/2$	$-\frac{3A}{4}$	$\sqrt{5}B$			
	-5/2		$-\frac{5A}{4}$				
-1/2	5/2		$\sqrt{5}B$	$-\frac{5A}{4}$			
	3/2		$2\sqrt{2}B$	$-\frac{3A}{4}$			
	1/2		3B	$-\frac{A}{4}$			
	-1/2		$2\sqrt{2}B$	$\frac{A}{4}$			
	-3/2		$\sqrt{5}B$	$\frac{3A}{4}$			
	-5/2			$\frac{5A}{4}$			
-3/2	5/2			$\sqrt{15}B/2$	$-\frac{15A}{4}$		
	3/2			$\sqrt{6}B$	$-\frac{9A}{4}$		
	1/2			$3\sqrt{3}B/2$	$-\frac{3A}{4}$		
	-1/2			$\sqrt{6}B$	$\frac{3A}{4}$		
	-3/2			$\sqrt{15}B/2$	$\frac{9A}{4}$		
	-5/2				$\frac{15A}{4}$		

All non-indicated elements are zero.

perturbation procedure. This transformation is effectively the coefficient matrix from above since $\underline{\underline{C}}^{\dagger}\underline{\underline{HC}} = \underline{\underline{C}}^{\dagger}\underline{\underline{CE}}$ and so $\underline{\underline{C}}^{\dagger}\underline{\underline{AC}}$ is the correct matrix.

After this transformation $(\mathcal{H}_o + \mathcal{H}_1)$ and $\mathcal{H}_2$ were both in the same basis and $\mathcal{H}_2$ was applied as a perturbation, solutions were obtained again correct to seventh order in energy. In order to find the field for the transition between any two of the resulting 24 energy levels, a new field independent term $\Delta E_o'$ was defined for the difference polynomial.

$$\Delta E_o' = \text{Energy of level 1 - Energy of level 2 - } 2h\nu \qquad \ldots(22)$$

It is implicit in this definition that the hyperfine structure levels $|M_s'M_I\rangle$ are parallel to the $|M_s'\rangle$ fine structure levels, or in other words a strong field approximation with respect to the hyperfine terms. Since $g\beta_e H + D \sim 1\text{cm}^{-1}$ and $A \sim 0.01\ \text{cm}^{-1}$ this is quite valid.

Fig. 10 shows this procedure in detail.

Finally, this new difference polynomial was solved by the Newton-Raphson method and the hyperfine transition field was obtained. This process was repeated for a whole range of values of the parameters until the best fit with experiment was obtained.

The agreement between experiment and theory for the $'|-\tfrac{1}{2}\rangle' - '|+\tfrac{1}{2}\rangle'$ transition is very good and the results are shown in Table 2 together with the best fitting spin Hamiltonian parameters. Figs. 11 and 12 show the orientation dependence of the six hyperfine components and the five hyperfine splittings respectively, the solid line being calculated using the above method. A block diagram of the computer program used for the calculations is shown in Appendix II. All the computations were made in Fortran IV on an I.B.M. 7044 machine.

This method should be very generally applicable to E.S.R. spectra

Figure 10

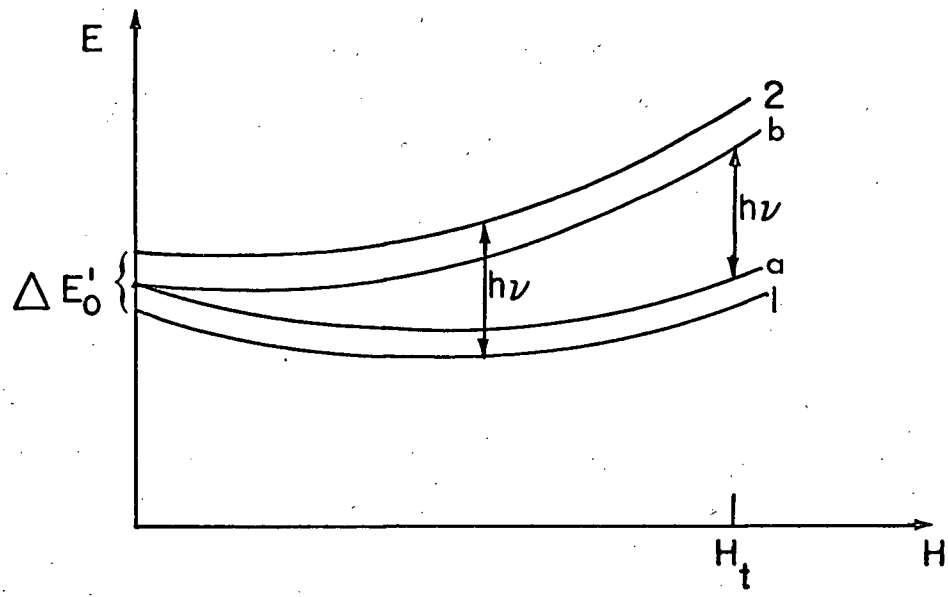

Initially $\Delta E_o = E(b)_{H=0} - E(a)_{H=0} - h\nu$

$= -h\nu$ for this case since $E(b)_{H=0} = E(a)_{H=0}$

For a fine structure transition

$$h\nu = E(b)_{H=H_t} - E(a)_{H=H_t}$$

For a hyperfine structure transition

$$\Delta E_o' = E(2)_{H=0} - E(1)_{H=0} - h\nu$$

But this is $= E(2)_{H=H_t} - E(1)_{H=H_t} - (E(b)_{H=H_t} - E(a)_{H=H_t}) - h\nu$

if the lines 1 and 2 are parallel to a and b.

But we have seen above that

$$E(b)_{H=H_t} - E(a)_{H=H_t} = h\nu$$

and so $\Delta E_o' = E(2)_{H=H_t} - E(1)_{H=H_t} - 2h\nu$

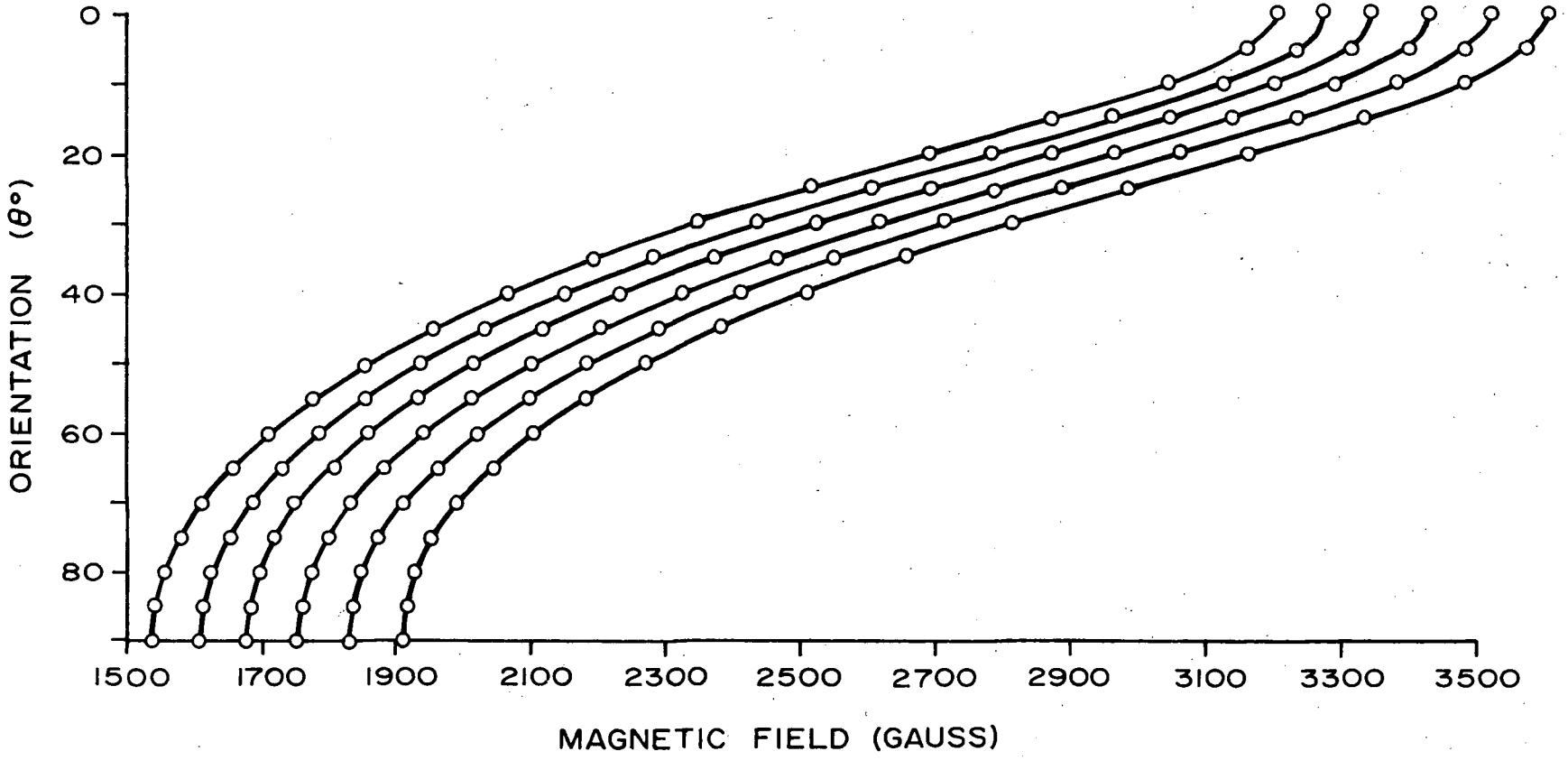

FIGURE 11 : The observed hyperfine transitions for the '$|+\frac{1}{2}\rangle$' - '$|-\frac{1}{2}\rangle$' transition, with the solid line indicating the theoretical curves

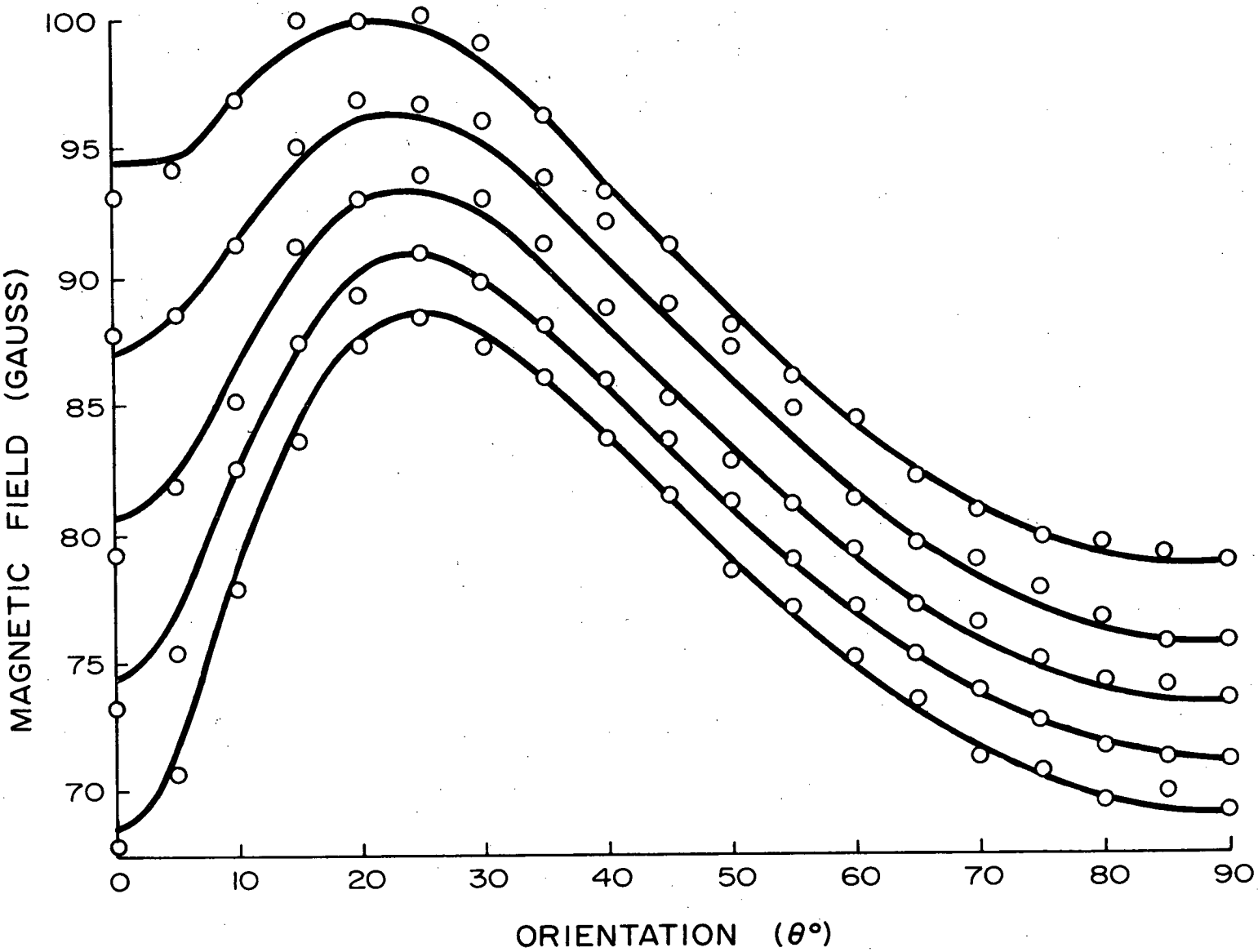

FIGURE 12 : The observed hyperfine splittings for the '$|+\frac{1}{2}\rangle$' - '$|-\frac{1}{2}\rangle$' transition, with the solid lines indicating theoretical curves

A PARALLEL = 0.00760CM-1, A-PERPENDICULAR = 0.00684CM-1, D = 0.861CM-1, G-PARALLEL = 1.9920, G-PERPENDICULAR = 1.9880

ORIENTATION (DEGREES)	FINE STRUCTURE TRANSITIONS MS=(1/2) - MS=(-1/2)	HYPERFINE STRUCTURE TRANSITIONS (FIELDS IN GAUSS) MI VALUES 5/2	3/2	1/2	-1/2	-3/2	-5/2
0.	3420.39	3209.47	3278.07	3352.54	3433.24	3520.58	3615.08
10.	3272.25	3044.31	3123.19	3205.68	3292.37	3383.91	3481.00
20.	2938.71	2696.18	2784.09	2874.36	2967.36	3063.58	3163.59
30.	2586.13	2347.56	2435.46	2525.50	2617.94	2713.15	2811.55
40.	2291.56	2065.65	2149.39	2235.24	2323.43	2414.26	2508.09
50.	2068.56	1856.32	1935.20	2016.15	2099.40	2185.22	2273.94
60.	1909.60	1708.86	1783.55	1860.28	1939.25	2020.74	2105.06
70.	1804.19	1611.77	1683.41	1757.05	1832.88	1911.18	1992.26
80.	1744.17	1556.71	1626.53	1698.31	1772.26	1848.65	1927.77
90.	1724.69	1539.28	1607.97	1678.91	1752.28	1828.32	1907.31

MEAN ERROR = 1.87

DEVIATIONS FROM EXPERIMENT

3.33	1.93	0.86	-0.64	-0.08	-1.98
4.09	3.01	3.22	1.73	1.49	1.30
5.12	4.51	3.54	3.64	4.32	4.31
3.24	2.64	2.50	3.16	4.15	4.35
1.45	1.01	1.26	1.97	3.34	2.81
1.78	1.40	1.75	1.20	2.58	1.96
-1.46	-1.05	-0.68	-0.25	-0.44	-0.26
0.13	-0.31	-0.15	0.52	1.32	1.04
-0.91	-1.23	-1.41	-1.16	-0.85	-0.27
-1.48	-1.07	-1.01	-0.88	-1.22	-1.61

TABLE 2

and it is trivial to extend the program to include quadrupolar and nuclear Zeeman terms; forbidden transitions are also simple to obtain.

One somewhat difficult point is the introduction of non-axial symmetry since this implies complex matrix elements. However, this problem has been overcome and a general program will soon be available (41).

In order to accommodate systems where $g\beta_e H > D$ the following method was used. As an example we will treat the transition observed at $\theta = 90^o$ at around 10.6 kilogauss, for which $g\beta_e H \sim 1 cm^{-1}$ and $D = 0.861 cm^{-1}$. Since, for the purposes of perturbation theory, there is no restriction on the way a Hamiltonian is divided into $\mathcal{H}_o$ and $\mathcal{H}_1$ providing $\mathcal{H}_1 \ll \mathcal{H}_o$; $\mathcal{H}_o$ was taken as

$$\mathcal{H}_o = D\{S_z^2 - \tfrac{1}{3}\hat{S}^2\} + (g_{\parallel} S_z \cos\theta + g_{\perp} S \sin\theta)\beta_e H'$$

where H' is some field less than $H_{transition}$ by about a few hundred gauss (H' = 10,000 gauss in our example). $\mathcal{H}_o$ was solved by numerical diagonalisation using Jacobi's (42) method and the resulting eigenstates and eigenvalues taken as new "zero field" parameters for the purposes of the calculation.

The transition field was then found using the method described previously except that the resultant value of H now had to be added to H' to find the correct value. This mode of calculation was used to calculate the positions of the "forbidden" transitions observed ar around 7000 and around 11,000 gauss and also for the "allowed" transition at around 15,000 g as plotted in Fig. 9.

This type of calculation covers the whole range of possible values for D and is thus more general than the equations of Bleaney (24) which only apply for $D < g\beta_e H$. Other methods (43,44) are equally useful for the fine structure transitions, but these are not easily extended

to treat hyperfine nuclear Zeeman or quadrupolar effects, and these are often important. For example, in the present case it is not valid to take the fine structure transition as occuring midway between the third and fourth hyperfine structure lines, as can be seen from the results in Table 2. This is a second order approximation which has often been used in the past, but is not always justified and in the present system third and fourth order terms are quite important.

5. Ligand Field Calculations on the Ground State of the Complex

The central manganese ion is surrounded by oxygen ions situated approximately at the corners of an octahedron. Thus we may consider the central ion as being in an environment which is the sum of two influences, a large octahedral field with a superposed smaller tri-trigonal field, due to the arrangement of the nine molybdenum-containing octahedra. The one electron d-orbitals are split by these two fields in the following manner (45).

Figure 13

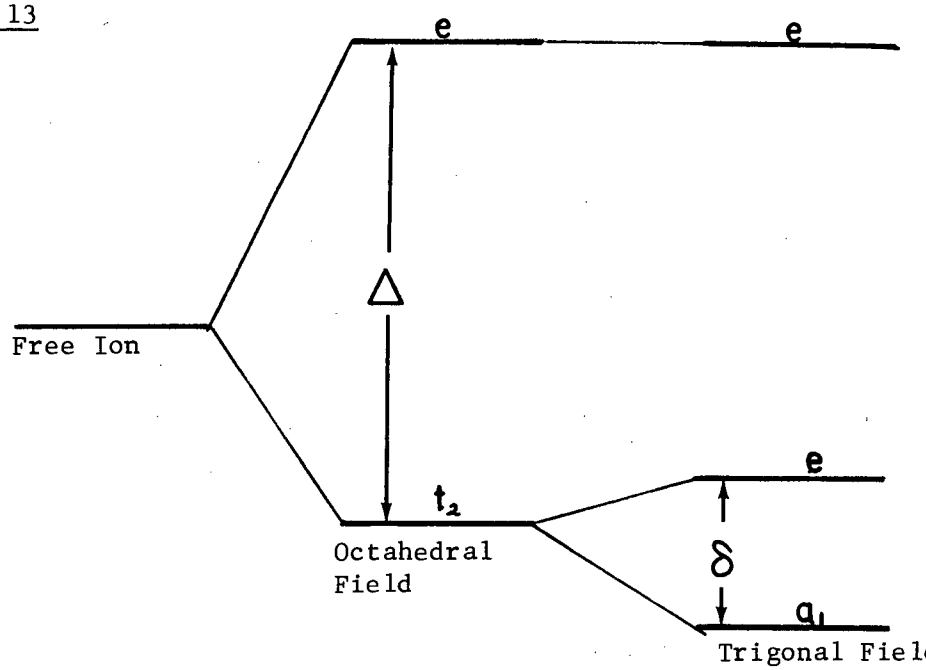

While the relative positions of the e and t_2 orbitals is fixed in the octahedral field, the order of the a_1 and lower e orbitals in the trigonal field is not unique but rather depends on the direction of the distortion from O_h symmetry whether by expansion or contraction along the threefold axis. There is no a priori way of finding the sign of δ and it is not always possible to decide upon this by calculation.

Ignoring the trigonal field for the moment, we can consider the strong field configurations t_2^3, t_2^2e, t_2e^2, e^3 for a d^3 system, each

separated by an amount Δ from the other. Electrostatic repulsion between the electrons splits these configurations into "strong field" states. Viewed from the weak field standpoint the free ion states of the d^3 configuration are split into various states by the octahedral field and we may draw a correlation diagram of the form shown in Fig. 14. The energy axis is not to scale, although the terms are in the correct order. From the available experimental results for optical spectra (46,47) the d^3 ions V^{2+}, Cr^{3+} and Mn^{4+} are found to occupy the approximate intermediate positions indicated. In performing calculations on the ground state of the ions, it seems reasonable to consider effects of the doublet states from t_2^3 and the quartets from t_2^2e. The calculations performed for d^3 systems previously are reviewed below, and it will be seen that most authors have neglected these lowest doublet states.

A. Survey of Previous Calculations on d^3 Systems

Many calculations have been made on d^3 systems and it is hoped that this survey will help to correlate all the results.

Let us first define some terms:

$$\mathcal{H}_{so} = \lambda \underline{L}\cdot\underline{S} = \sum_i \zeta_i \underline{l}_i \cdot \underline{s}_i \quad : \quad \lambda = \zeta/3$$

$$\mathcal{H}_z = \beta_e \underline{H}\cdot\underline{g}\cdot\underline{S} \quad : \quad \text{Z.F.S.} = 2D$$

$$\delta W_i = \sum_j \frac{|\langle i | \lambda \underline{L}\cdot\underline{S} | j \rangle|^2}{\Delta E_{ij}}$$

1939 Van Vleck (48) was the first to treat the problem using the data on the Cr^{3+} ion in chrome-alum. The ground state of a d^3 ion is ^4F and this is split by an octahedral and trigonal field as shown in Fig. 15. The ground state, $^4A_2$, is split by spin-orbit coupling in conjunction with the trigonal field

FIGURE 14 : Complete correllation diagram for a d^3 system (not to scale)

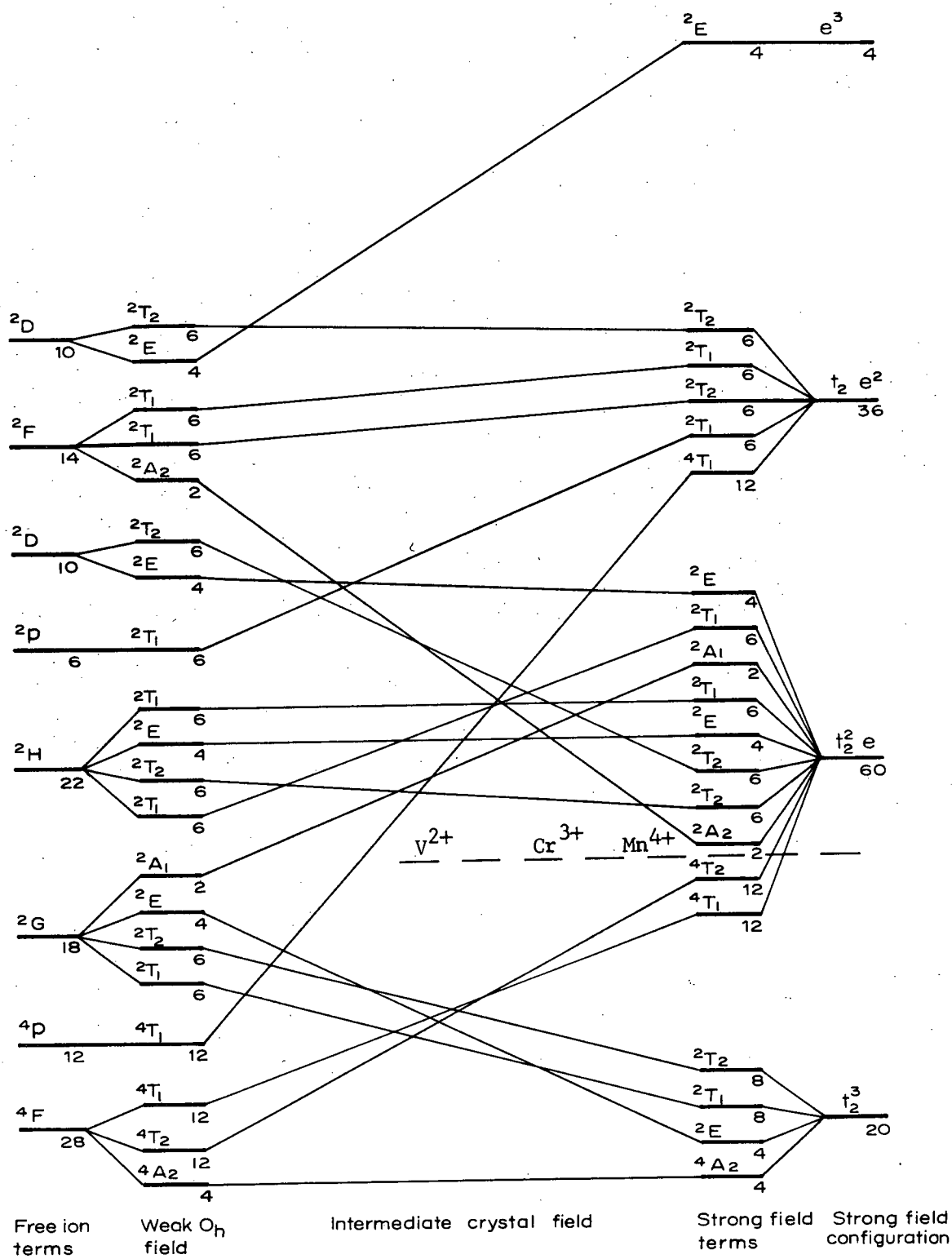

effect. The difference in energy between the two resulting doublets, 2D, is given by

$$2D = \delta W(\tfrac{1}{2}) - \delta W(3/2) = \frac{+72K\lambda^2}{9\Delta_{\parallel}^2} \quad \text{(i.e. } \pm 3/2 \text{ lowest for } K>0) \qquad \cdots(23)$$

This comes from spin-orbit coupling between $^4A_2$ and the split levels of $^4T_2$, this latter splitting being due to the trigonal field.

Figure 15

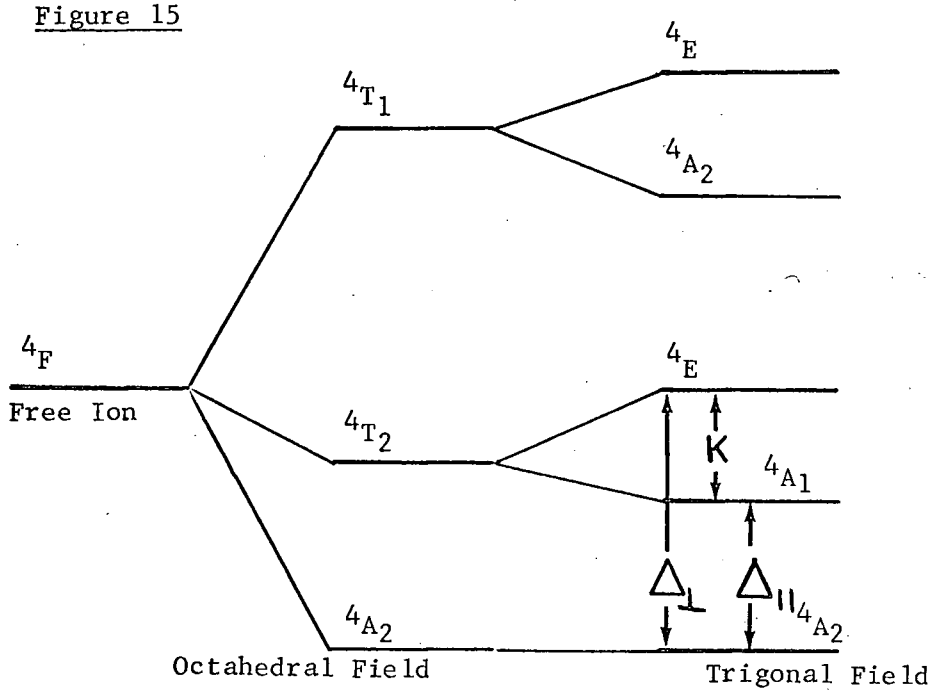

Van Vleck also thought that the sign of 2D was correct, since K is positive from crystal structure arguments.

1942 Broer (49) performed a similar calculation with a slightly different crystal field operator and obtained

$$2D = \frac{88}{9}\frac{K\lambda^2}{\Delta_{\parallel}^2}$$

1948 Weiss (50) used the same operator and found the same value as Van Vleck

$$2D = \frac{72}{9}\frac{K\lambda^2}{\Delta_{\parallel}^2} \qquad : \qquad g = 2\left(1 - \frac{4\lambda}{\Delta_{\parallel} + 2K/3}\right)$$

1955 Meijer and Gerritson (51) performed the calculation using

zero order functions for the spin-orbit coupling perturbation which were already eigenstates of the total crystal field. They suggested that Van Vleck's formula was derived using only octahedral field eigenstates.

$$2D = -\frac{152K\lambda^2}{9\Delta^2}$$

This is different in sign as well as magnitude from Van Vleck's result ($\pm\frac{1}{2}$ is lowest from this result, for $K > 0$).

1957 Jarrett (52) did not give a theoretical expression for 2D but only presented a graph of calculated splittings versus the ratio of the axial to the cubic components of the crystal field. He appears to agree with Meijer and Gerritson in that a negative value of K indicates that $\pm 3/2$ states are lowest.

1957 Davies and Strandberg (53) recalculated Van Vleck's result without mentioning the original result. They did however mention Meijer and Gerritson's paper but without comment on the discrepancies.

1958 Sugano and Tanabe (54) made a very careful study of the optical spectrum of ruby and found that 2D = 0.36 cm^{-1} and K was approximately -134 cm^{-1}. This difference in sign did not agree with Van Vleck's ideas and so they suggested the use of anisotropic spin-orbit coupling, defining the parameters as follows

$$\Delta g_{\parallel} = \frac{8\zeta_{\parallel}}{3E(^4T_2)} \quad \left(\frac{\sim 8\zeta}{3\Delta_{\parallel}}\right) \; : \; \Delta g_{\perp} = \frac{8\zeta_{\perp}}{3E(^4T_2)} \quad \left(\frac{\sim 8\zeta}{3\Delta_{\perp}}\right)$$

(Author's approximations in parentheses)

This is a very ad hoc definition of $\zeta_{\parallel}$ and $\zeta_{\perp}$ since the $^4T_2$ state is split by a trigonal distortion and all the unknowns

are lumped together into the spin-orbit coupling parameters. Their expression for 2D was

$$2D = \frac{8}{9}\left(\frac{\zeta_{\parallel}^2\,\zeta_{\perp}^2}{E(^4T_2)}\right) + \frac{4}{9}\left(\frac{\zeta_{\parallel}^2\,\zeta_{\perp}^2}{(E(^4T_2))^2}\right)\frac{2K}{3} - \frac{8}{9}\left(\frac{2}{3}\right)^{\frac{1}{2}}\left(\frac{\zeta_{\perp}^2+2\zeta_{\parallel}^2}{E(^4T_2)E(^4T_1)}\right)\frac{2K}{3}$$

The final cross term comes from doing the calculation by using the trigonal field and the spin-orbit coupling together as the perturbing terms.

By a little algebra and some approximations this can be brought into the same form as Van Vleck's formulation. By making the approximation that $E(^4T_1) = 2E(^4T_2)$ which is reasonable from the spectroscopic results, we find

$$2D \sim \frac{\lambda^2 K}{\Delta_{\parallel}^2}\,(16 + 8 - 9)$$

$$= \frac{15\lambda^2 K}{\Delta^2}$$

which is similar in magnitude to Meijer and Gerritson's result, but opposite in sign. This predicts a negative value for 2D since K is itself negative. In their paper Sugano and Tanabe said that since the last two terms in the expression are nearly equal and opposite, then 2D is positive for $\zeta_{\parallel} > \zeta_{\perp}$ whatever the sign of K. Unfortunately using their definition, $\zeta_{\parallel} > \zeta_{\perp}$ implies that $\Delta_{\perp} > \Delta_{\parallel}$ and that K is positive. This contradiction arises, I feel, because of the obscuring of the exact effect of the trigonal field on the system by the use of the parameters $\zeta_{\parallel}$ and $\zeta_{\perp}$. g-values are far more sensitive to covalency than is 2D, and the error may lie in the transferring of g-value parameters directly to those for 2D.

Spin-orbit coupling parameters, being radial integrals, may

well be anisotropic if treated correctly. However, the assumptions involved in using this form of the spin-orbit coupling terms for n-electron systems have already been discussed in Section 2B. One of these assumptions is that since the radial integral varies as r^{-3} then the contribution is greatest near the nucleus, where the surrounding electric field is approximately spherical. This spherical field implies isotropic spin-orbit coupling factors for an electron in a nl orbital. When the electron is in a molecular orbital then ligand contributions to ζ_{nl} must be considered. Most common ligands (O, F, N) have small values of ζ and produce only small deviations from the free ion value for the central metal ion.

1959 Stahl-Brada and Low (55) measured the zero field splitting in spinel by E.S.R. and gave Van Vleck's result although in a different form

$$2D = -8\lambda^2 \left(\frac{\Delta_{\parallel} - \Delta_{\perp}}{\Delta_{\parallel}\Delta_{\perp}}\right)$$

$$\frac{8\lambda^2_K}{\Delta_{\parallel}\Delta_{\perp}} \qquad \frac{8\lambda^2_K}{\Delta^2_{\parallel}}$$

They were puzzled by the large value of 2D (0.990 cm^{-1}) compared with the results for ruby.

1961 Sugano and Peter (56) solved an 80 x 80 secular equation for ruby by a numerical method and varied parameters to get the best fit with experimental results. It is difficult to argue with such a result, but it gives little insight into the physical situation and each problem has to be attacked separately. However, they were the first to consider states other than the $^4T_2$.

1962 Kamimura (57) used the idea of distortion of the t_{2g} molecular orbitals through π-covalency in a complex. This distortion, represented by a parameter q ($=\zeta_{\parallel}/\zeta_{\perp}$), gives a formula for 2D which is very similar to Van Vleck's

$$2D = 8\lambda^2 \left(\frac{\beta_{\perp}^2}{\Delta_{\perp}} - \frac{\beta_{\parallel}^2 q^2}{\Delta_{\parallel}} \right)$$

where $\beta_{\parallel}$ and $\beta_{\perp}$ are coefficients from configuration mixing. This is similar to Sugano and Tanabe's anisotropic spin-orbit coupling but not as ad hoc.

1963 Lohr and Lipscomb (58) used the Sugano-Tanabe-Kamimura formulation but pointed out that all previous calculations had neglected the considerable contribution to the Z.F.S. from the $^2T_{2g}$ levels of t_{2g}^3 which occurs as well as the $^4T_{2g}$ from $t_{2g}^2 e_g$. The formula that they arrived at is

$$2D = -8 \left(\frac{\lambda_{\parallel}^2 - \lambda_{\perp}^2}{E(^4T_2)} \right) - 6 \left(\frac{\lambda_{\perp}'^2 - \lambda_{\parallel}'^2}{E(^2T_2)} \right) - \text{smaller terms}$$

with $\lambda_{\parallel}$ and $\lambda_{\perp}$ (closely related to $\zeta_{\parallel}$ and $\zeta_{\perp}$ respectively), defined in terms of one-electron operators and molecular orbital functions. The energy terms in the denominators are taken from experiment, and the molecular orbitals are arrived at by the extended Huckel method. The trigonal fields involved are assumed to be small in this treatment and in this situation they point out that the g-value can be isotropic even if a sizeable zero field splitting is observed.

1964 McGarvey (59) calculated 2D for systems with large trigonal fields and introduced the effect of distortion of the one-electron d-orbitals by the ligands. Both this, and a para-

llel extended Huckel molecular orbital calculation were used to get values of the distortion parameters using experimental values for energy levels in the system, and for the zero field splitting. Estimates of g-values were made, and it was found necessary to include the effect of including excited states obtained by promoting a bonding electron into the anti-bonding d-orbitals.

1966 Owen and Thornley (60) give a very general review of covalent bonding and its effect on magnetic properties of transition metal ions. They discuss the effects of σ and π bonding on the orbital magnetic moment, spin-orbit coupling and Racah parameters, and after considering all the available calculations and experimental evidence, their conclusion is that the effects of covalency on zero field splittings, g-values and hyperfine constants are at best imperfectly understood.

In view of these previous results it was decided to perform a calculation on the d^3 system within the ligand field framework, in order to obtain more insight into the problem, and to arrive at a less empirical expression for the Z.F.S. than that obtained by McGarvey (59).

It was found useful to classify the three-electron determinantal functions according to the double group D_3^*, since this is correct for spinors within an S = 3/2 manifold, and it reduces the algebra to a reasonable level. The combination of d-orbitals, first used by Pryce and Runciman (61), in which the trigonal axis of the octahedron is the axis of quantization, seemed the logical basis to use. The five orbitals are

$$t_o = 1/\sqrt{3}(d_{xy} + d_{yz} + d_{xz})$$

$$t_{\pm} = \mp 1/\sqrt{3}(d_{xy} + w^{\pm 1} d_{yz} + w^{\pm 2} d_{xz})$$

$$e_{\pm} = \mp 1/\sqrt{2}(d_{z^2} \pm i d_{x^2-y^2}) \qquad \ldots(24)$$

where $w = e^{2\pi i/3}$, in terms of the usual real orbitals having the four-fold axis for quantization.

A diagram of the way in which the strong field configurations, t_2^3 and $t_2^2 e$, are split by electron repulsion and a trigonal field are shown in Fig. 16. The classification is given in terms of the representations of D_3^* as well as the more usual D_3.

Instead of using all the 120 functions of d^3, which would be a very large task, it was decided to use just the 20 arising from the t_{2g}^3 configuration and 24 from the $t_{2g}^2 e_g$ configuration which gave rise to the $^4T_{1g}$ and $^4T_{2g}$ states of the O_h scheme; these latter were obtained by the use of shift operators on determinants like $|e_- t_- t_+|$. This selection is justified since the other states have considerably higher energies and would thus contribute much less to the Z.F.S. Subshell configuration mixing was neglected since the energy corrections are of the order of $50B^2/\Delta$ (62) where B is Racah's (63) electron repulsion parameter and Δ is the strength of the octahedral field. For the free ion Mn^{4+}, B is estimated to be 1060 cm^{-1} (6) and Δ is approximately 22,000 cm^{-1} from the optical spectrum (46,47) and previous work on Mn^{4+} (11-22). So the correction is fairly small ($\sim$10% of the energy of the lowest doublet).

Table 3 gives the 44 determinants used for this calculation, and Fig. 5 shows the co-ordinate axes used for the spin and the orbital manifolds. These were chosen so as to make the algebraic manipulation as simple as possible.

The complete character table for D_3^* is given in Table 4. We may

FIGURE 16 : Diagram of the splitting of strong octahedral field configurations, under the influence of electron repulsion and trigonal field operators. The left side of the diagram is not to scale, but the right-hand side indicates both the labelling of the states in the D_3^* group, and the correct ordering of levels when B = 700 cm^{-1}, δ = 7000 cm^{-1} and Δ = 22000 cm^{-1}

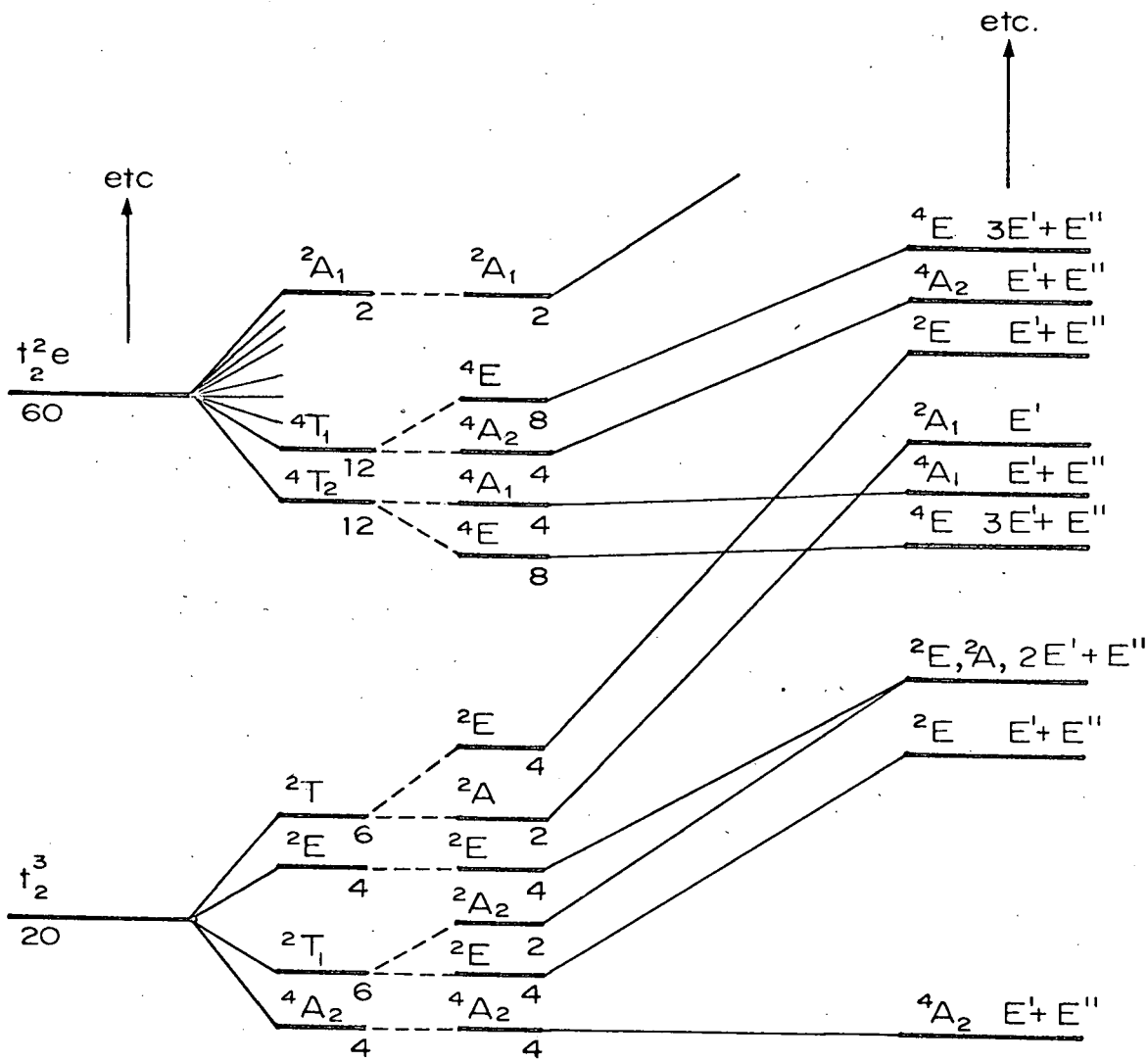

Strong field configuration | Strong field terms.

O_h | + Electron repulsion | $+D_3$ | D_3 | D_3^*

TABLE 3

The 44 determinantal basis functions

t^3 configuration

$\psi_1 = |\bar{t}_o t_+ t_-|$

$\psi_2 = |\bar{t}_o t_+ \bar{t}_-|$

$\psi_3 = |\bar{t}_o \bar{t}_+ t_-|$

$\psi_4 = |\bar{t}_o t_+ t_-|$

$\psi_5 = |\bar{t}_o \bar{t}_+ \bar{t}_-|$

$\psi_6 = |\bar{t}_o t_+ \bar{t}_-|$

$\psi_7 = |\bar{t}_o \bar{t}_+ t_-|$

$\psi_8 = |\bar{t}_o \bar{t}_+ \bar{t}_-|$

$\psi_9 = |\bar{t}_o \bar{t}_o t_+|$

$\psi_{10} = |\bar{t}_o t_o \bar{t}_+|$

$\psi_{11} = |\bar{t}_o \bar{t}_o t_-|$

$\psi_{12} = |\bar{t}_o t_o \bar{t}_-|$

$\psi_{13} = |\bar{t}_o t_+ \bar{t}_+|$

$\psi_{14} = |\bar{t}_o t_+ \bar{t}_+|$

$\psi_{15} = |\bar{t}_o t_- \bar{t}_-|$

$\psi_{16} = |\bar{t}_o t_- \bar{t}_-|$

$\psi_{17} = |\bar{t}_+ \bar{t}_+ t_-|$

$\psi_{18} = |\bar{t}_+ t_+ \bar{t}_-|$

$\psi_{19} = |\bar{t}_+ t_- \bar{t}_-|$

$\psi_{20} = |\bar{t}_+ \bar{t}_- \bar{t}_-|$

t^2e configuration (quartets only).

$\phi_1 = |\bar{e}_- t_- t_+|$

$\phi_2 = 1/\sqrt{3}[|\bar{e}_- t_- t_+| + |\bar{e}_- \bar{t}_- t_+| + |\bar{e}_- t_- \bar{t}_+|]$

$\phi_3 = 1/\sqrt{3}[|\bar{e}_- \bar{t}_- t_+| + |\bar{e}_- t_- \bar{t}_+| + |\bar{e}_- \bar{t}_- \bar{t}_+|]$

$\phi_4 = |\bar{e}_- \bar{t}_- \bar{t}_+|$

$\phi_5 = |\bar{e}_- t_- t_o|$

$\phi_9 = |\bar{e}_- t_+ t_o|$

$\phi_{13} = |\bar{e}_+ t_- t_+|$

$\phi_{17} = |\bar{e}_+ t_- t_o|$

$\phi_{21} = |\bar{e}_+ t_+ t_o|$

The remaining components of the quartets are found by operating with S_- on these +3/2 components.

where $|....|$ stands for a normalised Slater determinant

TABLE 4

Character table for D_3^*, together with the behaviour of spin and spatial basis functions

		E	C_3	$\bar{C}_3$	C_2^1R	C_2^2	C_2^3	R	C_3R	$\bar{C}_3R$	C_2^1	C_2^2R	C_2^3R
	A_1	1	1	1	1	1	1	1	1	1	1	1	1
	A_2	1	1	1	-1	-1	-1	1	1	1	-1	-1	-1
	E	$\begin{bmatrix}1&0\\0&1\end{bmatrix}$	$\begin{bmatrix}\omega^2&0\\0&\omega\end{bmatrix}$	$\begin{bmatrix}\omega&0\\0&\omega^2\end{bmatrix}$	$\begin{bmatrix}0&-1\\-1&0\end{bmatrix}$	$\begin{bmatrix}0&-\omega\\-\omega^2&0\end{bmatrix}$	$\begin{bmatrix}0&-\omega^2\\-\omega&0\end{bmatrix}$	$\begin{bmatrix}1&0\\0&1\end{bmatrix}$	$\begin{bmatrix}\omega^2&0\\0&\omega\end{bmatrix}$	$\begin{bmatrix}\omega&0\\0&\omega^2\end{bmatrix}$	$\begin{bmatrix}0&-1\\-1&0\end{bmatrix}$	$\begin{bmatrix}0&-\omega\\-\omega^2&0\end{bmatrix}$	$\begin{bmatrix}0&-\omega^2\\-\omega&0\end{bmatrix}$
E′	α	$\begin{bmatrix}1&0\\0&1\end{bmatrix}$	$\begin{bmatrix}-\omega&0\\0&-\omega^2\end{bmatrix}$	$\begin{bmatrix}-\omega^2&0\\0&-\omega\end{bmatrix}$	$\begin{bmatrix}0&-i\\-i&0\end{bmatrix}$	$\begin{bmatrix}0&-i\omega^2\\-i\omega&0\end{bmatrix}$	$\begin{bmatrix}0&-i\omega\\-i\omega^2&0\end{bmatrix}$	$\begin{bmatrix}-1&0\\0&-1\end{bmatrix}$	$\begin{bmatrix}\omega&0\\0&\omega^2\end{bmatrix}$	$\begin{bmatrix}\omega^2&0\\0&\omega\end{bmatrix}$	$\begin{bmatrix}0&i\\i&0\end{bmatrix}$	$\begin{bmatrix}0&i\omega^2\\i\omega&0\end{bmatrix}$	$\begin{bmatrix}0&i\omega\\i\omega^2&0\end{bmatrix}$
	β												
E″	ϵ_1	1	-1	-1	i	i	i	-1	1	1	-i	-i	-i
	ϵ_2	1	-1	-1	-i	-i	-i	-1	1	1	i	i	i
a_1	t_0	t_0	t_0	t_0	t_0	t_0	t_0	t_0	t_0	t_0	t_0	t_0	t_0
e	t_+	t_+	$\omega^2 t_+$	ωt_+	$-t_-$	$-\omega^2 t_-$	$-\omega t_-$	t_+	$\omega^2 t_+$	ωt_+	$-t_-$	$-\omega^2 t_-$	$-\omega t_-$
	t_-	t_-	ωt_-	$\omega^2 t_-$	$-t_+$	$-\omega t_+$	$-\omega^2 t_+$	t_-	ωt_-	$\omega^2 t_-$	$-t_+$	$-\omega t_+$	$-\omega^2 t_+$
e	e_+	e_+	$\omega^2 e_+$	ωe_+	$-e_-$	$-\omega^2 e_-$	$-\omega e_-$	e_+	$\omega^2 e_+$	ωe_+	$-e_-$	$-\omega^2 e_-$	$-\omega e_-$
	e_-	e_-	ωe_-	$\omega^2 e_-$	$-e_+$	$-\omega e_+$	$-\omega^2 e_+$	e_-	ωe_-	$\omega^2 e_-$	$-e_+$	$-\omega e_+$	$-\omega^2 e_+$
e′	α	α	$-\omega\alpha$	$-\omega^2\alpha$	$-i\beta$	$-i\omega\beta$	$-i\omega^2\beta$	$-\alpha$	$\omega\alpha$	$\omega^2\alpha$	$i\beta$	$i\omega\beta$	$i\omega^2\beta$
	β	β	$-\omega^2\beta$	$-\omega\beta$	$-i\alpha$	$-i\omega^2\alpha$	$-i\omega\alpha$	$-\beta$	$\omega^2\beta$	$\omega\beta$	$i\alpha$	$i\omega^2\alpha$	$i\omega\alpha$

where $\omega = e^{2\pi i/3}$, α and β are spin functions

note here that two of the original C_2 operators in D_3 form a class with one of the C_2R operators of D_3^*, and the remaining C_2 operator is in another class with the other two C_2R operators. The particular C_2 operator depends on the axis system chosen. For the present system $C_2^{(1)}$, $C_2^{(2)}R$ and $C_2^{(3)}R$ form a class. The final six operators of D_3^* have characters identical to the first six except for the E" representation where the sign is different for the two sets.

Table 4 also gives the summary of the way in which the five orbitals together with the α and β spin vectors transform in D_3^*. The transformation of the α and β spin vectors was derived using the formulation given by Ballhausen (64). The matrix

$$\begin{pmatrix} e^{i(\psi+\phi)/2}\cos\theta/2 & ie^{i(\psi-\phi)/2}\sin\theta/2 \\ ie^{-i(\psi-\phi)/2}\sin\theta/2 & e^{-i(\psi+\phi)/2}\cos\theta/2 \end{pmatrix}$$

is given for co-ordinate system rotation and so for vector rotation $C_3 = \overline{C_3}$ for co-ordinates.

e.g. for a vector

$$C_3 = \begin{pmatrix} e^{i(-2\pi/3)/2} & 0 \\ 0 & e^{-i(-2\pi/3)/2} \end{pmatrix}$$

since $\phi = 120^\circ$, $\psi = 0^\circ$, $\theta = 0^\circ$

$$= \begin{pmatrix} -\omega & 0 \\ 0 & -\omega^2 \end{pmatrix}$$

All the other operators can be treated similarly.

By operating with the various operators in the group on the determinants in Table 3 we arrive at the symmetry adapted set given in Table 5.

The first step in the partial removal of degeneracy from these 44

TABLE 5

Symmetry adapted determinantal functions

	E′		E′′	
	α	β	ρ_1	ρ_2
	ψ_2	ψ_6	$1/\sqrt{2}(\psi_1-\psi_8)$	$1/\sqrt{2}(\psi_1+\psi_8)$
t^3 configuration	ψ_3	ψ_7	$1/\sqrt{2}(\psi_9-\psi_{12})$	$1/\sqrt{2}(\psi_1+\psi_{12})$
	ψ_4	ψ_5	$1/\sqrt{2}(\psi_{17}-\psi_{20})$	$1/\sqrt{2}(\psi_{17}+\psi_{20})$
	ψ_{10}	ψ_{11}	$1/\sqrt{2}(\psi_{14}-\psi_{15})$	$1/\sqrt{2}(\psi_{14}+\psi_{15})$
	ψ_{16}	ψ_{13}		
	ψ_{18}	ψ_{19}		
	ϕ_1	$-\phi_{16}$	$1/\sqrt{2}(\phi_9+\phi_{20})$	$1/\sqrt{2}(\phi_9-\phi_{20})$
	ϕ_4	$-\phi_{13}$	$1/\sqrt{2}(\phi_{17}+\phi_{12})$	$1/\sqrt{2}(\phi_{17}-\phi_{12})$
t^2e configuration	ϕ_7	$-\phi_{22}$	$1/\sqrt{2}(\phi_6+\phi_{23})$	$1/\sqrt{2}(\phi_6-\phi_{23})$
	ϕ_{10}	$-\phi_{19}$	$1/\sqrt{2}(\phi_{14}+\phi_3)$	$1/\sqrt{2}(\phi_{14}-\phi_3)$
	ϕ_{15}	$-\phi_2$		
	ϕ_{18}	$-\phi_{11}$		
	ϕ_{21}	$-\phi_8$		
	ϕ_{24}	$-\phi_5$		

functions is to find the eigenvalues and eigenvectors of the electrostatic repulsion operator $\sum_{i>j} e^2/r_{ij}$. Various quantities like the Coulomb integral $J(t_+,t_+)$ are needed in the calculation, and this one is worked out in detail in Appendix III. The rest of the set of integrals in Table 6 may be worked out similarly. The results are expressed in terms of Racah's parameters.

The matrices of $\sum_{i>j} e^2/r_{ij}$ for the $E''(\rho_1)$ and $E'(\alpha)$ symmetry species are given in Table 7. $E''(\rho_2)$ and $E'(\beta)$ functions will have identical matrices and these are not shown.

On solving these matrices completely, we arrive at the set of eigenfunctions and eigenvalues given in Table 8. It will be noticed that the eigenvalues and their respective degeneracies are identical regarding the electrostatic part, to those given by Ballhausen (64). For convenience the eigenfunctions are renamed at this point.

The second step in this calculation is to find the eigenfunctions and eigenvalues of the trigonal field operator. This field is introduced via the one-electron parameters δ and Δ, defined in Figure 13. The original determinants have their energies modified as shown in Table 9.

The matrices for the trigonal field operator in the basis of the newly defined functions are given in Table 10. Only trivial 2 x 2 determinants have to be solved to find the eigenfunctions and eigenvalues and these are given in Table 11.

In order to introduce spin-orbit coupling into these eigenfunctions it is necessary to calculate the matrix of $\sum_i \xi_i \underline{l}_i \cdot \underline{s}_i$ in the basis $|t_+^+\rangle$ etc., with the spin and orbital parts of the spinor referred to the same axis system. This was done by referring the t and e orbitals defined in Equ. #24 to the spin axis system given earlier. The result-

TABLE 6

Electrostatic repulsion integrals, given in terms of Racah's parameters

$$J(t_o,t_o) = A + 4B + 3C$$

$$J(t_+,t_+) = A + B + 2C$$

$$= J(t_-,t_-)$$

$$= J(t_-,t_+)$$

$$J(t_o,t_+) = A - 2B + C$$

$$= J(t_o,t_-)$$

$$J(e_-,t_-) = A + C = J(e_j,t_i) \quad , \; j = \pm, \; i = \pm, o.$$

$$K(t_o,t_+) = 3B + C$$

$$= K(t_o,t_-) = \tfrac{1}{2}K(t_+,t_-)$$

$$K(e_i,t_j) = 2B + C \quad , \quad i = \pm, \; j = \pm \text{ or } o.$$

$$(t_o t_+ | t_- t_-) = 0 = (t_o t_- | t_+ t_+)$$

$$(t_o t_o | t_- t_+) = -(3B + C)$$

$$(e_- t_- | e_+ t_o) = 4B$$

$$= -(e_+ t_+ | e_- t_o)$$

$$= -(e_- t_+ | e_+ t_-)$$

$$(e_- t_o | t_+ e_+) = 2B$$

$$= (e_- t_+ | t_- e_+)$$

$$= -(e_- t_- | t_o e_-)$$

where $J(a,b) = \int a^*(1)\, b^*(2)\, \frac{e^2}{r_{12}}\, a(1)\, b(2) d\tau$

$$K(a,b) = \int a^*(1)\, b^*(2)\, \frac{e^2}{r_{12}}\, a(2)\, b(1) d\tau$$

$$(ab|cd) = \int a^*(1)\, b^*(2)\, \frac{e^2}{r_{12}}\, c(1)\, d(2) d\tau .$$

TABLE 7

Matrices of $\sum_{i>j} \frac{e^2}{r_{ij}}$ in the $E''(\rho_1)$ and $E'(\alpha)$ basis for t^3 and t^2e configurations, given in terms of Racah's parameters

$E''(\rho_1)\ t^3$

$1/\sqrt{2}(\psi_1-\psi_8)$	$1/\sqrt{2}(\psi_{14}-\psi_{15})$	$1/\sqrt{2}(\psi_9-\psi_{12})$	$1/\sqrt{2}(\psi_{17}-\psi_{20})$
3A - 15B	0	0	0
0	3A-6B+3C	0	0
0	0	3A-3B+4C	3B + C
0	0	3B + C	3A-3B+4C

$E'(\alpha)\ t^3$ divides into two 3 x 3 matrices

ψ_2	ψ_3	ψ_4
3A-6B+3C	-(6B+2C)	-(3B+C)
-(6B+2C)	3A-6B+3C	-(3B+C)
-(3B+C)	-(3B+C)	3A-9B+2C

ψ_{16}	ψ_{10}	ψ_{18}
3A-6B+3C	0	0
0	3A-3B+4C	3B+C
0	3B+C	3A-3B+4C

$E''(\rho_1)\ t^2e$ divides into two identical 2 x 2 matrices

$1/\sqrt{2}(\phi_9+\phi_{20})$	$1/\sqrt{2}(\phi_{17}+\phi_{12})$
3A-9B	-6B
-6B	3A-9B

and similarly for $1/\sqrt{2}(\phi_6-\phi_{23})$ and $1/\sqrt{2}(\phi_{14}-\phi_3)$

$E'(\alpha)\ t^2e$ divides into four identical 2 x 2 matrices, each having the same elements as the $E''(\rho_1)\ t^2e$ above.

Pairs of functions

$$\begin{Bmatrix} \phi_1 & \phi_4 & \phi_7 & \phi_{10} \\ \phi_{21} & \phi_{24} & \phi_{15} & \phi_{18} \end{Bmatrix}$$

TABLE 8

Eigenfunctions and eigenvalues of the electrostatic repulsion operator

Eigenfunction	Symmetry species		Eigenvalue
$\chi_1 = 1/\sqrt{2}(\psi_1-\psi_8)$	ρ_1	E''	3A - 15B
$\chi_2 = 1/\sqrt{2}(\psi_1+\psi_8)$	ρ_2	E''	
$\chi_3 = 1/\sqrt{2}(\psi_2+\psi_3+\psi_4)$	α	E'	
$\chi_4 = 1/\sqrt{2}(\psi_5+\psi_6+\psi_7)$	β	E'	
$\chi_5 = 1/\sqrt{2}(\psi_2-\psi_3)$	α	E'	3A + 5C
$\chi_6 = 1/\sqrt{2}(\psi_6-\psi_7)$	β	E'	
$\chi_{17} = \frac{1}{2}(\psi_9-\psi_{12}+\psi_{17}-\psi_{20})$	ρ_1	E''	
$\chi_{18} = \frac{1}{2}(\psi_9+\psi_{12}+\psi_{17}+\psi_{20})$	ρ_2	E''	
$\chi_{19} = 1/\sqrt{2}(\psi_{10}+\psi_{18})$	α	E'	
$\chi_{20} = 1/\sqrt{2}(\psi_{11}+\psi_{19})$	β	E'	
$\chi_7 = 1/\sqrt{6}(2\psi_4-\psi_2-\psi_3)$	α	E'	3A - 6B + 3C
$\chi_8 = 1/\sqrt{6}(2\psi_5-\psi_6-\psi_7)$	β	E'	
$\chi_9 = \frac{1}{2}(\psi_9-\psi_{12}-\psi_{17}+\psi_{20})$	ρ_1	E''	
$\chi_{10} = \frac{1}{2}(\psi_9+\psi_{12}-\psi_{17}-\psi_{20})$	ρ_2	E''	
$\chi_{11} = 1/\sqrt{2}(\psi_{10}-\psi_{18})$	α	E'	
$\chi_{12} = 1/\sqrt{2}(\psi_{11}-\psi_{19})$	β	E'	
$\chi_{13} = 1/\sqrt{2}(\psi_{14}-\psi_{15})$	ρ_1	E''	
$\chi_{14} = 1/\sqrt{2}(\psi_{14}+\psi_{15})$	ρ_2	E''	
$\chi_{15} = \psi_{16}$	α	E'	
$\chi_{16} = \psi_{13}$	β	E'	

TABLE 8A

Eigenfunction		Eigenvalue
$E'(\alpha)$	$E'(\beta)$	
$\beta_1 = 1/\sqrt{2}(\phi_1-\phi_{21})$	$\beta_9 = -1/\sqrt{2}(\phi_{16}-\phi_8)$	
$\beta_3 = 1/\sqrt{2}(\phi_4-\phi_{24})$	$\beta_{11} = -1/\sqrt{2}(\phi_{13}-\phi_5)$	3A - 3B
$\beta_5 = 1/\sqrt{2}(\phi_7-\phi_{15})$	$\beta_{13} = -1/\sqrt{2}(\phi_{22}-\phi_2)$	
$\beta_7 = 1/\sqrt{2}(\phi_{10}-\phi_{18})$	$\beta_{15} = -1/\sqrt{2}(\phi_{19}-\phi_{11})$	
$\beta_2 = 1/\sqrt{2}(\phi_1+\phi_{21})$	$\beta_{10} = -1/\sqrt{2}(\phi_{16}+\phi_8)$	
$\beta_4 = 1/\sqrt{2}(\phi_4+\phi_{24})$	$\beta_{12} = -1/\sqrt{2}(\phi_{13}+\phi_5)$	3A - 15B
$\beta_6 = 1/\sqrt{2}(\phi_7+\phi_{15})$	$\beta_{14} = -1/\sqrt{2}(\phi_{22}+\phi_2)$	
$\beta_8 = 1/\sqrt{2}(\phi_{10}+\phi_{18})$	$\beta_{16} = -1/\sqrt{2}(\phi_{19}+\phi_{11})$	
$E''(\rho_1)$	$E''(\rho_2)$	
$\alpha_1 = \frac{1}{2}(\phi_9+\phi_{20}-\phi_{17}-\phi_{12})$	$\alpha_5 = \frac{1}{2}(\phi_9-\phi_{20}-\phi_{17}+\phi_{12})$	3A - 3B
$\alpha_3 = \frac{1}{2}(\phi_6+\phi_{23}-\phi_{14}-\phi_3)$	$\alpha_7 = \frac{1}{2}(\phi_6-\phi_{23}-\phi_{14}+\phi_3)$	
$\alpha_2 = \frac{1}{2}(\phi_9+\phi_{20}+\phi_{17}+\phi_{12})$	$\alpha_6 = \frac{1}{2}(\phi_9-\phi_{20}+\phi_{17}-\phi_{12})$	3A - 15B
$\alpha_4 = \frac{1}{2}(\phi_6+\phi_{23}+\phi_{14}+\phi_3)$	$\alpha_8 = \frac{1}{2}(\phi_6-\phi_{23}+\phi_{14}-\phi_3)$	

TABLE 9

Function	Crystal Field Energy
$\psi_1 \rightarrow \psi_8$	0
$\psi_9 \rightarrow \psi_{12}$	$-\delta$
$\psi_{13} \rightarrow \psi_{16}$	0
$\psi_{17} \rightarrow \psi_{20}$	$+\delta$
$\phi_1 \rightarrow \phi_4$	$\Delta + \frac{2\delta}{3}$
$\phi_5 \rightarrow \phi_{12}$	$\Delta - {}^{\delta}/_{3}$
$\phi_{13} \rightarrow \phi_{16}$	$\Delta + {}^{2\delta}/_{3}$
$\phi_{17} \rightarrow \phi_{24}$	$\Delta - {}^{\delta}/_{3}$

TABLE 10

Matrices of the crystal field operator and $\sum_{i>j} \frac{e^2}{r_{ij}}$

$E''(\rho_1)\ t^3$ $\quad \chi_1, \chi_{13}$ are eigenfunctions with unchanged eigenvalues

	χ_{17}	χ_9
	$3A + 5C$	$-\delta$
	$-\delta$	$3A-6B+3C$

$E'(\alpha)\ t^3$ $\quad \chi_3, \chi_5, \chi_7$, and χ_{15} are eigenfunctions with unchanged eigenvalues.

	χ_{19}	χ_{11}
	$3A + 5C$	$-\delta$
	$-\delta$	$3A - 6B + 3C$

$E''(\rho_1)t^2e$ divides into two 2 x 2 matrices

	α_1	α_2
	$3A - 3B + \Delta - \delta/3$	0
	0	$3A - 15B + \Delta - \delta/3$

	α_3	α_4
	$3A - 3B + \Delta - \delta/3$	$-\delta/2$
	$-\delta/2$	$3A - 15B + \Delta - \delta/3$

$E'(\alpha)\ t^2e$ divides into four 2 x 2 blocks

	β_1	β_2
	$X+\Delta+\delta/6$	$\delta/2$
	$\delta/2$	$Y+\Delta+\delta/6$

	β_3	β_4
	$X+\Delta+\delta/6$	$\delta/2$
	$\delta/2$	$Y+\Delta+\delta/6$

	β_5	β_6
	$X+\Delta+\delta/6$	$-\delta/2$
	$-\delta/2$	$Y+\Delta+\delta/6$

	β_7	β_8
	$X+\Delta-\delta/3$	0
	0	$Y+\Delta-\delta/3$

where $X = 3A - 3B$, $Y = 3A - 15B$

TABLE 11

Eigenfunctions of both the crystal field and electrostatic repulsion operators

$E''(\rho_1)$	$E''(\rho_2)$	eigenvalue
χ_1	χ_2	$3A - 15B$
χ_{13}	χ_4	$3A - 6B + 3C$
$\chi_{17}' = a_1\chi_{17} + b_1\chi_9$	$\chi_{18}' = a_1\chi_{18} + b_1\chi_{10}$	$3A - 3B + 4C + (E^2 + \delta^2)^{\frac{1}{2}}$
$\chi_9' = a_2\chi_{17} + b_2\chi_9$	$\chi_{10}' = a_2\chi_{18} + b_2\chi_{10}$	$3A - 3B + 4C - (E^2 + \delta^2)^{\frac{1}{2}}$
α_1	α_5	$3A - 3B + \Delta - \delta/3$
α_2	α_6	$3A - 15B + \Delta - \delta/3$
$\alpha_3' = a_3\alpha_3 + b_3\alpha_4$	$\alpha_7' = a_3\alpha_7 + b_3\alpha_8$	$3A - 9B + (G^2 + \delta^2)^{\frac{1}{2}} + \Delta + \delta/6$
$\alpha_4' = a_4\alpha_3 + b_4\alpha_4$	$\alpha_8' = a_4\alpha_7 + b_4\alpha_8$	$3A - 9B - (G^2 + \delta^2)^{\frac{1}{2}} + \Delta + \delta/6$

$E'(\alpha)$	$E'(\beta)$	
χ_3	χ_4	$3A - 15B$
χ_5	χ_6	$3A + 5C$
χ_7	χ_8	$3A - 6B + 3C$
χ_{15}	χ_{16}	$3A - 6B + 3C$
$\chi_{19}' = a_1\chi_{19} + b_1\chi_{11}$	$\chi_{20}' = a_1\chi_{20} + b_1\chi_{12}$	$3A - 3B + 4C + (E^2 + \delta^2)^{\frac{1}{2}}$
$\chi_{11}' = a_2\chi_{19} + b_2\chi_{11}$	$\chi_{12}' = a_2\chi_{20} + b_2\chi_{12}$	$3A - 3B + 4C - (E^2 + \delta^2)^{\frac{1}{2}}$
$\beta_1' = +a_3\beta_1 - b_3\beta_2$	$\beta_9' = a_3\beta_9 - b_3\beta_{10}$	$F + \frac{1}{2}(G^2 + \delta^2)^{\frac{1}{2}}$
$\beta_2' = -a_4\beta_1 + b_4\beta_2$	$\beta_{10}' = -a_4\beta_9 + b_4\beta_{10}$	$F - \frac{1}{2}(G^2 + \delta^2)^{\frac{1}{2}}$
$\beta_3' = +a_3\beta_3 - b_3\beta_4$	$\beta_{11}' = a_3\beta_{11} - b_3\beta_{12}$	$F + \frac{1}{2}(G^2 + \delta^2)^{\frac{1}{2}}$
$\beta_4' = -a_4\beta_3 + b_4\beta_4$	$\beta_{12}' = -a_4\beta_{11} + b_4\beta_{12}$	$F - \frac{1}{2}(G^2 + \delta^2)^{\frac{1}{2}}$
$\beta_5' = a_3\beta_5 + b_3\beta_6$	$\beta_{13}' = a_3\beta_{13} + b_3\beta_{14}$	$F + \frac{1}{2}(G^2 + \delta^2)^{\frac{1}{2}}$
$\beta_6' = a_4\beta_5 + b_4\beta_6$	$\beta_{14}' = a_4\beta_{13} + b_4\beta_{14}$	$F - \frac{1}{2}(G^2 + \delta^2)^{\frac{1}{2}}$
β_7	β_{15}	$3A - 3B + \Delta - \delta/3$
β_8	β_{16}	$3A - 15B + \Delta - \delta/3$

where $E = 3B + C$, $F = 3A - 9B$, $G = 12B$
$+\Delta + \delta/6$

ing matrix for the ten spinors is given in Table 12 in units of ζ which is equal to the radial integral $\hbar^2\int R_{n1}^2 \xi(r) r^2 dr$. Here R_{n1} is the radial part of the wave function and ζ is thus positive. We are most interested in calculating the zero field splitting of the ground quartet and a second order spin-orbit coupling calculation should be adequate for this purpose. Accordingly only the top row elements of the spin-orbit coupling matrix have been evaluated and these are also given in Table 12.

Expressions for the zero field splitting can now be written and these are given below, correct to second order in ζ. For χ_1, χ_2 the second order correction to the energy is given by

$$E_1^{(2)} = -\zeta^2\left[\frac{a_1^2}{4E+J} + \frac{a_2^2}{4E-J} + \frac{1}{\Delta - \delta/3} + \frac{2b_3^2}{3(H+K)} + \frac{2b_4^2}{3(H-K)}\right]$$

and for χ_3, χ_4 we have

$$E_2^{(2)} = -\zeta^2\left[\frac{2}{15E} + \frac{a_1^2}{3(4E+J)} + \frac{a_2^2}{3(4E-J)} + \frac{14b_3^2}{9(H+K)} + \frac{14b_4^2}{9(H-K)} + \frac{1}{9(\Delta - \delta/3)}\right]$$

where $E = 3B+C$; $G = 12B$; $H = G/2 + \Delta + \delta/6$ ...(25)

And thus, the zero field splitting is given by

$$E_1^{(2)} - E_2^{(2)} = -\zeta^2\left[\frac{-2}{15E} + \frac{2a_1^2}{3(4E+J)} + \frac{2a_2^2}{3(4E-J)} + \frac{8}{9(\Delta - \delta/3)} - \frac{8b_3^2}{9(H+K)} - \frac{8b_4^2}{9(H-K)}\right] \quad ...(26)$$

χ_3 and χ_4 comprise the "$|\pm\frac{1}{2}\rangle$" doublet and so we can write expressions for the spin-orbit coupling corrections to these wave functions, correct to first order in ζ.

$$\tilde{\chi}_3 = \frac{1}{N}\left[\chi_3 - \zeta\left\{\frac{-2}{5\sqrt{6}E}\chi_5 - \frac{a_1 i}{\sqrt{3}(4E+J)}\chi'_{19} - \frac{a_2 i}{\sqrt{3}(4E-J)}\chi'_{11} + \frac{2ib_3}{\sqrt{6}(F+K)}\beta'_1 + \frac{2ib_4}{\sqrt{6}(F-K)}\beta'_2 - \frac{2\sqrt{2}ib_3}{3(F+K)}\beta'_5 - \frac{2\sqrt{2}ib_4}{3(F-K)}\beta'_6 - \frac{\beta_8}{3\Delta - \delta}\right\}\right] \quad ...(27)$$

$$\tilde{\chi}_4 = \frac{1}{N}\left[\chi_4 + \zeta\left\{(\ )\chi_6 + (\ )\chi'_{20} + (\ )\chi'_{12} + (\ )\beta'_9 + (\ )\beta'_{10} - (\ )\beta'_{13} - (\ )\beta'_{14} - (\ )\beta_{16}\right\}\right]$$

where $(E^2+\delta^2)^{\frac{1}{2}} = J$ and $\frac{1}{2}(G^2+\delta^2)^{\frac{1}{2}} = K$, and N = normalization constant.

TABLE 12

Matrix of $\underline{l}.\underline{s}$ in the one-electron spinor basis

$\underline{\ell}.\underline{s}$	$\overset{+}{t}_o$	$\bar{t}_o$	$\bar{t}_+$	$\overset{+}{t}_-$	$\overset{+}{t}_+$	$\bar{t}_-$	$\overset{+}{e}_+$	$\bar{e}_+$	$\overset{+}{e}_-$	$\bar{e}_-$
$\overset{+}{t}_o$	o	o	$i/\sqrt{2}$	o	o	o	o	$-i$	o	o
$\bar{t}_o$	o	o	o	$-i/\sqrt{2}$	o	o	o	o	i	o
$\bar{t}_+$	$-i/\sqrt{2}$	o	$\frac{1}{2}$	o	o	o	o	$1/\sqrt{2}$	o	o
$\overset{+}{t}_-$	o	$i/\sqrt{2}$	o	$\frac{1}{2}$	o	o	o	o	$1/\sqrt{2}$	o
$\overset{+}{t}_+$	o	o	o	o	$-\frac{1}{2}$	o	$-1/\sqrt{2}$	o	o	i
$\bar{t}_-$	o	o	o	o	o	$-\frac{1}{2}$	i	o	o	$-1/\sqrt{2}$
$\overset{+}{e}_+$	o	o	o	o	$-1/\sqrt{2}$	$-i$	o	o	o	o
$\bar{e}_+$	i	o	$1/\sqrt{2}$	o	o	o	o	o	o	o
$\overset{+}{e}_-$	o	$-i$	o	$1/\sqrt{2}$	o	o	o	o	o	o
$\bar{e}_-$	o	o	o	o	$-i$	$-1/\sqrt{2}$	o	o	o	o

Spin-orbit coupling matrix elements for the lowest energy quartet and the higher energy functions.

For E''(ρ_1), (E''(ρ_2) in brackets

	$\chi_1(\chi_2)$	$\chi_{17}'(\chi_{18}')$	$\chi_9'(\chi_{10}')$	$\chi_{13}(\chi_{14})$	$\alpha_1(\alpha_5)$	$\alpha_2(\alpha_6)$	$\alpha_3'(\alpha_7')$	$\alpha_4'(\alpha_8')$
$\chi_1(\chi_2)$	(3A-15B)	$-i\zeta a_1$	$-\zeta a_2 i$	0	0	ζ	$\frac{2ib_3\zeta}{\sqrt{6}}$	$\frac{2ib_4\zeta}{\sqrt{6}}$

and for E'α (E'β in brackets)

	$\chi_3(\chi_4)$	$\chi_5(\chi_6)$	$\chi_7(\chi_8)$	$\chi_{15}(\chi_{16})$	$\chi_{19}'(\chi_{20}')$	$\chi_{11}'(\chi_{12}')$
$\chi_3(\chi_4)$	(3A-15B)	$\frac{-2\zeta}{\sqrt{6}}$	0	0	$\frac{a_1 i\zeta}{\sqrt{3}}$	$\frac{a_2 i\zeta}{\sqrt{3}}$

	$\beta_1'(\beta_9')$	$\beta_2'(\beta_{10}')$	$\beta_3'(\beta_{11}')$	$\beta_4'(\beta_{12}')$	$\beta_5'(\beta_{13}')$	$\beta_6'(\beta_{14}')$	$\beta_7(\beta_{15})$	$\beta_8(\beta_{16})$
$\chi_3(\chi_4)$	$\frac{-2ib_3\zeta}{\sqrt{6}}$	$\frac{-2ib_4\zeta}{\sqrt{6}}$	0	0	$\frac{2\sqrt{2}ib_3\zeta}{3}$	$\frac{2\sqrt{2}ib_4\zeta}{3}$	0	$-\zeta/3$

In order to calculate g-values for this doublet we have to find eigenvalues of the Zeeman operator.

$$\mathcal{H}_z = \beta_e \underline{H} \cdot \left(\sum_i \underline{l}_i + g_e \sum_i \underline{s}_i \right)$$

If, for a given direction of the applied magnetic field we have eigenvalues of $x\,\beta_e H$ and $y\,\beta_e H$ then $g_\theta = x-y$.

For the axial system under consideration it is sufficient to calculate only two principal values for g, $g_{//}$ and $g_\perp$, where $g_\perp$ equals either g_x or g_y. In order to make these calculations, matrix elements of l_z and l_x are needed in the $t_\pm$, t_o, $e_\pm$ basis and these are given in Table 13. The matrices of the Zeeman operator in the doublet for $H /\!/ z$ and $H /\!/ x$ are

$$\langle \; | \text{"z"} | \; \rangle = \frac{1}{N^2} \begin{pmatrix} & \chi_3 & \chi_4 \\ \chi_3 & A + g_e B & 0 \\ \chi_4 & 0 & -(A + g_e B) \end{pmatrix}$$

$$\langle \; | \text{"x"} | \; \rangle = \frac{1}{N^2} \begin{pmatrix} & \chi_3 & \chi_4 \\ \chi_3 & 0 & C + g_e D \\ \chi_4 & C + g_e D & 0 \end{pmatrix}$$

where A, B, C and D are all real. Calculations were taken to second order in ζ, but it was found that only the first order terms were significant and that N was effectively unity. B and D contain only zeroth and second order terms, and these latter were found to be negligible. Thus to first order

$$A = -(4\zeta)/(3\Delta - \delta)$$

$$B = 0.5$$

$$C = -(8\zeta/3)\left\{ \frac{b_3^2}{H+K} + \frac{b_4^2}{H-K} \right\}$$

$$D = 1.0$$

and the resulting g-values are

$$g_{//} = 2(g_e B + A) = g_e + 2A$$

$$g_\perp = 2(g_e D + C) = 2g_e + 2C \qquad \ldots(28)$$

TABLE 13

Matrices of l_z and l_x in the one-electron orbital basis

ℓ_z	t_o	t_+	t_-	e_+	e_-
t_o	o	o	o	o	o
t_+	o	-1	o	$-\sqrt{2}$	o
t_-	o	o	1	o	$\sqrt{2}$
e_+	o	$-\sqrt{2}$	o	o	o
e_-	o	o	$\sqrt{2}$	o	o

ℓ_x	t_o	t_+	t_-	e_+	e_-
t_o	o	$i/\sqrt{2}$	$-i/\sqrt{2}$	-i	i
t_+	$-i/\sqrt{2}$	o	o	o	i
t_-	$i/\sqrt{2}$	o	o	i	o
e_+	i	o	-i	o	o
e_-	-i	-i	o	o	o

Similar calculations for the "$|\pm 3/2\rangle$" doublet lead to equivalent formulae for the apparent g-values. Since E.S.R. transitions for this doublet could only be observed at $\theta = 90^{o}$, then only the expression for $g_{\perp}$ was calculated. To second order this was found to be identically zero, indicating no splitting of the doublet for this orientation. In fact transitions were observed indicating some splitting and this will be discussed later with the rest of the numerical results.

B. Hyperfine Coupling Calculations

Term ($\mathcal{H}_{SI}$) of Equ. #1 may be treated by the equivalent operator technique and can be shown (6) to reduce to

$$\mathcal{H} = P(\underline{L}.\underline{I} - k\underline{S}.\underline{I} + [1/7]\sum_{k=1}^{N} \underline{a}_k.\underline{I}) \qquad \ldots(29)$$

where $\underline{a}_k = 4\underline{s}_k - (\underline{l}_k.\underline{s}_k)\underline{l}_k - \underline{l}_k(\underline{l}_k.\underline{s}_k)$

and $P = g_e g_N \beta_e \beta_N \langle r^{-3} \rangle$

We may write this as

$$\mathcal{H} = P(\underline{l} + [1/7]\,\underline{a}_k).\underline{I} - Pk\underline{s}.\underline{I}$$
$$= \mathcal{H}_{\text{dipolar}} + \mathcal{H}_{\text{contact}}$$

where $\underline{l}$ and $\underline{a}$ are sums of one electron operators. The first term becomes, on expansion,

$$\mathcal{H}_{\text{dipolar}} = P\left\{(l_x+[1/7]\,a_x)I_x+(a_y+[1/7]a_y)I_y+(l_z+[1/7]\,a_z)I_z\right\} \qquad \ldots(30)$$

Now Griffith (6) has shown that for an operator ρ which obeys the conditions $\rho = \bar{\rho} = \rho^{*}$ we have the following form of matrix within a Kramers doublet (α,β)

ρ	α	β
α	c	a + ib
β	a - ib	c

with a, b and c real.

The operator $2aS_x + 2bS_y + 2cS_z$ has exactly this matrix within $|+\tfrac{1}{2}\rangle$, $|-\tfrac{1}{2}\rangle$. Thus any operator ρ which satisfies the above conditions may be represented by a linear form in the components of S, having real coefficients. In particular

$$\mathcal{H}(s) = AS_zI_z + BS_xI_x + CS_zI_z$$

and $$\mathcal{H} = P(\underline{1} + (1/7)\underline{a}).\underline{I} - Pk\ \underline{S}.\underline{I}$$

are covered by this treatment.

We now wish to compare these three forms of the Hamiltonian, and we will consider first the z components.

$$2\langle\alpha|\rho|\alpha\rangle S_z = 2cS_z = AS_z$$

where ρ is given by Equ. #30

Thus $2P\langle\alpha|1_z + (1/7)a_z|\alpha\rangle\ I_zS_z = AS_zI_z$

and so

$$A = 2P(\langle\alpha|1_z + (1/7)a_z|\alpha\rangle)$$

We have seen that $2\langle\alpha|1_z|\alpha\rangle = \Delta g_{zz}$ to first order, and so

$$A = P(\Delta g_{zz} + (2/7)\langle\alpha|a_z|\alpha\rangle)$$

It may be shown similarly that

$$B = P(\Delta g_{xx} + (2/7)\langle\beta|a_x|\alpha\rangle)$$

$$C = P(\Delta g_{yy} + (2i/7)\langle\alpha|a_y|\beta\rangle)$$

For an axial system with B = C, $\Delta g_{xx} = \Delta g_{yy}$

$$A_{\parallel} = P(\Delta g_{\parallel} + (2/7)\langle\alpha|a_z|\alpha\rangle)$$

$$A_{\perp} = P(\Delta g_{\perp} + (1/7)\langle\beta|a_-|\alpha\rangle) \qquad \ldots(31)$$

In order to make comparison with the experimentally observed results we have to estimate the two matrix elements above, with

$$|\alpha\rangle = \tilde{\chi}_3$$

$$|\beta\rangle = \tilde{\chi}_4$$

from our previous calculation. Tables 14 and 15 give the matrices of a_z and a_- within the basis $t_\pm$, t_o, $e_\pm$, compiled with the help of Table A.41, Appendix 2, of reference 6.

To zeroth order a_z and a_- have vanishing matrix elements within α and β. This is to be expected since the zeroth order functions are equivalent to one electron occupying each of the d_{xy}, d_{yz}, d_{xz} orbitals and this spherically symmetric situation should average dipolar contributions to zero. To first order in ζ the matrix elements are

$$\langle\alpha|a_z|\alpha\rangle = (\zeta/3)(2\sqrt{6}/(4E+J) + (2P_4-P_1)/3 + (P_2-P_1))$$

$$\langle\beta|a_-|\alpha\rangle = (\zeta/3)(4P_5 + 8P_3 + 1/(3\Delta - \delta))$$

where $P_1 = a_1(a_1 + b_1)/(4E + J) + a_2(a_2 + b_2)/(4E - J)$

$P_2 = a_1(a_1 - b_1)/(4E + J) + a_2(a_2 - b_2)/(4E - J)$

$P_3 = a_3b_3/(H + K) + a_4b_4/(H - K)$

$P_4 = b_3(a_3 - b_3)/(H + K) + b_4(a_4 - b_4)/(H - K)$

$P_5 = a_1b_1/(4E + J) + a_2b_2/(4E - J)$

TABLE 14

Matrix of a_z in the one-electron spinor basis

a_z	$\overset{+}{t}_o$	$\overset{-}{t}_o$	$\overset{+}{t}_+$	$\overset{-}{t}_+$	$\overset{+}{t}_-$	$\overset{-}{t}_-$	$\overset{+}{e}_+$	$\overset{-}{e}_+$	$\overset{+}{e}_-$	$\overset{-}{e}_-$
$\overset{+}{t}_o$	2	o	o	$-i/\sqrt{2}$	o	o	o	i	o	o
$\overset{-}{t}_o$	o	-2	o	o	$-i/\sqrt{2}$	o	o	o	i	o
$\overset{+}{t}_+$	o	o	-1	$[1/\sqrt{2}](1+i)$	o	$-\sqrt{2}i$	$-\sqrt{2}$	$\frac{1}{2}(1+i)$	o	$\frac{1}{2}(3+i)$
$\overset{-}{t}_+$	$i/\sqrt{2}$	o	$[1/\sqrt{2}](1-i)$	1	o	o	$-(1-i)$	$\sqrt{2}$	o	o
$\overset{+}{t}_-$	o	$i/\sqrt{2}$	o	o	-1	$[-1/\sqrt{2}](1-i)$	o	o	$\sqrt{2}$	1-i
$\overset{-}{t}_-$	o	o	$\sqrt{2}i$	o	$[-1/\sqrt{2}](1+i)$	1	$-\frac{1}{2}(3+i)$	o	$-\frac{1}{2}(1+i)$	$\sqrt{2}$
$\overset{+}{e}_+$	o	o	$-\sqrt{2}$	$-(1+i)$	o	$-\frac{1}{2}(3-i)$	o	$[-1/\sqrt{2}](1+i)$	o	$\sqrt{2}i$
$\overset{-}{e}_+$	-i	o	$\frac{1}{2}(1-i)$	$\sqrt{2}$	o	o	$[-1/\sqrt{2}](1-i)$	o	o	o
$\overset{+}{e}_-$	o	-i	o	o	$-\sqrt{2}$	$-\frac{1}{2}(1-i)$	o	o	o	$[1/\sqrt{2}](1-i)$
$\overset{-}{e}_-$	o	o	$\frac{1}{2}(3-i)$	o	1+i	$\sqrt{2}$	$-\sqrt{2}i$	o	$[1/\sqrt{2}](1+i)$	o

TABLE 15

Matrix of a_- in the one-electron spinor basis

a_-	$\overset{+}{t}_o$	$\overset{-}{t}_o$	$\overset{+}{t}_+$	$\overset{-}{t}_+$	$\overset{+}{t}_-$	$\overset{-}{t}_-$	$\overset{+}{e}_+$	$\overset{-}{e}_+$	$\overset{+}{e}_-$	$\overset{-}{e}_-$
$\overset{+}{t}_o$	0	0	$-i/\sqrt{2}$	$-2(1-i)$	0	$2(1+i)$	i	$-\sqrt{2}(1-i)$	0	$\sqrt{2}(1+i)$
$\overset{-}{t}_o$	-2	0	0	$i/\sqrt{2}$	0	0	0	$-i$	0	0
$\overset{+}{t}_+$	0	$-2(1-i)$	$\{1/\sqrt{2}(1+i)$	0	$-\sqrt{2}i$	0	$\frac{1}{2}(1-i)$	0	$\frac{1}{2}(3+i)$	0
$\overset{-}{t}_+$	0	0	1	$\{-1/\sqrt{2}(1+i)$	0	$\sqrt{2}i$	$\sqrt{2}$	$-\frac{1}{2}(1+i)$	0	$-\frac{1}{2}(3+i)$
$\overset{+}{t}_-$	$i/\sqrt{2}$	$2(1+i)$	0	2	$\{-1/\sqrt{2}(1-i)$	0	0	$-2\sqrt{2}$	$1-i$	0
$\overset{-}{t}_-$	0	$-i/\sqrt{2}$	0	0	1	$\{1/\sqrt{2}(1-i)$	0	0	$\sqrt{2}$	$-(1-i)$
$\overset{+}{e}_+$	0	$-\sqrt{2}(1-i)$	$-(1+i)$	0	$-\frac{1}{2}(3-i)$	0	$\{1/\sqrt{2}(1-i)$	0	$\sqrt{2}i$	0
$\overset{-}{e}_+$	0	0	$\sqrt{2}$	$1+i$	0	$\frac{1}{2}(3-i)$	0	$\{1/\sqrt{2}(1+i)$	0	$-\sqrt{2}i$
$\overset{+}{e}_-$	$-i$	$\sqrt{2}(1+i)$	0	$-2\sqrt{2}$	$-\frac{1}{2}(1-i)$	0	0	4	$\{1/\sqrt{2}(1-i)$	0
$\overset{-}{e}_-$	0	i	0	0	$\sqrt{2}$	$\frac{1}{2}(1-i)$	0	0	0	$\{-1/\sqrt{2}(1-i)$

6. Discussion

Before comparing the experimental results with the foregoing theoretical calculations and the survey of previous work, it would seem useful to establish the relationship between the principal g-values obtained from the spin Hamiltonian of Equ. #16, where the spin manifold was a quartet, and the apparent g-values obtained by considering just the $|\pm\frac{1}{2}\rangle$, $|\pm 3/2\rangle$ states as Kramers' doublets. From fitting the experimental results to the quartet Hamiltonian, we find $g_{//} = 1.9920$ and $g_{\perp} = 1.9880$; whereas the apparent g-values, which are those calculated by the ligand field method are from Equ. #28, $g'_{//} \sim g_e$ and $g'_{\perp} \sim 2g_e$. Thus straight away we can compare the two values for $g_{//}$, but we have to reconsider the situation for $g_{\perp}$.

We may write the matrix of Equ. #18 in the basis $|\pm\frac{1}{2}\rangle$, $|\pm 3/2\rangle$ as

+3/2	-3/2	+1/2	-1/2
$D + 3G_{//}/2$	0	$\sqrt{3}G_{\perp}/2$	0
0	$D - 3G_{//}/2$	0	$\sqrt{3}G_{\perp}/2$
$\sqrt{3}G_{\perp}/2$	0	$-D + G_{//}/2$	$G_{\perp}$
0	$\sqrt{3}G_{\perp}/2$	$G_{\perp}$	$-D - G_{//}/2$

where $G_{//} = g\beta_e H\cos\theta$ and $G_{\perp} = g\beta_e H\sin\theta$

Using the method of matrix partitioning (65) we may replace the element H_{rs} by

$$\tilde{H}_{rs} = H_{rs} + \sum_t \frac{H_{rt}H_{ts}}{E_r^o - E_t^o}$$

and this leads to the following matrix, correct to second order, where the basis is now two isolated doublets $|\pm 3/2\rangle$ and $|\pm\frac{1}{2}\rangle$

$+3/2$	$-3/2$	$+1/2$	$-1/2$
$D+3/2G_{\parallel}+3G_{\perp}^2/8D$	0	0	0
0	$D-3/2G_{\parallel}+3G_{\perp}^2/8D$	0	0
0	0	$-D+\frac{1}{2}G_{\parallel}+3G_{\perp}^2/8D$	$G_{\perp}$
0	0	$G_{\perp}$	$-D-\frac{1}{2}G_{\parallel}+3G_{\perp}^2/8D$

Thus the apparent splitting of the $|+\frac{1}{2}\rangle$, $|-\frac{1}{2}\rangle$ states is given by the solution of the lower 2 x 2 determinant.

$$(-D + 3G_{\perp}^2/8D - E)^2 - G_{\parallel}^2/4 - G_{\perp}^2 = 0$$

therefore $$E = -D + 3G_{\perp}^2/8D \pm \sqrt{G_{\parallel}^2/4 + G_{\perp}^2}$$

For $H /\!/$ to z then $G_{/\!/} = g\beta_e H$ and $G_{\perp} = 0$; so $E = \pm G_{\parallel}/2 = \pm g_{\parallel}\beta_e H/2$ and the splitting is $g_{/\!/}\beta_e H$, i.e. an effective g-value of $g_{/\!/}$. But for $H \perp z$ then $G_{\perp} = g_{\perp}\beta_e H$ and $G_{\parallel} = 0$ so $E = \pm G_{\perp} = \pm g_{\perp}\beta_e H$ and the splitting is $2g_{\perp}\beta_e H$, i.e. an effective g-value of $2g_{\perp}$. By inspection the effective g-values of the other doublet $|\pm 3/2\rangle$ and $|-3/2\rangle$ are given by

$$g'_{/\!/} = 3g_{/\!/} \quad \text{and} \quad g'_{\perp} = 0$$

With these results in mind, we may now proceed to compare the experimental results for D, g and A with the calculated values.

The equations for zero field splitting and apparent g-values are expressed in terms of the parameters B, C, δ, Δ and ζ. We make the approximation that C = 4B (62) and that Δ may be taken as approximately 22,000 cm^{-1} from other studies on the $[MnO_6]$ system (11-22). This leaves the parameters B, δ and ζ which are to be determined. For a strict crystal field calculation it would be correct to take the free ion values for B and ζ. However, this would neglect all co-

valency effects and these are not negligible in complexes with oxygen as ligands (59) and are observed in the present system as superhyperfine lines, visible in Fig. 6 which will be discussed in more detail later. In view of the approximations (see Section 2B) involved in using a sum over one electron operators for ζ this parameter is taken as isotropic with a value fairly close to that of the free ion (Mn^{4+}; ζ = 402 cm^{-1}) (6). The electron repulsion parameter B is much more susceptible to electron delocalization effects and is thus taken as a variable parameter in the calculations, with values up to that for the free ion (1060 cm^{-1}) (6). δ, the effective one-electron trigonal field, is left to be determined.

The previous calculations of McGarvey mentioned, indicated that an approximate formula for 2D is given by (for small trigonal fields):

$$2D \sim 8\lambda^2 \left(1/E(^4E) - 1/E(^4A_1)\right) + 6\lambda^2 \left(1/E(^2A_1) - 1/E(^2E)\right)$$

$$= 8\lambda^2 \left(1/\Delta_{\parallel} - 1/\Delta_{\perp}\right) + 6\lambda^2 \left(1/E(^2A_1) - 1/E(^2E)\right)$$

$$\sim 8\lambda^2 K/\Delta_{\parallel}^2 + 6\lambda^2 \left(1/E(^2A_1) - 1/E(^2E)\right) \qquad \ldots(32)$$

which is very similar in form to that given by Lohr and Lipscomb (58). In fact, assuming their $\lambda_{\parallel}$ and $\lambda_{\perp}$ to be defined in a similar manner to those of Sugano and Tanabe (54), their formulae differ by a factor of two from the above. It will be noticed that the term $8\lambda^2 K/\Delta_{\parallel}^2$ is that derived by Van Vleck and others. Lohr and Lipscomb's work gives a value of about $15\lambda^2 K/\Delta_{\parallel}^2$ for this term, and this seems to be in error for the same reasons as the treatment of Sugano and Tanabe. The second term of Equ. #32 is similarly half that of Lohr and Lipscomb.

The detailed formula from the present work, Equ. #26, reduces to

the following for small δ when

$a_1 \sim 1 : a_2 \sim 0 : b_3 \sim 0 : b_4 \sim 1$ (see Table 10)

Thus $2D \sim -(2/3)\zeta^2(1/E(^2E) + 4/3(E(^4A_1)) - 1/E(^2A_1) - 4/3(E(^4E)))$

$= -(2/3)\zeta^2(1/E(^2E) - 1/E(^2A_1)) - (8/9)\zeta^2(1/E(^4A_1) - 1/(^4E))$

$= (6/9)\zeta^2(1/E(^2A_1) - 1/E(^2E)) + (8/9)\zeta^2(1/E(^4E) - 1/E(^4A_1))$

$= 6\lambda^2(1/E(^2A_1) - 1/E(^2E)) + 8\lambda^2(1/E(^4E) - 1/E(^4A_1))$

when $\zeta = 3\lambda$

which is McGarvey's formula, Equ. #32 above, for very small δ, and it is felt that these are fairly equivalent descriptions, although that of McGarvey differs from the present work in using more empirical parameters. It may be noted in passing, that there is an error or misprint in McGarvey's paper. The last + sign of Equation #23, Page 3754 should in fact be -.

By substituting values of 400 cm^{-1} (6) and 22,000 cm^{-1} for ζ and Δ respectively in Equ. #26 and varying B and δ, several values of the Z.F.S. were obtained. The experimental value of 2D is $\pm$1.72 cm^{-1} and the nearest approaches to this value were obtained as shown below.

B	δ	Z.F.S.
500	5000	-1.67
600	6000	-1.65
700	7000	-1.67
800	8000	-1.73

B	δ	Z.F.S.
900	8900	-1.82
1000	9800	-1.79

A graph of the energies of the first eight excited states calculated using these parameter values is shown in Fig. 17. The optical spectrum of the manganese polymolybdate has been observed (46, 47) and this is shown in Fig. 18. The first spin-allowed transition occurs at about 21,500 cm^{-1} and there is a small spin-forbidden doublet at about 14,500 cm^{-1}. It can be seen from Fig. 17 that the energies calculated for B = 700 cm^{-1} and δ = 7000 cm^{-1} fit these observed values quite well. The small splitting of the line at 14,500 cm^{-1} is probably due to sub-shell configuration mixing of the two states labelled $^2E_2(^2T_1)$ and $^2A_2(^2T_1)$ in the D_3 classification. The measured splitting is 640 cm^{-1}. We may compare this with the theoretical expression given by Jorgensen (62) which is $66B^2/\Delta$ with the $^2E(^2T_1)$ the lower. For B = 700 cm^{-1} and Δ = 22,000 cm^{-1} this expression gives a value of 1470 cm^{-1}, which is larger than the experimental value. However, the graph on Page 261 of reference #6 for this splitting indicates a smaller value, more in line with that observed.

The strong peak at 21,500 cm^{-1} is very broad and may consist of transitions to both the $^4A(^4T_2)$ and $^4E(^4T_2)$ states, since both transitions are formally allowed. A more highly resolved spectrum taken in polarised light would have been desirable, but unfortunately the crystals were very fragile at low temperatures and this could not be obtained (47).

This interpretation is open to the objection that the $^2E_1(^2T_1)$ level could well be the one to which the spin-forbidden transition

FIGURE 17 : Variation of the energy levels with the combination of parameters which give a Z.F.S. of approximately 1.7 cm^{-1}. ($^4A_2$ defined as 0)

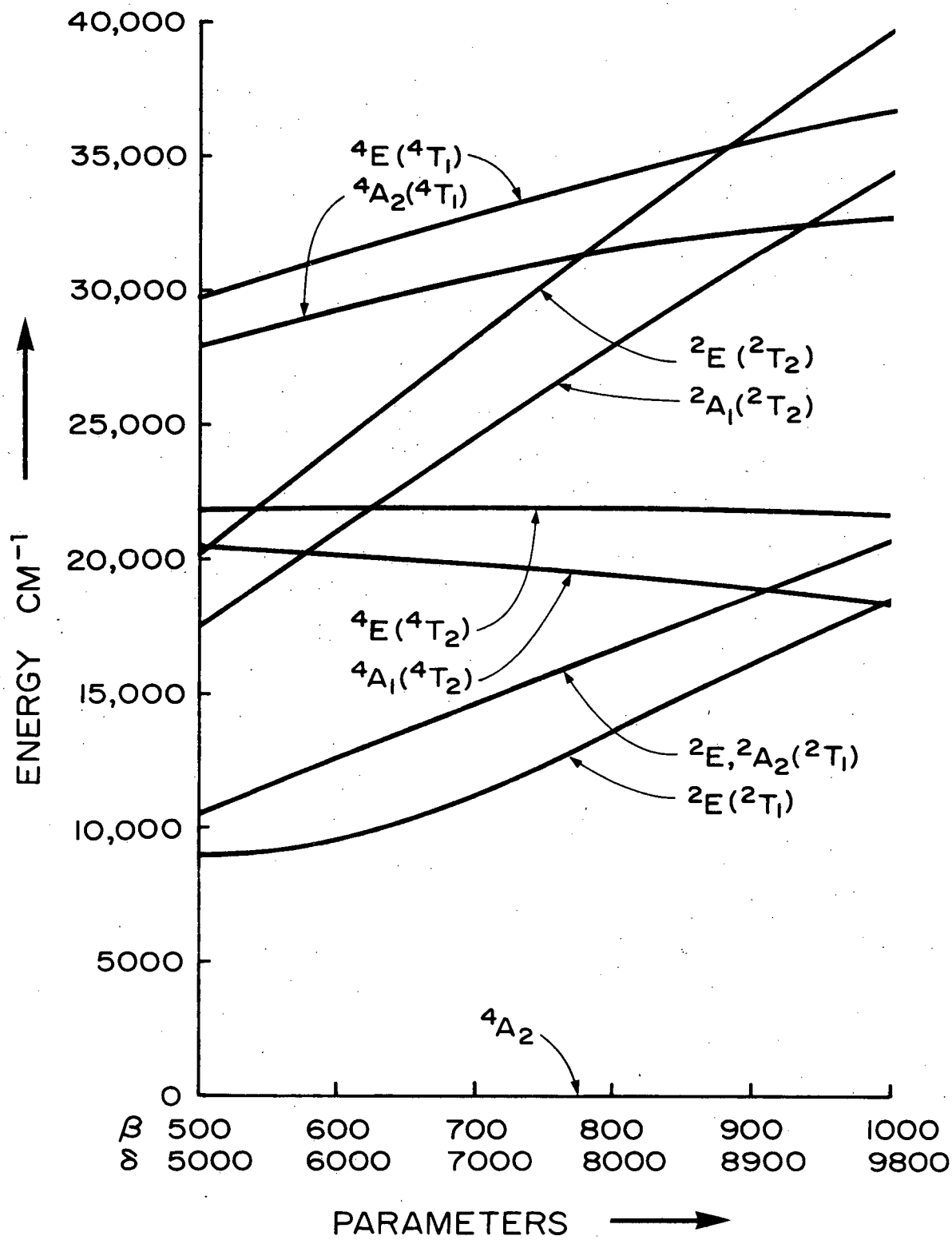

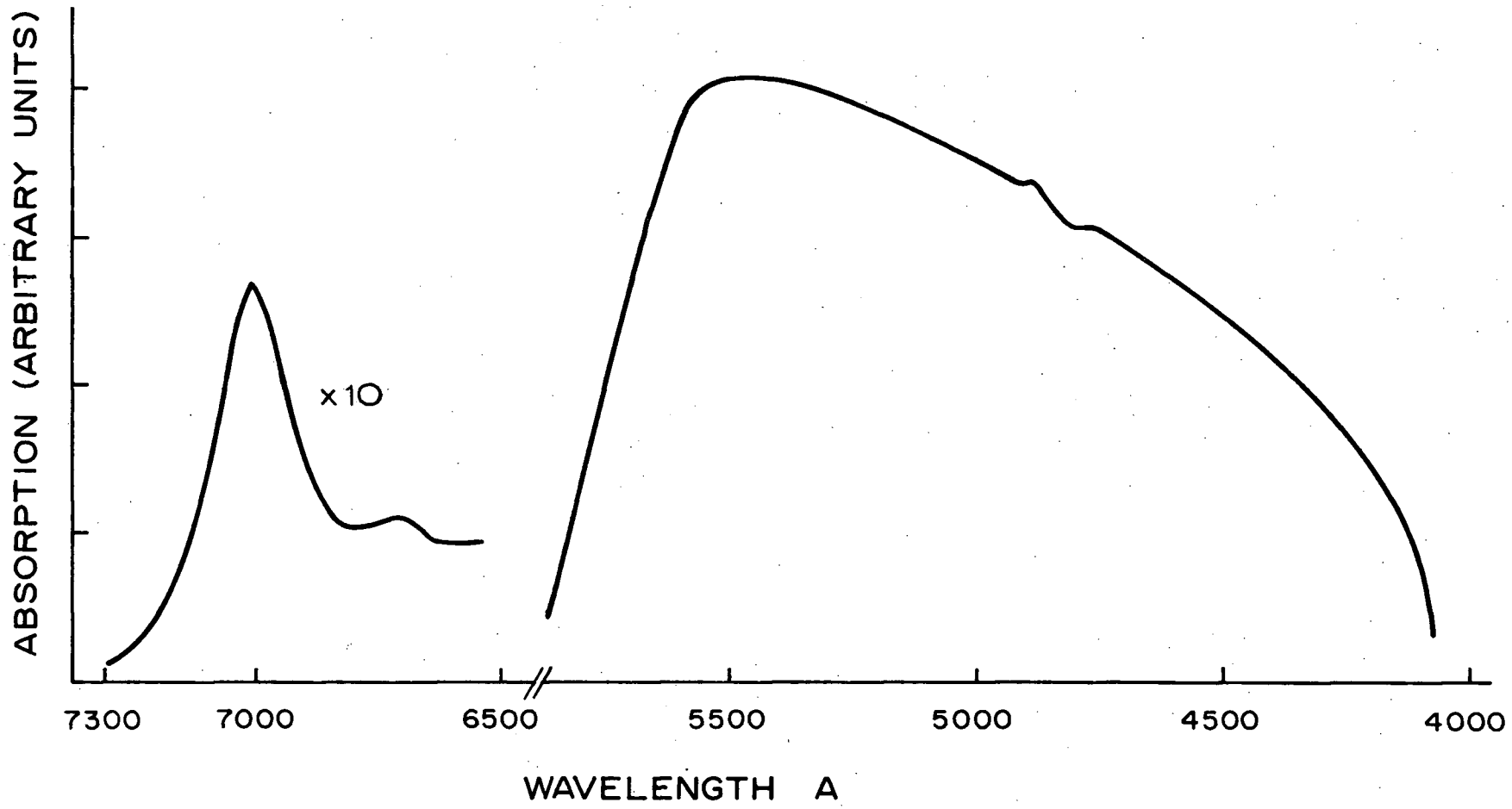

FIGURE 18 : Visible absorption spectrum of ammonium 9-molybdomanganate

occurred as this would be correct for values of B = 900 cm^{-1} and δ = 9000 cm^{-1}. However, there is no easily seen mechanism for this state to give rise to a doublet splitting and so the former discussion seems valid.

The value of δ, approximately 7000 cm^{-1} is very high, but in view of the very strong axial field produced by the molybdenum-centred octahedra in the structure of the ion, this high value is quite acceptable.

There is no a priori reason for choosing δ to be positive, since the splitting of the one electron orbitals could well be in the opposite direction to that indicated in Fig. 13 and the t_o orbital could well have higher energy than the t_+ and t_- orbitals. Calculations were also made with δ assumed negative in Equ.#26, but it was found not possible to produce a large zero field splitting with reasonable values of B and δ. It would thus seem that δ must be positive in this case, and thus also that the $|\pm 3/2\rangle$ states have lower energy than the $|\pm\frac{1}{2}\rangle$ doublet, since 2D is negative.

Applying the two chosen values of B and δ to Equ. #28 for the calculation of $g_{//}$ and $g_{\perp}$ it was found that $g_{//} = 1.950$ and $g'_{\perp} = 3.91$ ($g_{\perp} = 1.955$). These deviations from g_e are much larger than those observed experimentally. McGarvey (59) has suggested that a very important contribution to the g-factor, and which produces a positive contribution to g, is the effect produced by those states resulting from the promotion of an electron from the filled ligand-metal molecular orbitals to the d orbitals of the metal. It is not possible to calculate the size of this effect using the current scheme, although a molecular orbital treatment would be very illuminating, perhaps carried out along the lines of Maki and McGarvey's (66) d^1 calculation,

the only drawback being the much larger amount of book-keeping necessary for a d^3 system and consequent determinantal functions.

We may also use the fitted values of B and δ to make an estimate of the size of the dipolar contribution to the hyperfine coupling tensor. The matrix elements in Equ. #31 were calculated and their values to second order are

$$\langle \tilde{\chi}_3 | a_z | \tilde{\chi}_3 \rangle = 0.015$$
$$\langle \tilde{\chi}_4 | a_- | \tilde{\chi}_3 \rangle = 0.016$$

Since the g-values predicted by the ligand field theory are in such poor agreement with experiment it was decided to use those from experiment. Substitution in Equ. #31 gives

$$A_{//} = \pm 0.0076 = P(-0.010 + \tfrac{2}{7}(0.015)) - Pk$$
$$A_{\perp} = \pm 0.0068 = P(-0.050 + \tfrac{1}{7}(0.016)) - Pk$$

There is an ambiguity of sign for the components of A as measured by E.S.R. and this is indicated above. Since the values are nearly isotropic then $A_{//}$ and $A_{\perp}$ must have the same sign, but this may be + or -. The free ion value of P is $+0.024\ cm^{-1}$ and this will produce a difference in the dipolar terms of $A_{//}$ and $A_{\perp}$ of $\pm 0.0010\ cm^{-1}$.

This compares favourably with the experimental value of $\pm 0.0008\ cm^{-1}$ and so we can justifiably solve equations (33) for approximate values of P and Pk. Choosing both $A_{//}$ and $A_{\perp}$ to be positive then, we find

$$P = +0.02\ cm^{-1};\quad Pk = -0.0078\ cm^{-1}$$

and for both $A_{//}$ and $A_{\perp}$ negative

$$P = -0.02\ cm^{-1};\quad Pk = +0.0078\ cm^{-1}$$

Now P, being a radial integral, must necessarily be positive and so this latter result is not admissable. The ratio Pk/P is -0.39 which is consistent with the values for most first row transition metals (6).

The small lines observed at the wings and in the centre of the

spectrum in Fig. 6 need to be explained. These cannot arise from any form of "forbidden" transition, since such lines would necessarily lie within the outer two strong manganese lines. A good possibility is that they are superhyperfine lines due to delocalization of the manganese d-electrons onto the surrounding molybdenum nuclei. The lines are not observable for all orientations, probably due to overlapping with the wide manganese lines, and so it was not possible to make any definite measurement of their variation with angle. It is hoped that an ENDOR study of this system could clarify this situation (67).

Molybdenum has three naturally occurring isotopes, of which one (^{96}Mo) has zero nuclear spin and would thus not give extra superhyperfine lines. The other two isotopes ^{95}Mo and ^{97}Mo both have nuclear spin of 5/2 and magnetic moments within 2% of each other. Thus we can treat them, effectively, as one isotope whose abundance is approximately 25%.

Since there are nine molybdenum nuclei around the central manganese then it is a problem in probabilities to calculate the possible spectra resulting from various possible occupation of these nine sites by zero spin or 5/2 spin nuclei.

PART II

E.S.R. of X-Ray Irradiated Single Crystals of Deuterated Ammonium Paramolybdate Tetrahydrates

1. Introduction

The E.S.R. spectrum of ammonium paramolybdate tetrahydrate was measured recently (34) and this work was carried out to verify that the observed doublet super-hyperfine splittings were in fact due to a hydrogen nucleus near the central molybdenum.

2. Experimental

Single crystals were readily grown from D_2O and a typical crystal is shown in Fig. 19 together with the chosen axes for the monoclinic class. Lindquist (68) determined the crystal structure and the present axis system differs from his in the choice of the a axis, since an orthogonal right-handed set is most useful for the purposes of experiment. The crystals were irradiated with 50 kv. x-rays at room temperature for one hour and a discolouration of the material after irradiation was noticed, this being typical of crystals with disrupted electronic structure. The crystal was rotated about the a, b and c axes and spectra were obtained at 15^{o} intervals. The method of mounting the crystal consists of a small perspex device with three mutually perpendicular faces and each of these can be mounted with their plane parallel to the direction of the magnetic field.

The spectra were obtained at room temperature on a standard x-band spectrometer described previously (69) and a typical spectrum is shown in Fig. 20. This shows the single strong central line due to the molybdenum isotope (^{96}Mo) with zero nuclear spin and six outer lines due to

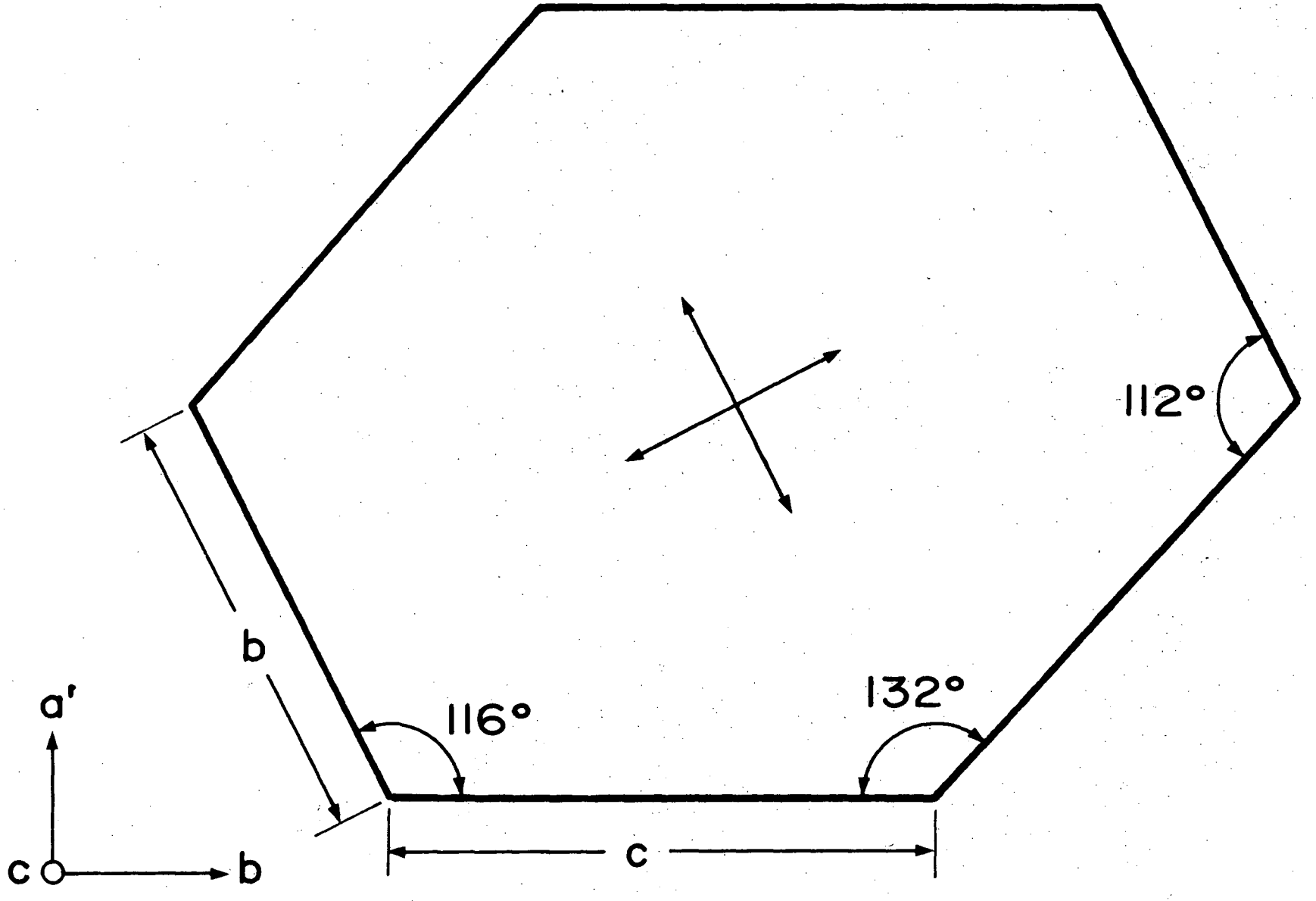

FIGURE 19 : A typical crystal of ammonium paramolybdate, showing the chosen axis-system. The cross in the centre indicates the extinction positions under polarised light

FIGURE 20 : An E.S.R. spectrum of an irradiated single crystal of deuterated ammonium paramolybdate tetrahydrate, with the magnetic field in the a' - c plane

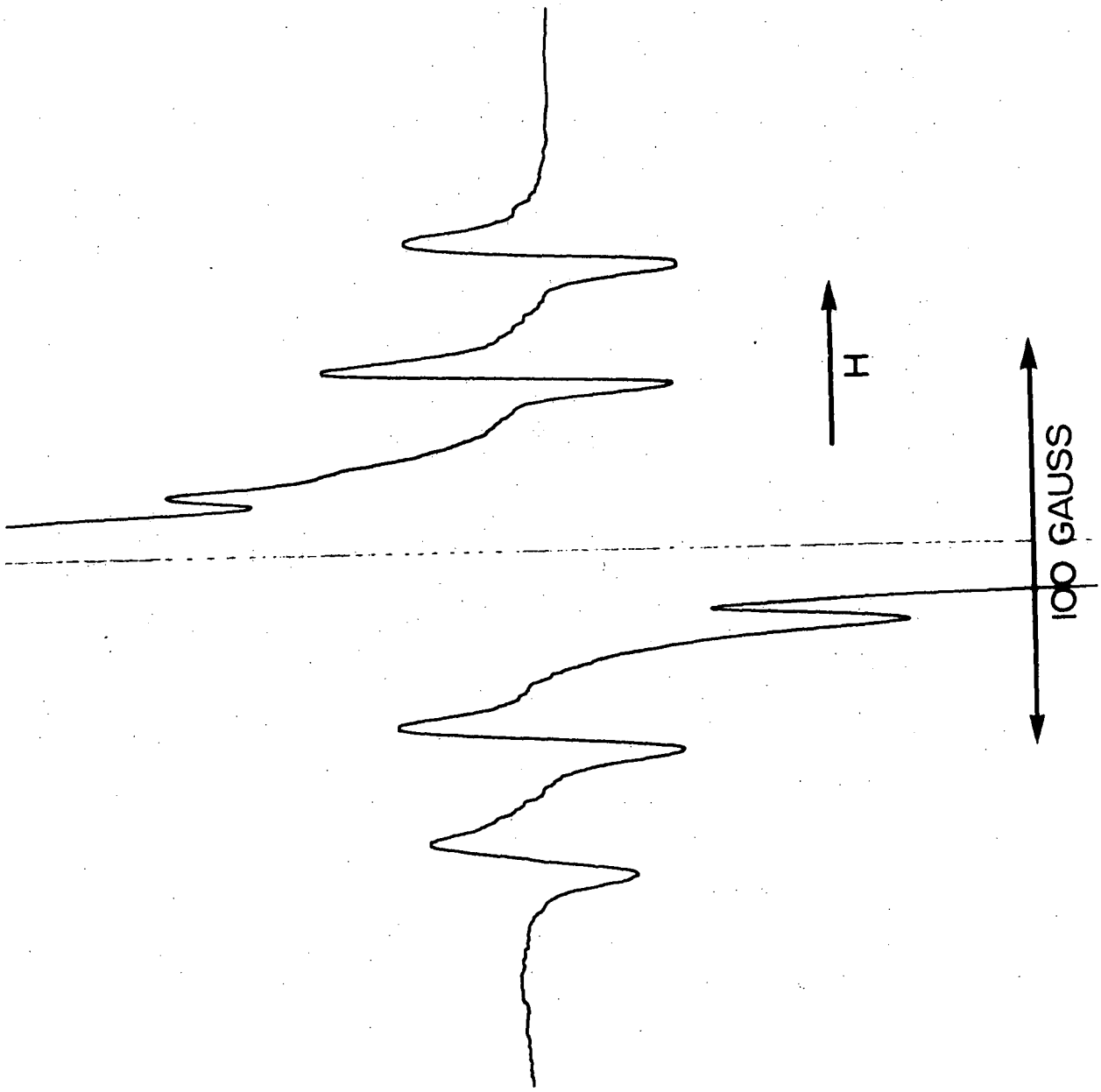

the isotopes ^{95}Mo and ^{97}Mo, both of which have a nuclear spin of 5/2. The difference between the nuclear magnetic moments of these species is only 2% and so the two possible sets of hyperfine lines merge into one set with the observed line-width (the ratio of line-width to hyperfine splitting is of the order of 1:8). In the normal hydrated crystals the spectra showed a doublet splitting of all lines, of the order of 7 gauss in magnitude. Because of the much smaller nuclear magnetic moment of deuterium this splitting is reduced to about 1.2 gauss in the deuterated crystals and is thus not resolved.

When spectra were measured in the b-c and a'-b planes they were found to consist of two superposed spectra since the monoclinic symmetry allows two non-equivalent sites for the molecules in the unit cell for these orientations. Despite this superposition it was quite simple to trace the variation of the lines with orientation. The variation with angle of the observed hyperfine splitting and g-values for each of the three planes is shown in Figs. 21 - 23.

In order to obtain the components of the hyperfine coupling tensor the first-order approximation, of dividing the splitting between the second and fifth hyperfine lines by three was used. The two centre components of the hyperfine structure were often obscured by overlap with the strong central line, whereas the lines chosen were sharp and distinct for all orientations.

3. Theoretical

Since Mo has a fairly large spin orbit coupling constant and $\underline{\underline{g}}$ and the hyperfine tensor are not parallel, it is not justifiable to take the usual $\hbar g_N \beta_N \beta_e \underline{S} \cdot \underline{\underline{A}} \cdot \underline{I}$ term in the spin Hamiltonian as a good description of the hyperfine coupling. Cross terms from Equ. #1 give

FIGURE 21 : The variation of hyperfine splitting and g-values, for an irradiated single crystal of deuterated ammonium paramolybdate tetrahydrate, for the orientations where the magnetic field is perpendicular to the a' axis

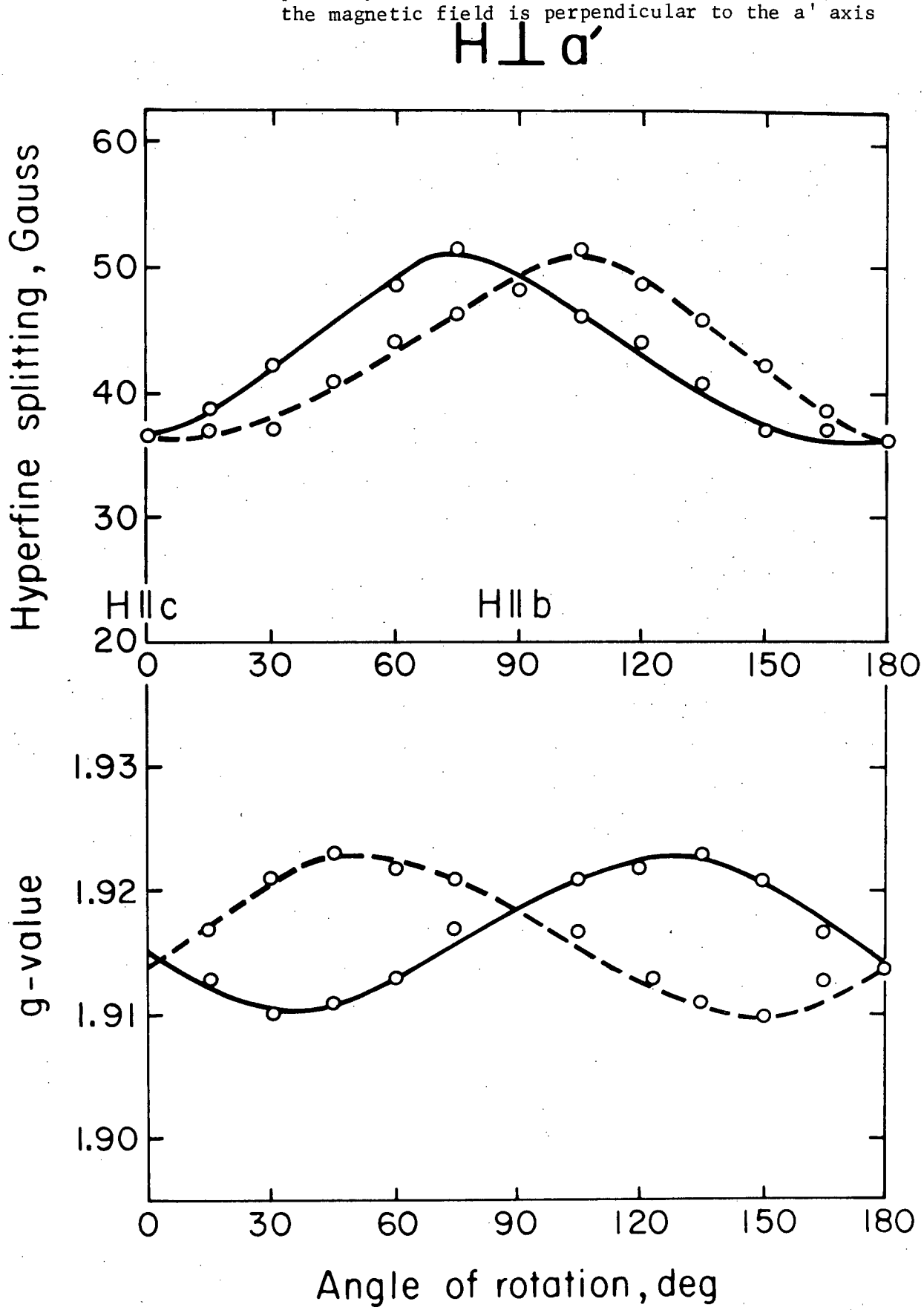

FIGURE 22 : The variation of hyperfine splitting and g-values for an irradiated single crystal of deuterated ammonium paramolybdate tetrahydrate for the orientations where the magnetic field is perpendicular to the b axis

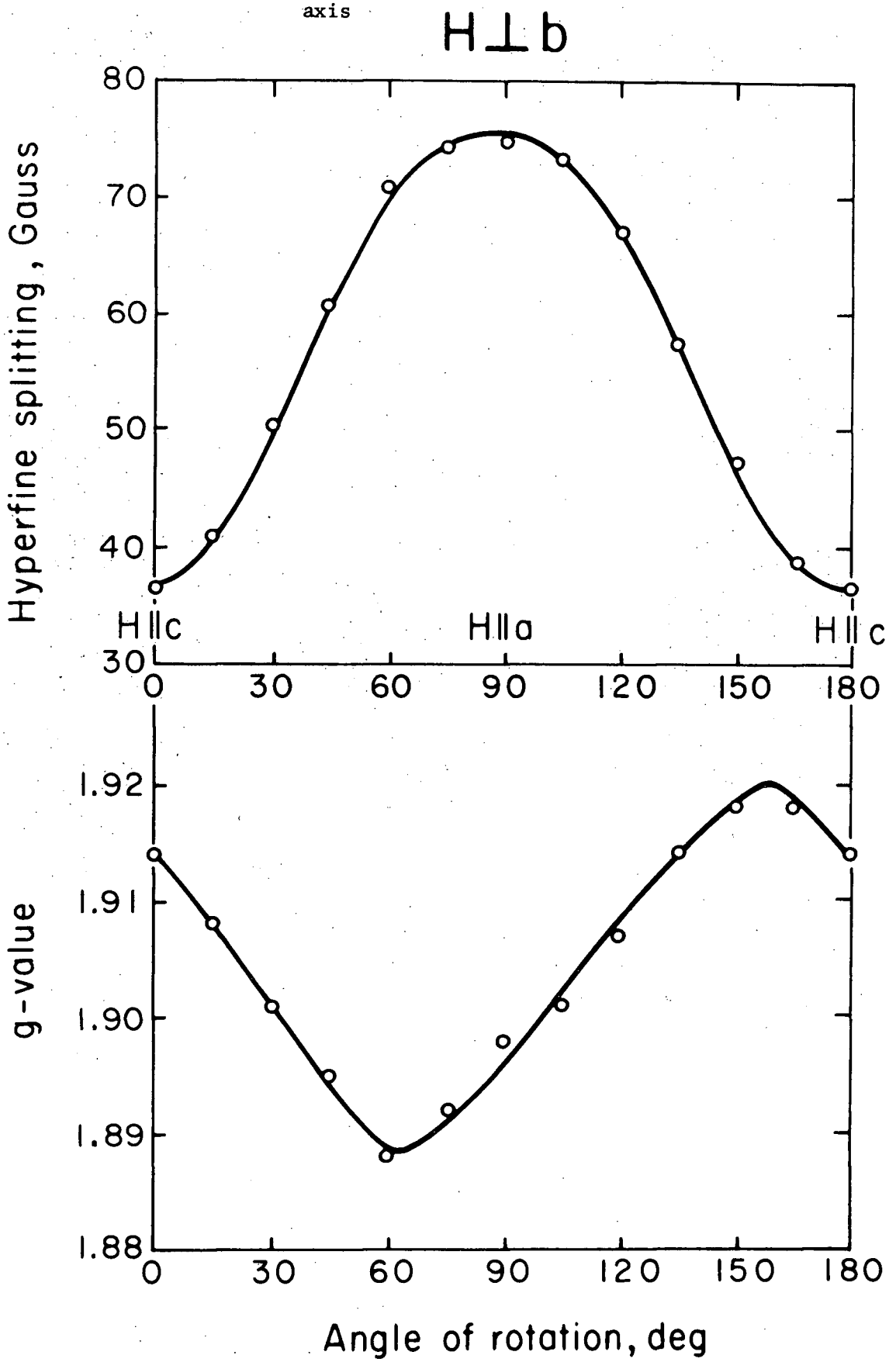

FIGURE 23 : The variation of hyperfine splittings and g-values for an irradiated single crystal of deuterated ammonium paramolybdate tetrahydrate for the orientations where the magnetic field is perpendicular to the c axis

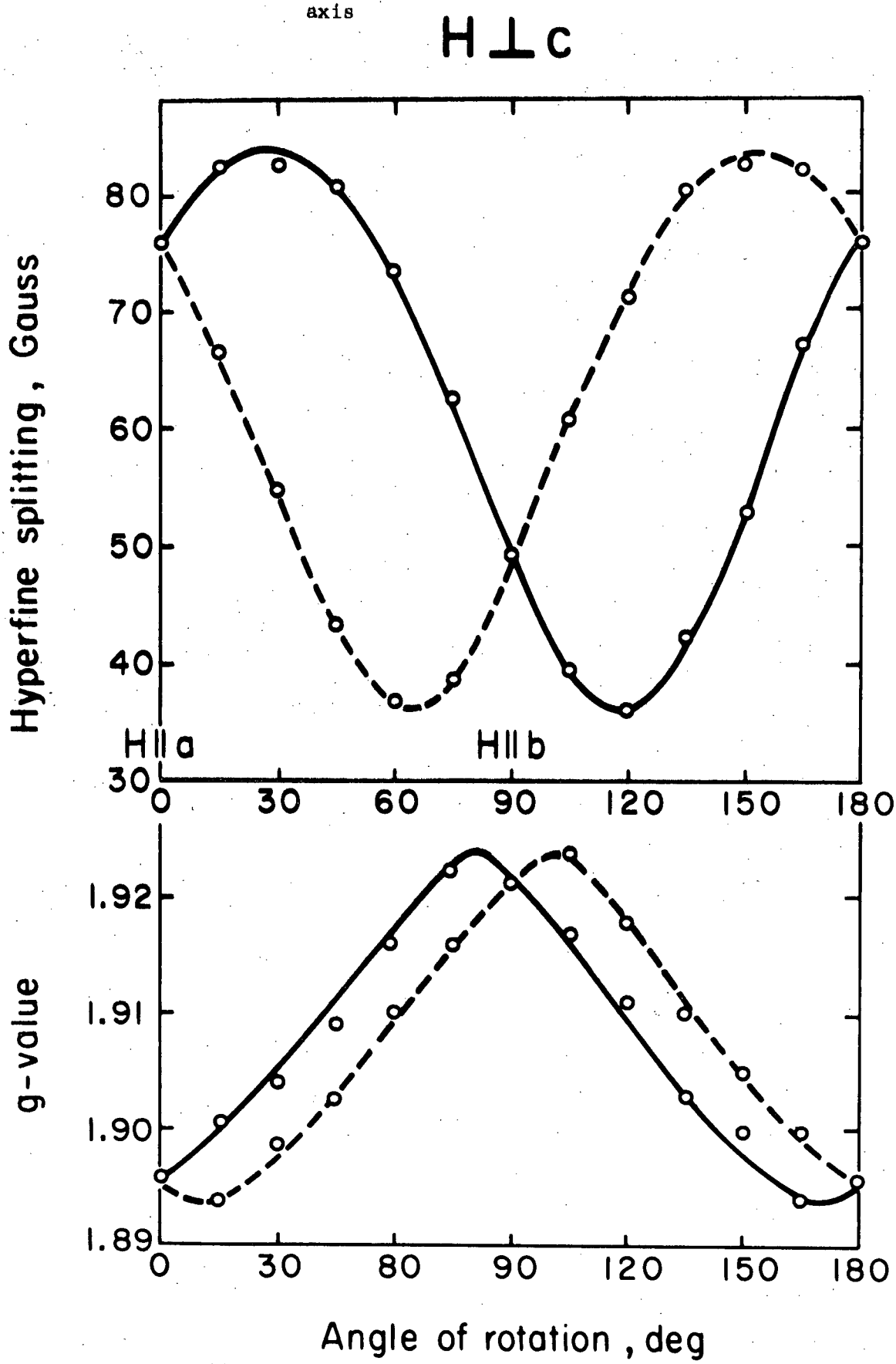

rise to a pseudo-dipolar hyperfine coupling which can rather be described by a term $\underline{S}.\underline{\underline{g}}.\underline{\underline{T}}.\underline{I}$ (70, 71) where $\underline{\underline{A}}$ has been replaced by $\underline{\underline{g}}.\underline{\underline{T}}$. The phenomenological spin Hamiltonian used for this work is thus

$$\mathcal{H} = \beta_e \underline{H}.\underline{\underline{g}}.\underline{S} + g_N \beta_N \beta_e \hbar \underline{S}.\underline{\underline{g}}.\underline{\underline{T}}.\underline{I}$$ which neglects the nuclear Zeeman term and which reduces the more usual equation when $\underline{\underline{g}}$ is very nearly isotropic and equal to the free electron value g_e. Since the measured deviation from g_e is about 0.1, this equation has been used.

One can see from Figs. 21 - 23 that the principal axes of the $\underline{\underline{g}}$ and hyperfine coupling tensors are not parallel and a method of determining the principal values of $\underline{\underline{g}}$ and $\underline{\underline{T}}$ has been given for this case (34).

The square of the observed g-value for a particular orientation is given by

$$g^2 = \sum Lij(\underline{\underline{g}}.\underline{\underline{g}})_{ij}$$

where Lij = lilj, li being the direction cosines of the magnetic field. The square of the observed hyperfine splitting is given by

$$(hfs)^2 = \frac{1}{g^2} \sum_{i,j} \frac{K_{ij}}{Tr(K)} (\underline{\underline{A}}.\underline{\underline{A}}^t)_{ij}$$

where $\underline{\underline{K}} = \underline{\underline{g}}.\underline{\underline{L}}.\underline{\underline{g}}$ and $\underline{\underline{A}}^t$ = transpose of $\underline{\underline{A}}$, $\underline{\underline{A}} = \underline{\underline{g}}.\underline{\underline{T}}$.
The derivation of these equations assumes that the electron spin $\underline{s}$ is quantized along the direction $\underline{H}.\underline{\underline{g}}$ and the nuclear spin in the direction of $\underline{S}.\underline{\underline{A}}$ (with $\underline{\underline{A}} = \underline{\underline{g}}.\underline{\underline{T}}$).

The tensor components $(\underline{\underline{g}}.\underline{\underline{g}})_{ij}$ and $(\underline{\underline{A}}.\underline{\underline{A}}^t)_{ij}$ were evaluated using a least squares technique on all the experimental data. The $(\underline{\underline{g}}.\underline{\underline{g}})$ tensor was diagonalized to give elements whose square roots are the principal values of $\underline{\underline{g}}$. Then from the definition of $\underline{\underline{A}}$ we have

$$\underline{\underline{T}}.\underline{\underline{T}} = \underline{\underline{g}}^{-1}.(\underline{\underline{A}}.\underline{\underline{A}}^t).\underline{\underline{g}}^{-1}$$

and since the $\underline{\underline{g}}$ tensor is already known, it is possible to calculate the components of $(\underline{\underline{T}}.\underline{\underline{T}})$ from the previous values of $(\underline{\underline{A}}.\underline{\underline{A}}^t)$. Diagonalization

of ($\underline{\underline{T}}.\underline{\underline{T}}$) gives the diagonal elements which are the squares of the principal values of $\underline{\underline{T}}$. In order to remove the ambiguity of the relative signs for off-diagonal elements of ($\underline{\underline{A}}.\underline{\underline{A}}^t$) in the a'-b and b-c planes, the "skew-axis" technique (72) was employed.

These calculations were all carried out on an I.B.M. 7040 computer using programs written by Dr. F.G. Herring and the final results are given in Table 16. The values for the normal hydrated crystal are also given for comparison.

4. Discussion

The E.S.R. spectrum of normal tetrahydrate crystal shown in Fig. 24 is for the same orientation as for the deuterated compounds in Fig. 20. It thus seems very probable that the doublet splitting is caused by the anion $(Mo_7O_{24})^{6-}$ capturing a hydrogen atom upon x-irradiation, giving the ion $(Mo_7O_{24}H)^{6-}$.

The undamaged crystal of $(NH_4)_6Mo_7O_{24}.4H_2O$ has discrete units which consist of seven distorted MoO_6 octahedra which are similar and nearly parallel to each other and which share corners and edges. The distortion makes and O - Mo - O axes unequal and non-orthogonal.

Since the principal hyperfine structure observed is that of an Mo nucleus, it seems reasonable to suppose that the odd electron orbital has considerable contributions from the 5s and 4d atomic orbitals of the Mo. Under S_2 symmetry these orbitals transform as A_g, as also do the angular momentum operators $\underline{l}_x$, $\underline{l}_y$, $\underline{l}_z$. As a result of this, matrix elements of the form

$\langle \phi_i | \lambda(r) \underline{l}_a | \phi_j \rangle \langle \phi_j | \underline{l}_b | \phi_i \rangle$ with ϕ_i = 5s or 4d and a, b = x, y, z

which occur in the Maki and McGarvey (66) perturbation scheme for g-shifts would all be non-zero. This would account for the large rhombic char-

	Principal values*		Direction cosines with respect to		
	Non-deuterated	Deuterated	a'	b	c
g	1.891 + 0.005	1.900 + 0.005	0.917	+0.057	0.394
	1.913 + 0.005	1.921 + 0.005	-0.262	+0.658	0.706
	1.925 + 0.005	1.935 + 0.005	-0.300	+0.750	0.589
T	83.4 + 0.5	83.2 + 0.5	0.890	+0.451	0.053
	37.0 + 0.5	37.0 + 0.5	-0.308	+0.514	0.796
	34.6 + 0.5	35.4 + 0.5	0.331	+0.726	0.597

* The hyperfine coupling values are given in gauss

TABLE 16A : The spin Hamiltonian parameters for the $(Mo_7O_{24}H)^{6-}$ ion in their principal axes system

.....

Compound	$g_{\parallel}$	$g_{\perp}$†	$T_{\parallel}$ ℙ	$T_{\perp}$†	α^2	χ(A.U.)	Reference
$(MoOF_5)^{2-}$	1.874	1.918	99.8	48.2	0.97	-7.60	(14)
$(MoOCl_5)^{2-}$	1.963	1.940	74.7	32.6	0.88	-5.61	(9)
$(MoOBr_5)^{2-}$	2.090	1.945	66.0	30.0	0.60	-5.09 §	(10)
$(MoO(SCN)_5)^{2-}$	1.928	1.944	68.4	34.5	0.66	-5.44	(15)
$(Mo_7O_{24}H)^{6-}$	1.90	1.90‡	78.0	33.7	0.68	-5.25	This work
$(Mo_7O_{24}H)^{6-}$	1.891	1.915//	78.0	33.7	0.67	-5.35	This work

† Average taken of x and y values
‡ g-values in T frame
§ Estimate neglecting ligand spin-orbit coupling from data in (10)
// g tensor not parallel to T tensor
ℙ $T_{\parallel}$, $T_{\perp}$ in units of 10^{-4} cm^{-1}

TABLE 16B : Values of the g tensor and hyperfine interaction tensor for molybdenum complex anions

FIGURE 24 : An E.S.R. spectrum of an irradiated single crystal of ammonium paramolybdate tetrahydrate, with the magnetic field in the a' - c plane

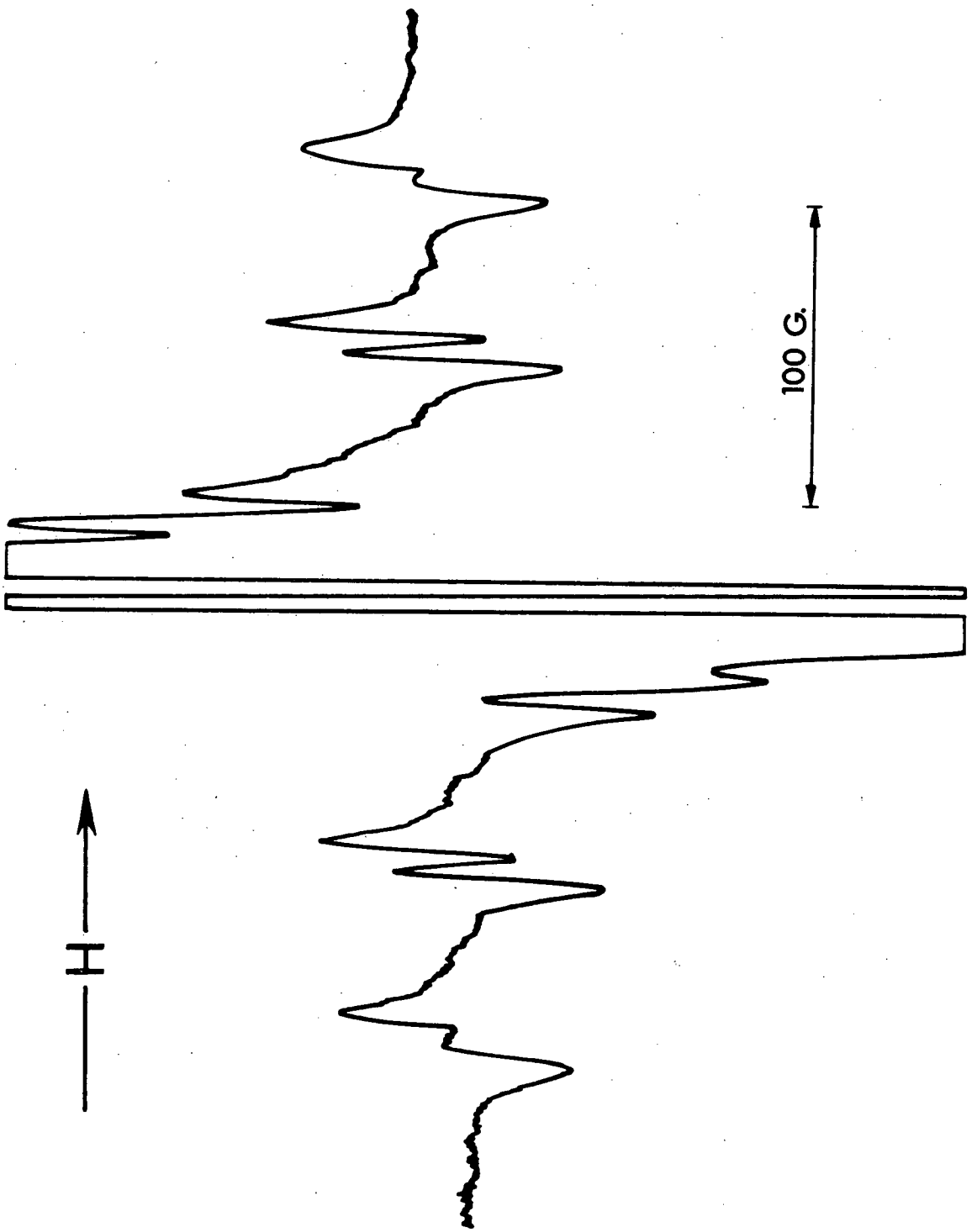

acter of the $\underline{g}$ tensor and, probably, for the fact that the principal axes of the $\underline{\underline{T}}$ and $\underline{g}$ tensors are not parallel.

The direction cosines of $\underline{\underline{T}}$ are nearly parallel to the Mo-O bonds in any one of the octahedra, whereas those for $\underline{g}$ are not. This is to be expected for molecules of low symmetry since $\underline{\underline{T}}$ depends primarily on the spin density in the immediate neighbourhood of the nucleus in question, but $\underline{g}$ depends on the electron distribution in the molecules as a whole (see Section 2).

In order to make an estimate of the bonding around the molybdenum, the non-orthogonality of the O-Mo-O axes was ignored (34) and the point group for a single octahedron regarded as D_{2h}. The anti-bonding orbitals for an MoO_6 unit can then be written as follows

$$|B_{1g}\rangle = \alpha|xy\rangle - \alpha'|L_{B_{1g}}\rangle$$

$$|B_{2g}\rangle = \beta|xz\rangle - \beta'|L_{B_{2g}}\rangle$$

$$|B_{3g}\rangle = \gamma|yz\rangle - \gamma'|L_{B_{3g}}\rangle$$

$$|A_g\rangle = \delta|x^2-y^2\rangle + \epsilon|z^2\rangle + \theta|s\rangle - \delta'|L_{A_g}\rangle$$

where L_Γ are the symmetry adapted linear combinations of oxygen orbitals belonging to the Γ-irreducible representation of D_{2h}.

The previous work on paramagnetic molybdenum complexes (78-81) has been done on species which have C_{4v} symmetry and a ground state which is principally a d_{xy} orbital. The hyperfine coupling tensor of the present species is very similar to those previously reported (Table 16) and accordingly B_{1g} has been chosen as the ground state, and a reasonable ordering of the orbitals in increasing energy would be $B_{1g} < B_{2g} \sim B_{3g} < A_g$.

Following the method of Maki and McGarvey (66) the following expressions were obtained (34) for the components of $\underline{\underline{T}}$

$$T_z = P(-k - (4/7)\alpha^2 - \Delta g_z - (3/14)(\Delta g_x + \Delta g_y))$$

$$T_x = P(-k + (2/7)\alpha^2 - \Delta g_x + (3/14)\Delta g_y - (3/14)(\epsilon/\delta)\Delta g_z)$$

$$T_y = P(-k + (2/7)\alpha^2 - \Delta g_y + (3/14)\Delta g_x + (3/14)(\epsilon/\delta)\Delta g_z)$$

where -Pk is the Fermi contact term. On substitution of the values of the components of $\underline{\underline{T}}$ and $\underline{\underline{g}}$ and a value of P for Mo^{5+}, the equations can be solved for α^2 and k. T_z was taken as 83.4 gauss, T_x as 37.0 gauss, and T_y as 34.6 gauss. The problem of $\underline{\underline{T}}$ and $\underline{\underline{g}}$ being non-parallel was treated in two ways:

(i) The non-parallel effect was ignored and the g-values assigned as $g_z = 1.891$, $g_x = 1.913$, $g_y = 1.925$, and

(ii) the $\underline{\underline{g}}$ tensor was transformed to the T-axes frame and these diagonal elements assigned to g_z, g_x and g_y. The elements all turn out to be 1.90 in this frame.

The value of P was taken as -67.95×10^{-4} cm^{-1}, quoted by McGarvey (82). The results of those two calculations are essentially identical.

The computed value of α^2 indicates a large contribution of in-plane bonding of the oxygen atoms to the molybdenum. There are two competing effects which determine whether $g_{\parallel} > g_{\perp}$ or $g_{\parallel} < g_{\perp}$. As α^2 becomes smaller in the halo-oxomolybdate series, the tendency for $g_{\parallel} > g_{\perp}$ increases (Table 16). However, the spin orbit coupling of F, Cl and Br increase in the same direction (84) and thus the effect of ligand spin-orbit coupling is also important (78). The spin-orbit coupling constant of O or O^- is smaller than that of the halogens (as is sulphur) and so we expect, in spite of the small value of α^2, that $g_{\parallel} < g_{\perp}$, as is observed.

The large value of χ indicates that there is little or no direct contribution to the contact term from the 5s orbital of molybdenum (82), and thus the hyperfine coupling arises primarily from core-polarization

affecting the 4d orbitals.

References

1. B.R. McGarvey, Transition Metal Chemistry, Vol. 3 (R.L. Carlin, ed.) 1966.
2. B. Bleaney & K.W.H. Stevens, Rept. Progr. Phys., 16, 108, 1953
3. K.D. Bower & J. Owen, ibid., 18, 304, 1955
4. J.W. Orton, ibid., 21, 204, 1958
5. J.H. Van Vleck, Phys. Rev., 41, 208, 1932
6. J.S. Griffith, The Theory of Transition Metal Ions, C.U.P., 1961
7. J.P. Dahl & C.J. Ballhausen, Quantum Chemistry, Vol. 4, 170, 1968
8. J. Owen & J.H.M. Thornley, Rept. Progr. Phys., 29, 675, 1966
9. A.M. Clogston, J.P. Gordon, V. Jaccarino, M. Peter & L.R. Walker, Phys. Rev., 117, 1222, 1960
10. E.U. Condon & G.H. Shortley, Theory of Atomic Spectra, C.U.P., 1951
11. S. Geschwind, P. Kisliuk, M.P. Klein, J.P. Remeika & D.L. Wood, Phys. Rev., 126, 1684, 1962
12. G.F. Imbusch, S.R. Chinn & S. Geschwind, ibid., 161, 295, 1967
13. W.H. From, P.B. Dorain & C. Kikuchi, ibid., 135, A710, 1964
14. H. Andresen, ibid., 120, 1606, 1960
15. E. Yamaka & R.G. Barnes, ibid., 135, A144, 1964
16. B. Henderson, Proc. Phys. Soc., 92, 1064, 1967
17. B. Henderson & T.P.P. Hall, ibid., 90, 511, 1967
18. K.A. Muller, Phys. Rev. Let., 2, 341, 1959
19. K.A. Muller, Helv. Phys. Acta., 33, 497, 1960
20. K.A. Muller, Conference on High-Frequency Spectroscopy, Leipzig, 31.3 - 2.4, 1960, Akademie Verlag Berlin, 1961, p. 138.
21. K.A. Muller, Paramagnetic Resonance, Vol. 1, (W. Low, ed.) 1963, Academic, New York, p. 17.
22. H. Gerritson, ibid., p. 3
23. B. Bleaney, R.J. Elliot & H.E.D. Scovil, Proc. Phys. Soc., A64, 933, 1951

24. H.A. Jahn & E. Teller, Proc. Roy. Soc., A161, 220, 1937

25. H.B. Kramers, Proc. Acad. Sci. Amsterdam, 33, 953, 1930 and 32, 1176, 1939

26. D.W. Davies, The Theory of the Electric and Magnetic Properties of Molecules, Wiley, 1967

27. E. Fermi, Z. Physik., 60, 320, 1930

28. S.M. Blinder, Adv. Quantum Chem., Vol. 2, 1965, Academic Press

29. A. Abragam & M.H.L. Pryce, Proc. Roy. Soc., A205, 135, 1951

30. M.H.L. Pryce, Proc. Phys. Soc., A63, 25, 1950

31. G.F. Koster & H. Statz, Phys. Rev., 115, 1568, 1959

32. R.M. Pitzer, C.W. Kern & W.N. Lipscomb, J. Chem. Phys., 37, 267, 1963

33. G.F. Kokoszka, H.C. Allen & G. Gordon, ibid., 46, 3013, 1967

34. C.R. Byfleet, F.G. Herring, W.C. Lin, C.A. McDowell & D.J. Ward, Mol. Phys., 15, 239, 1968

35. R. Lefebvre, ibid., 12, 417, 1967

36. B. Bleaney, Proc. Phys. Soc., A73, 939, 1959

37. W. Low, Paramagnetic Resonance in Solids, Solid State Physics, Supplement 2, Chap. 5

38. R. Stahl-Brada & W. Low, Nuovo Cimento, 15, 290, 1960

39. B. Bleaney, Phil. Mag., 42, 441, 1951

40. C-E. Froberg, Introduction to Numerical Analysis, Addison-Wesley, 1965

41. J.A. Hebden, Private Communication

42. C.G.J. Jacobi, Crelle's J., 30, 51, 1846 and A. Ralston, A First Course in Numerical Analysis, McGraw-Hill, 1965

43. J.A.R. Coope, J. Chem. Phys., 44, 4431, 1966

44. P. Kottis & R. Lefebvre, J. Chem. Phys., 39, 393, 1963

45. A. Carrington & A.D. McLachlan, Introduction to Paramagnetic Resonance, Harper & Row, 1967

46. Y. Shimura, H. Ito & R. Tsuchida, J. Chem. Soc., Japan, 75, 560, 1954

47. M. Mingardi, Private Communication

48. J.H. Van Vleck, J. Chem. Phys., 7, 61, 1939

49. L.J.F. Broer, Physica, 9, 547, 1942

50. P.R. Weiss, Phys. Rev., 73, 470, 1948

51. P.H.E. Meijer & H.J. Gerritson, Phys. Rev., 100, 742, 1955

52. H.S. Jarrett, J. Chem. Phys., 27, 1298, 1957

53. C.F. Davis & M.W.P. Strandberg, Phys. Rev., 105, 447, 1957

54. S. Sugano & Y. Tanabe, J. Phys. Soc., Japan, 13, 880, 1958

55. R. Stahl-Brada & W. Low, Phys. Rev., 116, 561, 1959

56. S. Sugano & M. Peter, Phys. Rev., 122, 381, 1961

57. H. Kamimura, ibid., 128, 1077, 1962

58. L.L. Lohr & W.N. Lipscomb, J. Chem. Phys., 38, 1607, 1963

59. B.R. McGarvey, ibid., 41, 3743, 1964

60. J. Owen & J.H.M. Thornley, Rept. Prog. Phys., 29, 675, 1966

61. M.H.L. Pryce & W.A. Runciman, Disc. Farad. Soc., 26, 34, 1958

62. C.K. Jorgensen, Adv. in Chem. Phys., Vol. 5 (I. Prigogine, ed.), 1963, Interscience, p. 33

63. G. Racah, Phys. Rev., 62, 438, 1942 and 63, 367, 1943

64. C.J. Ballhausen, Introduction to Ligand Field Theory, McGraw-Hill, 1962

65. P-O. Lowdin, J. Mol. Spec., 10, 12, 1963

66. A.H. Maki & B.R. McGarvey, J. Chem. Phys., 29, 31, 35, 1958

67. N.S. Dalal, Private Communication

68. J. Lindquist, Ark. Kemi., 2, 325, 1950 and Acta. Cryst., 3, 159, 1950

69. M.A. Hampton, B.Sc. thesis, U.B.C., 1965

70. H.M. McConnell, Proc. Nat. Acad. Sci., U.S.A., 44, 766, 1958

71. H.M. McConnell & R.E. Robertson, J. Chem. Phys., 29, 1361, 1959

72. F.G. Herring, J. Hwang, W.C. Lin & C.A. McDowell, J. Phys. Chem., 70, 2487, 1966

73. H. Eyring, J. Walter & G.E. Kimball, Quantum Chemistry, Wiley, 1944

74. J.O. Hirschfelder, W. Byers-Brown & S.T. Epstein, Adv. Quantum Chem., Vol. 1, p. 255, 1964, Academic Press

75. D.P. Chong, to be published

76. J.L.T. Waugh, D.P. Shomaker & L. Pauling, Acta. Cryst., 7, 438, 1954

77. C. Friedheim & M. Samuelson, Z. Anorg. Chem., 24, 67, 1900

78. K. De Armond, B.B. Garrett & H.S. Gutowsky, J. Chem. Phys., 42, 1091, 1965

79. H. Kon & N.E. Sharpless, J. Phys. Chem., 70, 105, 1966

80. N.S. Garifyanov, V.N. Fedotov & N.S. Kucheryavendo, Izv. Akad. Nauk SSSR, Ser. Khim., p. 743, 1964.

81. N.S. Garifyanov, B.M. Kozyrev & V.N. Fedotov, Dokl. Akad. Nauk SSSR, 156, 641, 1964

82. B.R. McGarvey, J. Phys. Chem., 71, 51, 1967

83. A. Abragam, J. Horowitz & M.H.L. Pryce, Proc. R. Soc. A., 230, 169, 1955

84. G. Malli & S. Fraga, Theor. Chim. Acta., 70, 80, 1967

APPENDIX I

Perturbation Theory

Let us consider a Hamiltonian $\mathcal{H}$ which can be written as $\mathcal{H}_o + \lambda V$ where the eigenvalues $E_i^{(o)}$ and eigenstates $\psi_i^{(o)}$ of $\mathcal{H}_o$ are known. If it is not possible, or not easy to find exact solutions to the total Hamiltonian $\mathcal{H}$ then, providing certain conditions are fulfilled, approximate solutions can be found as polynomials in λ. The most important condition is that the Hamiltonian λV, called the perturbing Hamiltonian, should be small compared with $\mathcal{H}_o$. Solutions for non-degenerate energies E_i, and wave functions ψ_i are given in terms of the solutions of $\mathcal{H}_o$ ($E_i^{(o)}$ and $\psi_i^{(o)}$), by (73, 74):

$$E_i = E_i^{(o)} + \lambda E_i^{(1)} + \lambda^2 E_i^{(2)} + \ldots + \text{etc.}$$

$$\psi_i = \psi_i^{(o)} + \lambda \psi_i^{(1)} + \lambda^2 \psi_i^{(2)} + \ldots + \text{etc.} \qquad \ldots(A1.1)$$

where

$$E_i^{(1)} = V_{ii}$$

$$E_i^{(2)} = \langle \psi_i^{(o)} | V' | \psi_i^{(1)} \rangle \qquad (V' = V - E_i^{(1)})$$

$$E_i^{(3)} = \langle \psi_i^{(1)} | V' | \psi_i^{(1)} \rangle$$

$$E_i^{(2n)} = \langle \psi_i^{(n+1)} | V' | \psi_i^{(n)} \rangle - \sum_{k=2}^{n} E_i^{(k)} \sum_{j=o}^{k-1} \langle \psi_i^{(n+j-1)} | \psi_i^{(n-j)} \rangle$$

$$E_i^{(2n+1)} = \langle \psi_i^{(n)} | V' | \psi_i^{(n)} \rangle - \sum_{k=2}^{n} E_i^{(k)} \sum_{j=o}^{k-1} \langle \psi_i^{(n-j+1-k)} | \psi_i^{(n-j)} \rangle$$

and

$$\psi_i^{(1)} = \sum_{k=1}^{n} a_k \psi_k^{(o)} \quad : \quad a_1 = V_{1i}/(E_i^{(o)} - E_1^{(o)})$$

$$\psi_i^{(2)} = \sum_{k=1}^{n} b_k \psi_k^{(o)} \quad : \quad b_1 = \sum_{k=1}^{n} a_k V'_{1k}/(E_i^{(o)} - E_1^{(o)})$$

$$\psi_i^{(3)} = \sum_{k=1}^{n} c_k \psi_k^{(o)} \quad : \quad c_1 = \sum_{k=1}^{n} b_k V'_{1k}/(E_i^{(o)} - E_1^{(o)}) - E_i^{(2)} a_1/(E_i^{(o)} - E_1^{(o)})$$

When λV is small these solutions are rapidly convergent. If the solutions to $\mathcal{H}_o$ contain degenerate energy levels then these formulae are not immediately applicable since $E_i^{(o)} - E_n^{(o)}$ would be zero for some terms in the summation. To remove this difficulty the $\psi_i^{(o)}$ are transformed so that there are no off-diagonal matrix elements connecting degenerate levels.

This transformation is found by arranging the matrix V so that states with degenerate solutions to $\mathcal{H}_o$ are adjacent, and diagonalizing the sub-matrices with dimensions equal to the number of degenerate levels. The solutions to this diagonalization are called "correct zeroth order wave functions". e.g. Consider the two matrices in the basis α, β, γ

$$\mathcal{H}_o = \begin{array}{c} \begin{matrix} \alpha & \beta & \gamma \end{matrix} \\ \begin{pmatrix} A & 0 & 0 \\ 0 & A & 0 \\ 0 & 0 & B \end{pmatrix} \end{array} \qquad V = \begin{array}{c} \begin{matrix} \alpha & \beta & \gamma \end{matrix} \\ \begin{pmatrix} x & z & 0 \\ z & -x & 2z \\ 0 & 2z & y \end{pmatrix} \end{array}$$

α and β are degenerate in $\mathcal{H}_o$ and so we have to apply the above treatment. The matrices are already arranged with the degenerate states adjacent. The correct zeroth order wave functions for λV are found by diagonalizing the 2 x 2 sub-matrix.

$$\begin{pmatrix} x & z \\ z & -x \end{pmatrix}$$

The solutions may be written

$E_1 = +(x^2 - z^2)^{\frac{1}{2}}$: $\psi_1 = j\alpha + k\beta$ $(j^2 + k^2 = 1)$

$E_2 = -(x^2 - z^2)^{\frac{1}{2}}$: $\psi_2 = j\alpha - k\beta$

The transformation matrix T must thus be applied to λV where T is

$$\begin{pmatrix} j & j & o \\ k & -k & o \\ o & o & 1 \end{pmatrix}$$

and $T^\dagger \lambda V T = \lambda \begin{pmatrix} E_1 & o & p \\ o & E_2 & q \\ p^* & q^* & y \end{pmatrix}$

where p and q are the off-diagonal elements after transformation. This transformation, T, has made the matrix element connecting the two degenerate states

of $\mathcal{H}_o$ equal to zero. Note that the matrix of $\mathcal{H}_o$ is unchanged by this transformation since any linear combination of α and β will have the same eigenvalue.

The degenerate case has been treated in general by D.P. Chong (75) and he gives equations similar to Equ. #A 1.1). A program (DPERT1) (75) for the general case is available from the Quantum Chemistry Program Exchange.

The equations A1.1 differ from the normal presentation of perturbation theory in that they are far more amenable to numerical calculations, since successive orders of energies and wave-functions are found by progressive substitution of parameters.

APPENDIX II

Block Diagram of Program to Calculate Transition Magnetic Fields from Spin Hamiltonian Parameters

1. Read parameters and experimental data

   Set up $\mathcal{H}_o$ and $\mathcal{H}_1$ matrices in $|M_s\rangle$ basis — Equ. #18

   If $g\beta_e H < D$ go to 3

   Diagonalize $\mathcal{H}_o + \mathcal{H}_1$ for chosen field

   Go to 4

3. Diagonalize $\mathcal{H}_1$ blockwise

4. Call perturbation subroutine DPERT1

   Construct difference polynomial — Equ. #21

   Solve for $H_{transition}$

   Call DPERT1 again to get correct wave functions at this field

   Set up $\mathcal{H}_2$ matrix and transform to correct basis set

   Set up $(\mathcal{H}_o + \mathcal{H}_1)$ matrix in this expanded $|M_s M_I\rangle$ basis

   Call DPERT1 to get hyperfine energy levels

2. Define new field independent term and solve difference polynomial again — Equ. #22

Repeat (2) for all hyperfine transitions

Return to (1) for new parameters

Compare calculated fields with experimental values

Write out these fields and deviations from experiment

APPENDIX III

Example Calculation of an Electron Repulsion Integral

Let $xy = d_{xy}$: $yz = d_{yz}$: $xz = d_{xz}$

Then $t_+ = -(1/\sqrt{3})(xy + w.yz + w^2.xz)$

and $J(t_+,t_+) = \int t_+^*(1)\, t_+^*(2).(e^2/r_{12}).(t_+(1)\, t_+(2).d\tau$

$$= (1/9)\int \{xy(1).xy(2) + w^2.xy(1).yz(2) + w.xy(1).xz(2)$$
$$+ w^2.yz(1).xy(2) + w.yz(1).yz(2) + yz(1).xz(2)$$
$$+ w.xz(1).xy(2) + .xz(1).yz(2) + w^2.xz(1).xz(2)\}.(e^2/r_{12}).$$
$$\{xy(1).xy(2) + w.xy(1).yz(2) + w^2.xy(1).xz(2)$$
$$+ w.yz(1).xy(2) + w^2.yz(1).yz(2) + yz(1).xz(2)$$
$$+ w^2.xz(1).xy(2) + xz(1).yz(2) + w.xz(1).xz(2)\}.d\tau$$

$$= (1/3)(J(i,i) + 2J(i,j) + 2K(i,j) + (w+w^2)K(i,j))$$

since $J(i,i) = A + 4B + 3C$

$J(i,j) = A - 2B + C$ $\Big\}$ $(i,j = xy,\ yz \text{ or } xz)$

$K(i,j) = 3B + C$

and $w + w^2 = -1$

Thus $J(t_+,t_+) = (1/3)\ (3A + 3B + 6C)$

$= A + B + 2C$